PHENOTYPIC AND MOLECULAR CHARACTERIZATION OF A NOVEL MOUSE MODEL OF NEUROFIBROMATOSIS TYPE 2

Jeff R. Gehlhausen

Submitted to the faculty of the University Graduate School
in partial fulfillment of the requirements
for the degree
Doctor of Philosophy
in the Department of Biochemistry and Molecular Biology,
Indiana University

May 2015

Accepted by the Graduate Faculty, of Indiana University, in partial fulfillment of the requirements for the degree of Doctor of Philosophy.

D. Wade Clapp, M.D.
Chair

Mark G. Goebl, Ph.D.

Doctoral Committee

Maureen A. Harrington, Ph.D.

April 3, 2015

Grzegorz J. Nalepa, M.D., Ph.D.

© 2015
Jeff R. Gehlhausen

ACKNOWLEDGEMENTS

I would first like to acknowledge Wade Clapp for being the person most responsible for cultivating my nascent interest in science and encouraging me to pursue a career as a physician-scientist. He employed me as a research technician (without any previous experience) on a whim, supported me throughout, and kept a spot open for me in his lab when it was time to complete my thesis work. His work ethic, passion for basic science, and focus on translating discoveries into actionable therapies for man are just a handful of the many, many traits I admire about Dr. Clapp. Irrespective of where I end up to continue my training and career, I have no doubt that Wade will always be close friend that's just a phone call away.

I am very thankful to my committee members Dr. Maureen Harrington, Dr. Mark Goebl, and Dr. Grzegorz Nalepa for their thoughtful contributions to my work. I have met with each member outside of committee meetings more than once in order to discuss finer points of experiments, and their willingingness to meet with me is a testament to their commitment to academics and education.

I thank all the members of the Clapp lab for their support throughout my four years. I believe nearly every single person in the lab has helped me in my studies at some point. In particular, I would like to thank Dr. Shi Chen and Dr. Su

Jung Park for their assistance and tutelage. I would never have gotten to this point without their advice and experience.

I thank the MSTP program for supporting my education, and I'd like to point out some current and past IU MSTP students for their special contribution to my work. Karl Staser was instrumental in fostering an enthusiasm for science, as well as teaching me to be a thoughtful experimenter. Steven Rhodes, who was seated next to me for two years in lab, taught me many different things about science, especially when it came to preparing figures and manuscripts. Jackie Lajiness was always a close friend and science confidante, but she also has aided me in critical experiments at many different points throughout my thesis. Donna Cerabona has helped with many experiments in the past year, and has also been a great mind to bounce ideas off from time to time. All of you have had a significant influence on my thesis work, and I sincerely appreciate the help.

Finally, I would like to acknowledge my financial support from the Children's Tumor Foundation and NIDCD training grants.

Jeff R. Gehlhausen

PHENOTYPIC AND MOLECULAR CHARACTERIZATION OF A NOVEL MOUSE MODEL OF NEUROFIBROMATOSIS TYPE 2

Neurofibromatosis Type 2 is a genetic disease that predisoposes patients to the development of multiple benign nervous system tumors, the most common being schwannoma. To date, there are no mainstream medical alternatives to surgical excision for these tumors, which has the potential to increase disease burden. To better study NF2 disease, we generated a conditional knockout mouse that excises the *Nf2* gene in the developing Schwann cell lineages. Phenotypically, this mouse recapitulates important aspects of human NF2 disease, including complete schwannoma penetrance and hearing loss that correlates with vestibular schwannoma development.

In parallel studies, we analyzed genomics data comparing human schwannomas and normal nerve tissue for deregulated signaling pathways that may be involved in schwannoma genesis. Our investigation suggested that the NF-κB signaling pathway is activated in schwannoma tumors. The NF-κB pathway is known to regulate cellular proliferation and survival, and has been implicated as the driver of other cancers, including ependymomas, which also frequently arise in NF2 patients. We validated these findings in our NF2 mouse model by demonstrating

increased nuclear accumulation of NF-κB transcription factors in schwannomas with a concomitant increase in NF-κB target gene expression. Analysis of human and mouse tumors for upstream kinases regulating NF-κB transcription factor localization revealed a fragment of the kinase domain of NIK, a potent oncogene in the NF KappaB signaling pathway. Transduction of primary Schwann cells with this NIK kinase fragment increased proliferation, survival, and adhesion, while also inducing a gene expression profile highly reminiscent of that observed in both human and mouse schwannoma. Altogether, these studies demonstrate the remarkable ability of a phenotypically accurate genetic murine model to provide molecular insights into human disease.

D. Wade Clapp, M.D., Chair

TABLE OF CONTENTS

List of Tables xi

List of Figures xii

List of Abbreviations xvi

Introduction to Chapter One 1

Neurofibromatosis Type 2 1

NF2 molecular biology 5

The Schwann cell lineage 10

Mouse models of NF2 11

Materials and Methods 13

Study approval 13

Statistical methods 13

Hearing screening 14

Mice and genotyping 14

Histology and immunohistochemistry 15

Tumor volume quantitation 15

Vestibular studies 16

Results 18

Postn-Cre+ mice develop schwannomas 18

Vestibular schwannomas in *Postn-Cre+* mice 25

Postn-Cre+ mice experience hearing loss and vestibular impariment 29

Embryonic analysis of *PostnCre+* progenitor populations 35

Discussion 39

Introduction to Chapter Two 42
NF-κB signaling pathway 42
NIK, NF-κB, and cancer 47
NF-κB and NF2 in the nervous system 50
Materials and Methods 55
Microarray and Ingenuity Pathway Analysis 55
Statistical methods 55
Preparation of mouse Trigeminal nerves for RNA and protein studies 56
RNA extraction from Trigeminal Nerves and primary Schwann cells 56
qRT-PCR Primer list 57
Procurement and preparation of human vestibular schwannoma tissue for protein and histological studies 58
Primary antibody list 58
Western Blot densitometry 59
Histology and immunohistochemistry 59
Cell culture and transfection 59
Plasmids and site-directed mutagenesis 60
Virus generation and titration 60
Primary Schwann cell procurement and culture 62
Transduction of primary Schwann cells 62
Schwann cell proliferation assays 63
Schwann cell survival assay 63
Schwann cell adhesion assay 64

Cycloheximide NIK protein stability assay 64

Immunoprecipitation experiments in 293T cells 64

In vitro Caspase-8 cleavage assay 65

Prediction of Caspase-8 cleavage sites and orthologous cleavage site analysis 65

Deconvolution microscopy 66

Results 67

Genomic studies indicate NF-κB is activated in schwannomas 67

Increased REL protein expression in schwannomas 70

Schwannomas exhibit an increase in NIK and fragments of the NIK kinase domain 78

Caspase-8 cleaves NIK to generate a fragment of the kinase domain 84

Bioinformatics analysis identifies clusters of Caspase-8 cleavage sites in NIK 93

p55 NIK demonstrates increased protein stability and activates

NF-κB 101

NIK signaling regulates Schwann cell function and gene expression 106

Evidence of persistent NIK signaling in schwannomas 111

Discussion 113

Future Directions 123

References 125

Curriculum Vitae

LIST OF TABLES

Table 1. *Postn-Cre; Nf2*$^{flox/flox}$ mice develop vestibular impairment..... 34

LIST OF FIGURES

Figure 1. Schematic representation of Rac-PAK-NF2 signaling axis 9

Figure 2. *Postn-Cre; Nf2*$^{flox/flox}$ mice develop schwannomas of the DRG and spinal nerves 21

Figure 3. Temporal analysis of spinal nerve tumors in *Postn-Cre; Nf2*$^{flox/flox}$ mice 22

Figure 4. A small percentage of schwannomas in *Postn-Cre; Nf2*$^{flox/flox}$ mice progress into MPNSTs 23

Figure 5. Schwannomas observed in *Postn-Cre; Nf2*$^{flox/flox}$ mice histologically resemble those observed in human patients 24

Figure 6. *Postn-Cre; Nf2*$^{flox/flox}$ mice develop schwannomas on CN V and CN VII 26

Figure 7. *Postn-Cre; Nf2*$^{flox/flox}$ mice develop schwannomas on CN VIII..... 27

Figure 8. The cochleas in *Postn-Cre; Nf2*$^{flox/flox}$ mice are structurally similar to *Cre*-negative controls 28

Figure 9. *Postn-Cre; Nf2*$^{flox/flox}$ mice show deficits in both threshold and supra-threshold auditory brainstem responses (ABRs) 32

Figure 10: *Postn-Cre* induces recombination in neural crest-derived tissues 36

Figure 11. *Postn-Cre* is expressed in multipotent embryonic Schwann cell lineages 37

Figure 12. Schematic representation of the NF-κB signaling pathway 45

Figure 13. Schematic representation of NIK degradation by an E3 Ligase protein complex including TRAF2, TRAF3, and c-IAP1/2. 48

Figure 14. Ingenuity Pathway Analysis and qRT-PCR in schwannomas suggests activation of the NF-κB pathway..... 68

Figure 15. Murine schwannomas exhibit increased levels of Rel transcription factors at the RNA and protein level. 72

Figure 16. Increased cytoplasmic and nuclear RELA reactivity observed by immunohistochemistry in murine and human schwannomas. 74

Figure 17. Expanded immunohistochemical panel of RELA in human schwannomas..... 75

Figure 18. Increased cytoplasmic and nuclear RELB reactivity observed by immunohistochemistry in human schwannomas 76

Figure 19. Increased cytoplasmic and nuclear RELA and RELB seen by subcellular fractionation in murine schwannomas 77

Figure 20. Accumulation of NIK and fragments of the NIK kinase domain in murine and human schwannomas. 80

Figure 21. Accumulation of FL NIK and p55 NIK in murine schwannomas. 81

Figure 22. Immunohistochemistry localizes NIK accumulation to tumorigenic cells in schwannomas..... 82

Figure 23. Expanded immunohistochemical panel of NIK-positive human schwannomas..... 83

Figure 24. Caspase-8 is sufficient to induce cleavage of NIK, resulting in a 55 kD fragment of the kinase domain 87

Figure 25. Caspase-8 is sufficient to cleave NIK *in vitro*..... 88

Figure 26. Decreased levels of Procaspase-8 seen at the protein level in schwannomas..... 89

Figure 27. Diagram indicating which STE family kinases are cleaved by caspases. 90

Figure 28. Caspase-8 co-immunoprecipitates with NIK in 293T cells. 91

Figure 29. Computational prediction of caspase-8 cleavage sites..... 95

Figure 30. Caspase cleavage sites on human NIK are conserved across mammalian species..... 96

Figure 31. Further characterization of the 55 kilodalton fragment of the NIK kinase domain in murine schwannomas using a peptide antibody targeting internal NIK residues 97

Figure 32. Caspase-8 cleavage of NIK renders the resulting kinase fragment resistant to known mechanisms of regulation of wild type NIK 98

Figure 33. 309-801 NIK demonstrates increased stability over FL NIK. 102

Figure 34. 309-801 NIK is sufficient to activate canonical and non-canonical NF-κB signaling 103

Figure 35. 309-801 NIK co-immunoprecipitates with IKKα in 293T cells 104

Figure 36. 309-801 NIK increases primary Schwann cell proliferation, survival, and adhesion 107

Figure 37. 309-801 NIK induces expression of Rel family transcription factors and NF-κB target genes that are deregulated in human and murine schwannomas..... 109

Figure 38. The genes encoding NIK, TRAF2, and TRAF3 are overexpressed in murine schwannomas 111

Figure 39. Schematic representation of hypothesized persistent NIK signaling present in schwannomas. 118

LIST OF ABBREVIATIONS

AA	Amino acid
ABR	Auditory Brainstem Response
ALL	Acute Lymphocytic Leukemia
ANOVA	Analysis of variance
Blbp	Brain Lipid Binding Protein
cDNA	cDNA
Co	Cochlea
CN	Cranial nerve
CNS	Central nervous system
CML	Chronic Myelogenous Leukemia
DEG	Differentially expressed genes
DNA	Deoxyribonucleic acid
DRG	Dorsal root ganglia
E	Embryonic day
ECM	Extracellular matrix
EGFP	Enhanced Green Fluorescent Protein
EMSA	Electrophoretic mobility shift assay
ERM	Ezrin, Radixin, and Moesin
FERM	4.1 protein, Ezrin, Radixin, and Moesin
GEM	Genetically engineered murine
GM-CSF	Granulocyte-Macrophage Colony Stimulating Factor
H&E	Hemotoxylin and eosin
HVS	Human vestibular schwannoma
IAP	Inhibitor of apoptosis
IHC	Immunohistochemistry
IκB	Inhibitor of κB
IKK	Inhibitor of κB kinase
IL-6	Interleukin 6
IRES	Internal ribosome entry site
LPS	Lipopolysaccharide
MAPK	Mitogen-activated protein kinase
MBP	Myelin Basic Protein

MIP-1β	Macrophage Inflammatory Protein 1β; CCL4
MM	Multiple Myeloma
mRNA	Messenger ribonucleic acid
NF-κB	Nuclear factor kappa light chain enhancer of activated B cells
NIK	NF-κB inducing kinase; MAP3K14
NIK-KO	NIK knockout
NRG1	Neuregulin-1
NF2	Neurofibromatosis Type 2
NF2-KO	NF2 knockout
P	Passage
PAK	P21-activated kinase
PBS	Phosphate-buffered saline
PCR	Polymerase chain reaction
PDL	Poly-D-Lysine
PFA	Paraformaldehyde
PNS	Peripheral nervous system
Postn-Cre	*Cre* expression driven by the 3.9kb upstream promoter of Periostin
qRT-PCR	Quantitative reverse transcription polymerase chain r reaction
RANTES	regulated on activation, normal T cell expressed and secreted; CCL5
RHD	Rel homology domain
RTK	Receptor tyrosine kinase
ScG	Scarpa's ganglion
SCM-1	Schwann cell media I
SCM-2	Schwann cell media II
SCP	Schwann cell precursor
SDS	Sodium dodecyl sulfate
SDS-PAGE	SDS polyacrylamide gel electrophoresis
SEM	Standard error of the mean
SP	Summation Potential
ST	Scala Tympani
SV	Scala Vestibuli
SVZ	Subventricular zone
TAD	Transactivation domain
TNF-α	Tumor Necrosis Factor Alpha

VS	Vestibular schwannoma
W1	ABR Wave 1
WT	Wild type

Some of the text in this dissertation was originally published in the journal Human Molecular Genetics, and the citation is seen below.

Gehlhausen, J.R., et al., *A murine model of neurofibromatosis type 2 that accurately phenocopies human schwannoma formation.* Human molecular genetics, 2015. **24**(1): p. 1-8.

INTRODUCTION TO CHAPTER ONE

Neurofibromatosis Type 2

Neurofibromatosis type 2 (NF2) is an autosomal dominant disorder that arises from germline heterozygosity of the *NF2* tumor suppressor gene located on the long arm of chromosome 22. Affected individuals have a high propensity for the acquisition of multiple tumors of the nervous sytem, especially schwannomas. NF2 disease is observed at a frequency of roughly 1 in 25,000 individuals [1]. Phenotypically, NF2 is known to demonstrate variable expressivity, but it is almost fully penetrant by the age of 60 [2, 3].

NF2 patients are predisposed to develop benign lesions of the skin, eyes, and nervous system. Bilaterial vestibular schwannomas (VS) are pathognomonic for NF2 disease, with up to 95% of patients acquiring these tumors. These tumors are referred to as VS because they grow on cranial nerve VIII (CN VIII), the vestibulocochlear nerve. This is the nerve that mediates both the sense of hearing and balance from structures in the inner ear. Most patients also develop multiple schwannomas in the cranial, spinal, and peripheral nerves [4-14]. Schwannomas are also the most common peripheral nerve tumor in non-NF2 patients and are almost universally NF2-deficient, underscoring the critical function of this tumor suppressor in the Schwann cell lineage [1]. Other tumors often seen in NF2 patients include intracranial meningioma (up to 58%) and

spinal cord ependymoma (up to 53%). Cutaneous tumors, typically schwannomas, are seen in up to 68% of patients [15, 16]. Cataracts and/or hamartomatous lesions of the eye are also common findings, present in up to 81% of patients.

Despite the fact that NF2 is a genetic disease, the diagnosis of patients remains one based on clinical criteria, and the presence of a germline *NF2* mutation is not required. The most popular tool used to diagnose patients, the Manchester criteria [17], primarily uses the knowledge that an individual has a known family history of NF2 or bilaterial vestibular schwannomas along with other NF2-related manifestations. The wide acceptance of these criteria is largely based on its sensitivity, as well as ability to diagnose patients with no family history of NF2, which occurs in more than half of patients [18].

Individuals afflicted with NF2 typically present as young adults with hearing loss resulting from a VS. Frequently, hearing loss is only on one side, and can be accompanied by vestibular symptoms including tinnitus (“ringing of the ears”), dizziness, and loss of normal balance [4, 5]. Interestingly, children often present with a different constellation of symptoms, including visual abnormalities (resulting from eye lesions or intracranial tumors), cutaneous tumors, spinal cord tumors, and mononeuropathy [19-21].

The first account of a patient with NF2 was in 1822, with the physician describing a deaf patient with multiple tumors in the skull, dura, and brain [22]. The disease was identified as having an autosomal dominant mode of transmission after following two families with NF2 manifestations, including VS, through multiple generations [23, 24]. NF2 was frequently confused with Neurofibromatosis Type 1, another autosomal dominant disease predisposing patients to tumors of the nervous system, until linkage analysis studies demonstrated these diseases to be genetically distinct [25, 26].

NF2 disease course and severity is frequently similar within families but can differ substantially between families, suggestive of a genotype-phenotype association [1]. More detailed genetic studies revealed this phenomenon to be true, with germline nonsense or frameshift mutations resulting in more severe disease when compared to those harboring missense mutations [27, 28]. Splice-site mutations can lead to variable disease phenotypes, but it has been noted that mutations affecting exons 1-5 of *NF2* result in increased disease severity than mutations in exons 11-15 [29]. The genotype-phenotype association is also observed with risk of mortality, as patients with more severe mutations end up with an increased disease burden including more spinal and peripheral nerve tumors, intracranial meningiomas, and cataracts [30]. Overall, NF2 patients do suffer from early mortality, but they also face substantial morbidities, as most become deaf and many will require wheelchair assistance.

VS are the chief source of morbidity for NF2 patients. They can also contribute to early mortality due to brainstem compression and surgical complications [1, 31]. Early surgical intervention in VS can preserve some degree of CN VII and CN VIII function, though the decision of when to intervene can be challenging [32]. Much of the difficulty comes from the knowledge that there appears to be little to no correlation between tumor size and hearing loss [33]. Further confounding the issue is that VS are known to have highly variable rates of growth [1]. Some clinicians may wait to intervene surgically until deterioration in hearing is noted, but operative morbidities increase with tumor size [1]. Surgical resection also remains the treatment of choice for symptomatic spinal schwannomas. Overall, this is a very challenging disease to manage surgically, as the surgeries inevitably take place in and around critical anatomical structures of the nervous system. With this in mind, compromised or total loss of nerve function after surgical intervention is not an unusual event.

Histopathological examination of human schwannomas reveals a few hallmark features that distinguish them from other tumors of the nervous system. They tend to demonstrate a biphasic growth pattern, with some regions displaying a dense arrangement of spindle-shapped schwannoma cells (“Antoni A”), and other regions appearing to be largely acellular (“Antoni B”). Verocay bodies are also observed, which are seen as with rows of tumor cells (nuclear palisades)

separated by acellular regions. Nuclear pleomorphism may also be observed. Schwannomas are found to be uniformly positive for the neural crest marker S100 [34].

NF2 molecular biology

NF2 is a 595 amino acid protein encoded by 17 exons. Two isoforms, I and II, exist in humans and are the result of alternative splicing. Isoform I includes exon 17 with exon 16 spliced out, while Isoform II includes exon 16 but not exon 17. There are conflicting data on which isoform predominantly functions as a tumor suppressor, as evidence has been found for both isoforms [35, 36]. NF2 is a member of the ERM family of proteins, where ERM stands for Ezrin, Radixin, and Moesin. Ezrin, Radixin, and Moexin are the canonical proteins of the ERM family, with an amino-terminal FERM domain followed by a coiled-coil domain and a C-terminal hyprohilic region [37, 38]. Though NF2 has the same organization of the ERM proteins, it also has distinct sequence motifs as well [38, 39]. Two major differences in NF2 when compared to other ERM proteins is the lack of a C-terminal actin-binding motif, as well as the inclusion of a seven amino-acid (AA) Blue-box motif in the FERM domain that is evolutionarily conserved.

ERM proteins are held in an inactivated state by an association between the C-terminus and FERM domain, and in response to activation by Rho kinases, a C-

terminal residue of the ERM protein is phosphorylated. This phosphorylation disrupts the closed FERM domain-C-terminal association, opening the ERM protein for interactions with binding partners. In their open configuration, ERM proteins bind the cytoplasmic regions of cell-adhesion receptors like CD44 and ICAM through their FERM domain. They are also free to bind actin filaments through their C-terminal actin-binding domains. Through these molecular interactions, ERM proteins function as regulators of the cell cytoskeleton [40-43].

NF2 has also been shown to be regulated in a similar fashion to other ERM proteins, switching from a closed, tumor-supressive form to an inactive, open configuration in response to phosphorylation at Serine 518 by P21-activated kinase (PAK1) [44]. Support of this relationship is seen through site-mutant studies, with mutation of Serine 518 to Alanine increasing the inhibitory function of NF2, while mutation to an Aspartic Acid abolishes NF2's tumor suppressive function [45-47]. Deletion of the Blue Box motif in NF2 is sufficient to induce dominant-negative behaviour, as overexpression of this mutant promotes cellular transformation *in-vitro* [48]. Additional evidence of the importance of this motif is seen in *Drosophila*, where overexpression of a Blue box deletion mutant causes excessive wing proliferation [49].

In response to various anti-mitogenic signals, such as growth factor starvation, contact inhibition, and loss of cell adhesion to the ECM, the dephosphorylated,

tumor suppressive form of NF2 is increased [50]. Activation of Integrin or receptor tyrosine kinase (RTK) signalling leads to activation of CDC42/Rac1, which are well-established activators of PAK1. Activated PAK1 then phosphorylates NF2 at S518, inactivating its tumor suppressive function [51, 52]. NF2 also exerts a negative regulatory function on PAK1, preventing it from being activated by upstream Rac singaling through binding to the P21-binding domain of PAK [53]. Overall, the molecular interplay present in the Rac-PAK-NF2 axis has been suggested to resemble a feed-forward inactivation loop, whereby Rac activates PAK1, which inactivates NF2, freeing PAK to promote downstream signalling [51-53].

In the context of contact inhibition of cell proliferation, homophilic cadherin interactions lead to inactivation of PAK1, resulting in an increase of the closed, tumor-supressive form of NF2 [50]. Considering NF2 is an ERM family member with prevalant cortical localization, it has been suggested that NF2 exerts its function as a tumor suppressor by regulating molecular events at the cell membrane. Support of this relationship is seen in NF2-deficient cells, which do not arrest in the cell cycle at confluency as do normal, contact-inhibited cells [51]. The localization of NF2 in confluent cell states also supports this hypothesis, as it has been observed to accumulate to cell-cell contacts in epithelial cell types at confluency in cell culture [51, 54]. Another study identified NF2 to accumulation and interaction with a protein complex at the tight junction in epithelial cells [55].

NF2 is also an inhibitor of mTORC1 signalling, a fundamental pathway known to control protein translation [56, 57]. mTORC1 activation increases cell proliferation and survival through phosphorylation and inhibition of two downstream targets, p70-S6K1 and 4E-BP1. In response to activation by integrin signalling, PAK1 phosphorylates and inactivates NF2, leading to an increase in downstream mTORC1 activation. A schematic of the relationship between Rac, PAK, NF2, and mTORC1 is seen in **Figure 1**. Support for this relationship is seen in constitutive activation of mTORC1 in NF2-deficient mesothelioma, meningnioma, and vestibular schwannoma cell lines. This activation appears to be independent of two well-established upstream regulators of mTORC1, AKT and ERK [57]. NF2-deficient mesothelioma cell lines are more sensitive to mTORC1 inhibition by Rapamycin than NF2-competent mesothelioma cell lines, which suggests an important role for mTORC1 signaling in NF2-deficient tumors [56].

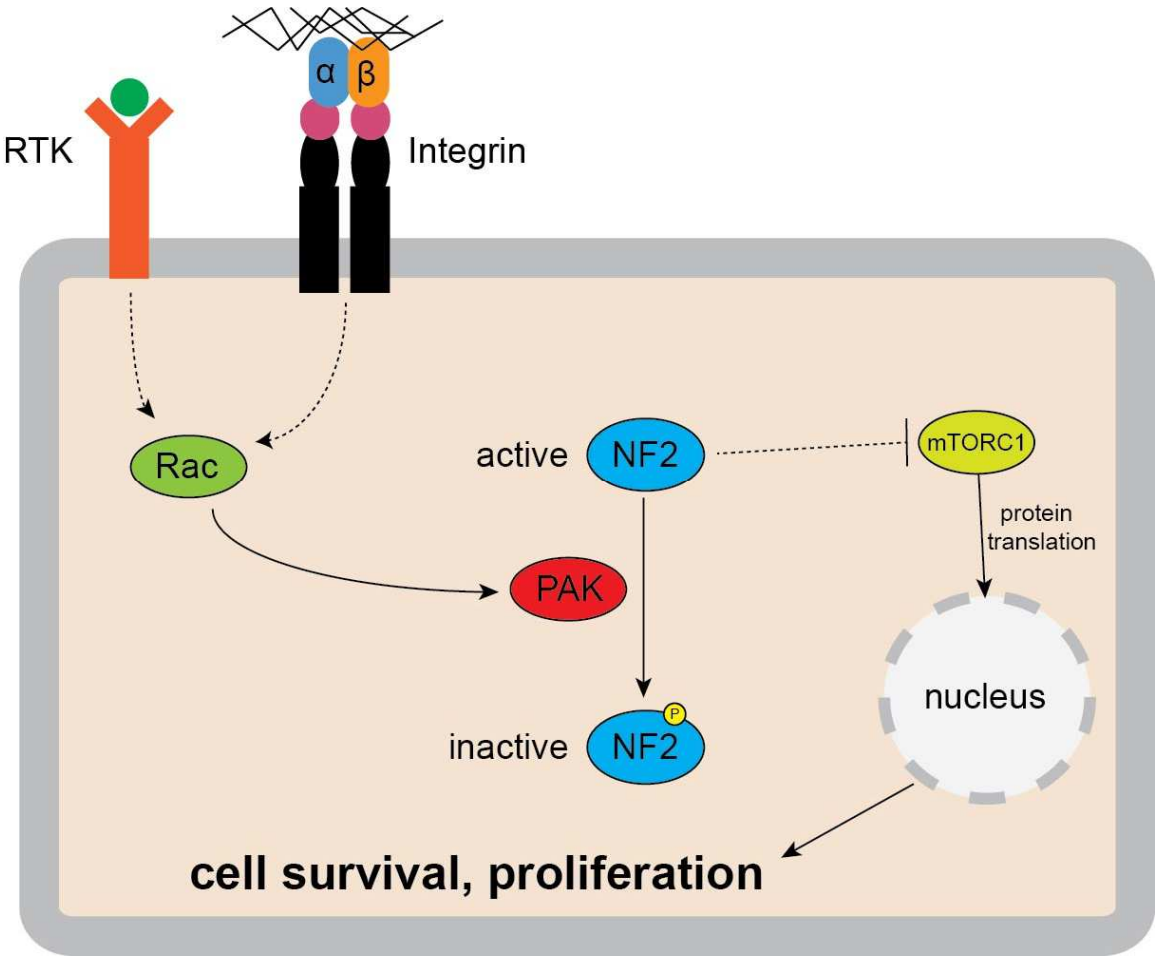

Figure 1. Schematic representation of Rac-PAK-NF2 signaling axis. In response to stimulation through activated RTKs or Integrin signaling, Rac's activated GTP-bound form is recruited to the cell cortex where it promotes PAK1 autophosphorylation and activation. Once activated, PAK1 phosphorylates NF2 at Serine 518, resulting in its inactivation. The inactivation of NF2 results in constitutive activation of mTORC1, which increases ribosomal biogenesis and protein translation. The net effect of mTORC1 activation is an increase in cell survival and proliferation, amongst other changes in cell function and behavior.

The Schwann cell lineage

Schwann cells are a neural crest-derived glial cell population and the primary glial cell found in peripheral nerves. They differ from oligodendrocytes, the myelinating CNS glial cell population, in that Schwann cells form myelin around single axons only. Developmentally, there are three different embryonic Schwann cell stages. The first stage includes neural crest cells, which gives rise to Schwann cell precursors (SCP, present from Embryonic day 12-13 in mice), and finally to Immature Schwann cells (present from Embryonic day 13-15 in mice) [58, 59]. These cell types are transient, and their ultimate fate as a myelinating or non-myelinating Schwann cells depends on the caliber of the axon they associate with. Myelinating Schwann cells are found in association with large caliber axons, whereas non-myelinating Schwann cells are found with small diameter axons [60].

Many different signals have been identified as important for the progression of glial cells from neural crest cells into a mature, myelinating phenotype [60]. SOX10, a transcription factor, is required for the development of all peripheral glial cells [61]. NRG1, a ligand for the ErbB family of receptors, is essential for SCP survival [59, 62]. Autocrine signalling is critical for Immature Schwann cells, especially signalling derived from NRG1-ErbB family of receptors and Laminin-β1 Integrin interactions [63-66]. Promotion from immature Schwann cells into a

myelinating phenotype involves the integration of many different signals, including those from NF-κB, Krox20, and OCT6 [67-70].

Mouse models of NF2

A useful preclinical animal model of human disease requires broad physiological relevance at both genotypic and phenotypic levels [71]. Therefore, genetically engineered murine (GEM) models of human disease should harbor mutations in gene(s) homologous to gene(s) mutated in human cancer. Moreover, this genetic perturbation should occur in cell types and gene doses similar to the hypothetical human tumor cell of origin. These tissue-specific genetic mutations should induce tumors that share histological and biological characteristics with the corresponding human tumors. Additionally, the GEM tumors should be expected to develop in a similar anatomical distribution and with similar functional consequence as human tumors. Since loss of *Nf2* expression results in embryonic lethality in mice and *Nf2*$^{+/-}$ mice do not have a Schwann cell phenotype, conditional knockout technologies must be employed for the generation of NF2 mouse models [72, 73]. Importantly, the first generation murine NF2 model demonstrated that *Nf2* disruption in Schwann cell lineages during embryogenesis promotes schwannoma formation [74, 75]. In existing models, however, schwannomas are incompletely penetrant (only occurring in about one-third of mice), and, generally, arise only late in life. Furthermore, vestibular schwannomas have not been observed in existing murine models of

NF2. These temporal, anatomical, and functional divergences from the human phenotype are critical barriers to *in vivo* genetic and pharmacologic studies that could facilitate better understanding of the molecular pathogenesis of NF2-associated schwannomas. Additionally, lack of an optimal mouse model NF2-associated schwannomas prevents the development and preclinical testing of novel therapeutics for these tumors.

The prior published murine *Nf2* conditional knockout model depends on Cre-mediated *Nf2* allele excision driven by the *P0* promoter element, which is expressed in neural crest cells at embryonic day 9.5 (E9.5) and in SCPs at E12.5 [75]. We hypothesized that an alternate promoter element with distinct developmental timing and anatomical distribution may provide an additional opportunity to recapitulate the phenotypic consequences of human *NF2* mutations and disease manifestations in mice. Therefore, we investigated *Cre* expression driven by the 3.9kb upstream promoter region of the *Periostin* gene (*Postn-Cre*), which prior studies have shown to drive robust reporter gene expression in Schwann cell progenitors beginning at E10 [76]. We intercrossed mice carrying *loxp* sequences flanking exon 2 of the *Nf2* gene ($Nf2^{flox/flox}$) [75] with *Postn-Cre* mice, generating *Postn-Cre*; $Nf2^{flox/flox}$ mice and their *Cre*-negative control littermates. Here, we present this intercross, which results in the consistent development of schwannomas that closely recapitulate features of the human disease, including hearing loss and vestibular impairment associated with vestibular schwannoma development.

MATERIALS AND METHODS

Study approval

All studies were carried out in accordance with, and approval of, the Institutional Animal Care and Use Committee (IACUC) of Indiana University Medical School, the U.S. Department of Agriculture's (USDA) Animal Welfare Act (9 CFR Parts 1, 2, and 3) and the Guide for the Care and Use of Laboratory Animals.

Statistical methods

Statistical analyses were performed with GraphPad Prism 5.0. The Kaplan-Meier method was used to analyze the survival outcomes of mice, and the Log Rank (Mantel-Cox) test was used to compare survival curves. As noted in the text, Analysis of Variance (ANOVA) with Bonferonni post-hoc analysis or Student's T-test was used to test for differences in tumor volume and hearing threshold. Specific tests and significance levels can be found in the figures and figure legends. Fischer's Exact test for Independence was performed on the vestibular phenotypic data using the R Statistical Programming Environment. *P* values less than .05 were considered significant.

Hearing screening

Auditory brainstem responses (ABRs) were recorded from left and right ears of anesthetized mice (100 mg/kg ketamine and 10 mg/kg xylazine by intraperitoneal injection) using subdermal needle electrodes. Stimuli were produced and responses were recorded with a Tucker-Davis Technologies (TDT) BioSigRZ system, using a RZ6 digital/analog converter (TDT). Responses to clicks (512 repetitions, 30-90 dB SPL in 10 dB steps, presented at 21/s with a closed-field system) were amplified, filtered (3 Hz - 3 kHz), averaged, and stored for offline analysis in Matlab (Mathworks, Natick, MA). ABR waveforms were additionally high-pass filtered (cutoff 200 Hz) to remove slow oscillations and emphasize characteristic ABR peaks. ABR threshold was defined as the lowest measured SPL at which a reproducible peak or trough was identified. Amplitude of the summating potential (SP) was calculated as baseline-to-peak, and amplitude of wave 1 (W1) was calculated as peak-to-trough.

Mice and genotyping

Postn-Cre and *Nf2*$^{flox/flox}$ transgenic lines were maintained on Teklad Lab Animal Diet (TD 2014, Harlan Laboratories USA) using a 12:12 (light/dark) photoperiod at 22-24 degrees Celsius. *Nf2*^{flox2} *and Nf2*$^{\Delta 2}$ bands were detected by PCR Analysis as described in Giovannini et al., *Genes and Dev*., 2000. The *Postn-Cre* transgene was detected by PCR analysis with the following primers: P1 (CAT-TTG-GGC-CAG-CTA-AAC-AT) and P2 (CCC-GGC-AAA-ACA-GGT-AGT-TA).

Band sizes are reported in **Figure 10**. *Postn-Cre; Nf2*$^{flox/flox}$ mice and *Cre*-negative controls possessed the same mixed genetic background, with SNP analysis indicating close relation to the FVB/NTac strain (87.37% identity).

Histology and immunohistochemistry

Tumors were excised from recently sacrificed animals, fixed with 10% formalin, embedded in paraffin, sectioned, and stained with H&E. Embryos were fixed in 4% Paraformaldehyde (PFA), stained with X-gal, embedded in paraffin, and then sectioned. Vector labs ABC (PK-6100), DAB (SK-4100), and Avidin/Biotin blocking (SP-2001) kits were used for immunoperoxidase staining. BLBP (Abcam, ab32423) primary antibody was detected with biotinylated Goat anti-Rabbit secondary antibody from Sigma (cat. B8896). For sectioning and staining of inner ear structures, mice were fixed with 4% PFA injected via intracardiac perfusion into the right atrium. Samples were then sent to Dr. Brian Faddis at the Otolaryngology Histology Core at Washington University in St. Louis for processing and staining.

Tumor volume quantitation

After fixation and decalcification in 5% formic acid, the DRG and spinal nerves were then dissected out under a microscope. Tumor volume was calculated

using the length and width values for a particular tumor in the formula *volume* = *length x width*^{2} *x .52*, the approximate volume of a spheroid.

Vestibular studies

All of the functional vestibular studies (trunk curl, contact righting, and swim) were performed on three consecutive days, with each test being performed once per day. The tests were scored by two independent observers experimentally blinded to the genotype of each animal. Fischer's Exact test was used to test for differences in the two genotypes.

For the trunk curl test, mice were individually suspended by their tails and presented with a horizontal platform roughly 2 cm outside their reach. Control mice will reach toward this platform, but mice with vestibular impairment will tend to curl in toward their abdomen with their head and upper-body. This inward-curling was scored as a failure for the test. Mice were scored on a two-point system, either succeeding or failing the test.

In the contact righting test, mice were placed in a 45 cm Plexiglas tube with a diameter of 6 cm, and the tube was re-oriented until the mouse was at the approximate center of the tube, facing toward the closed end. The tube was then rotated and the ability of the mice to correct their posture was assessed. Mice

that had significant difficulty adjusting to the rotation fell on their sides or on their backs. This was scored as a failure of the test. Mice were scored on a two-point system, either succeeding or failing the test.

For the swim test, a large sink (50 cm x 40 cm x 20 cm) was filled with tepid water to a depth of 18 cm and given several hours to equilibrate to room temperature. Mice were placed in the sink individually and their ability to swim was assessed for one minute. Normal swimming behavior was noted when the animal kept its body aligned horizontally in the water with its nose clearly above the surface. Abnormal swimming was noted when the animal made vertical deviations, had substantial head tilt, assumed an immobile floating position, or had significant lower limb thrashing. Any abnormal swimming was scored as a failure. Mice were scored on a two-point system, either succeeding or failing the test.

RESULTS

Postn-Cre+ mice develop schwannomas

Initial studies demonstrated that all *Postn-Cre*; *Nf2*$^{flox/flox}$ mice sacrificed at 15 months of age possessed significant enlargements of the dorsal root ganglion (DRG) and proximal spinal nerve roots (**Figure 2A** and **2B**). Subsequent histologic analyses indicated these enlargements are present at every vertebral level in *Postn-Cre*; *Nf2*$^{flox/flox}$ mice. To better understand the time course of these enlargements, we sacrificed and dissected mice at multiple time points. By five months of age, all *Postn-Cre*; *Nf2*$^{flox/flox}$ mice acquired enlargements of their DRG and proximal spinal nerve roots, with microscopic evidence of Schwann cell hyperplasia and/or schwannoma, featuring dense, intersecting fascicles of Schwann cells (**Figure 3**). By eight months, all *Postn-Cre*; *Nf2*$^{flox/flox}$ mice demonstrated DRG and proximal spinal nerve tumors with histological characteristics of frank schwannoma (**Figure 2C** and **2D**). Further analyses demonstrated diffuse S100-positivity of tumors from *Postn-Cre; Nf2*$^{flox/flox}$ mice, consistent with previously established criteria for genetically engineered mouse (GEM) Grade I schwannoma (**Figure 2E**) [34]. At fifteen months, dissected spinal cords from *Postn-Cre; Nf2*$^{flox/flox}$ mice demonstrated more than a five-fold increase in DRG volume as compared to *Cre*-negative control littermates (**Figure 2F**). Thus, *Postn-Cre; Nf2*$^{flox/flox}$ mice develop slow growing, low-grade

schwannomas highly reminiscent of schwannomas observed in individuals with NF2.

Detailed temporal analysis of cohorts revealed that *Postn-Cre*; *Nf2*$^{flox/flox}$ mice had a reduced lifespan as compared to *Cre*-negative *Nf2*$^{flox/flox}$ control mice (**Figure 2G**). In the majority of mice, only multiple large schwannomas were observed. However, 5/16 *Postn-Cre*; *Nf2*$^{flox/flox}$ mice analyzed required sacrifice due to the development of tumors that, upon histological examination, were found to be GEM Grade III lesions consistent with malignant peripheral nerve sheath tumors (MPNST) (**Figure 4**). MPNSTs, malignant sarcomas, and malignant carcinomas have also been observed with disruption of *Nf2* in other genetically engineered models [75].

Detailed examination of schwannomas excised from *Postn-Cre*; *Nf2*$^{flox/flox}$ mice indicated these tumors possessed an architecture highly reminiscent of schwannomas found in human NF2 disease. Some nerves demonstrated discrete nodules of schwannoma, similar to the Schwann cell tumorlets commonly observed in the cauda equina of NF2 patients (**Figure 5A**) [77]. In multiple cases, proliferating schwann cells caused diffuse expansion of the nerve and extended into its ramifications, simulating plexiform schwannomas frequently encountered in human NF2 patients (**Figure 5B**). Other focal lesions demonstrated pseudo-onion bulb formations comprised of proliferating Schwann

cells tightly whorled around a central axon, a histological feature also found in some human NF2-associated schwannomas (**Figure 5C**). Finally, in some nerves, proliferating Schwann cells did not form a discrete mass, but rather exhibited diffuse regions of hypercellularity, possibly representing an early neoplastic change prior to schwannoma development (**Figure 5D**).

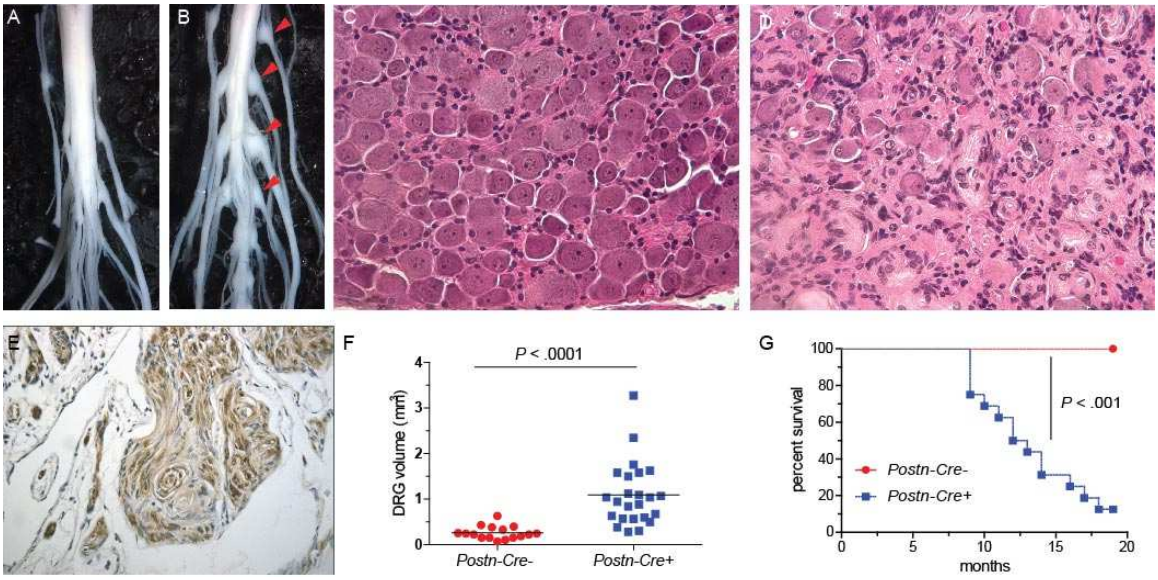

Figure 2. *Postn-Cre; Nf2$^{flox/flox}$* mice develop schwannomas of the DRG and spinal nerves. (**A** and **B**) Dissected spinal cord of 15 month old *Cre*-negative control (**A**) and *Postn-Cre; Nf2$^{flox/flox}$* (**B**) mice, with *Postn-Cre; Nf2$^{flox/flox}$* mice displaying diffusely enlarged DRG and spinal nerves (red arrowheads). (**C** and **D**) Hematoxylin and Eosin (H&E) stain of the DRG from seven month *Cre*-negative control and *Postn-Cre; Nf2$^{flox/flox}$* mice, respectively. The whorls of Schwann cell proliferation observed in **D** are characteristic of schwannoma histology. Original magnification x200. (**E**) Immunohistochemical S100 stain indicating tumors are comprised of mature Schwann cells. Original magnification x400. (F) DRG volume quantitation of 15 month old *Cre*-negative control mice (4) and *Postn-Cre; Nf2$^{flox/flox}$* mice (6). $P < .0001$, Unpaired Student's T-test with Welch's correction. (**G**) Kaplan-Meier survival analysis of *Cre*-negative control mice (8) and *Postn-Cre;Nf2$^{flox/flox}$* mice (16). $P < .001$, Log-Rank (Mantel-Cox) Test.

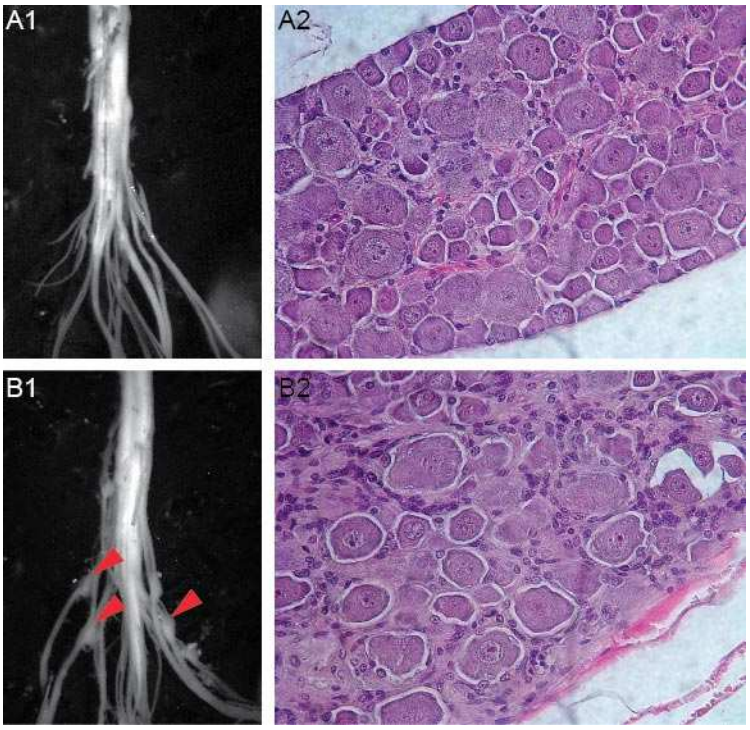

Figure 3. Temporal analysis of spinal nerve tumors in *Postn-Cre; Nf2$^{flox/flox}$* mice. (**A** and **B**) Gross dissected spinal cord and H&E stain from representative 5 month old *Cre*-negative control (**A1** and **A2**) and *Postn-Cre;Nf2$^{flox/flox}$* mouse (**B1** and **B2**), respectively. Red arrowheads in **B1** highlight the spinal enlargements observed in the *Postn-Cre; Nf2$^{flox/flox}$* mouse at 5 months of age. **A2** and **B2**, original magnification x400.

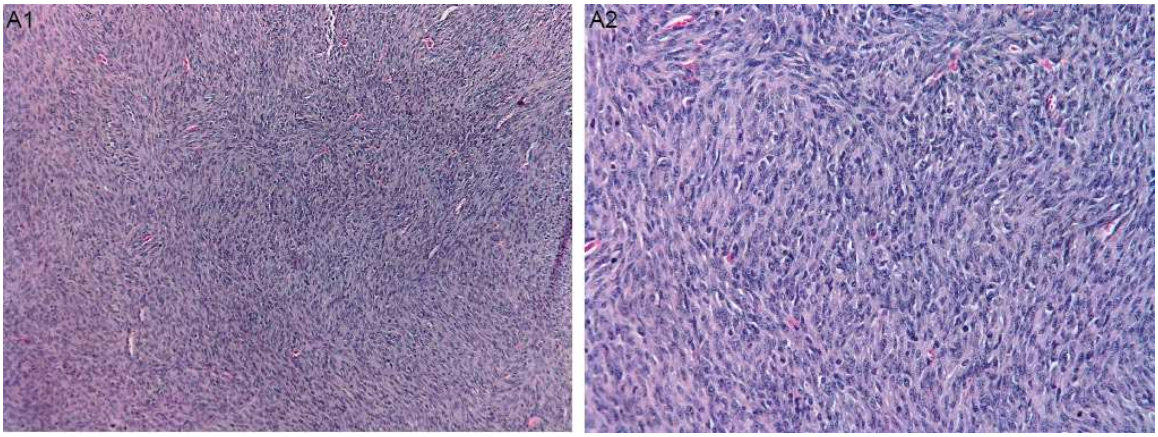

Figure 4. A small percentage of schwannomas in *Postn-Cre; Nf2$^{flox/flox}$* mice progress into MPNSTs. (**A**) H&E stain of a GEM Grade III tumor (MPNST) observed in a *Postn-Cre; Nf2$^{flox/flox}$* mouse, showing that some schwannomas progress into malignant Schwann cell tumors with large, pleomorphic cells arranged in intersecting fascicles. These tumors were diffusely infiltrative, possessed regions of necrosis, and also included mitotic figures. This mouse was sacrificed at the age of seven months. **A1**, original magnification x100. **A2**, original magnification x200.

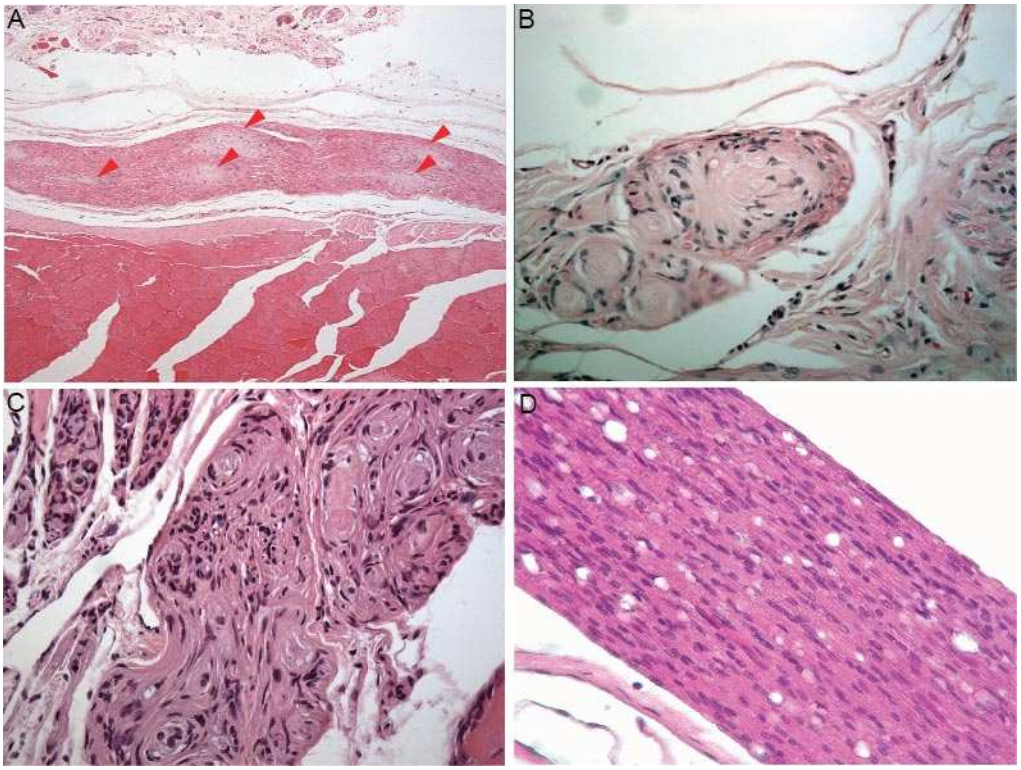

Figure 5. Schwannomas observed in *Postn-Cre; Nf2$^{flox/flox}$* mice histologically resemble those observed in human patients. (**A**) H&E stain showing a multifocal pattern of schwannoma growth along a nerve (red arrowheads). Original magnification x100. (**B**) Example of a plexiform schwannoma involving a nerve twig with peripheral axons. Original magnification x400. (**C**) Pseudo-onion bulb formation of proliferating Schwann cells forming whorls around centrally-located axons within a nerve. Original magnification x200. (**D**) Diffuse spinal nerve hyperplasia observed in the nerve of a *Postn-Cre; Nf2$^{flox/flox}$* mice. Original magnification x400.

Vestibular schwannomas in *Postn-Cre+* mice

NF2 patients develop schwannomas in multiple anatomic regions, including peripheral, cranial, and spinal nerves [78]. Interestingly, by ten months of age, thorough dissection and histological analysis of each *Postn-Cre; Nf2*$^{flox/flox}$ mouse revealed schwannomas in nearly all histological specimens of peripheral, cranial, and spinal nerves. For example, all *Postn-Cre; Nf2*$^{flox/flox}$ mice examined for cranial nerve pathology featured schwannomas of the Trigeminal (CN V) and Facial (CN VII) nerves (**Figure 6**). Given the high correlation between human NF2 disease and the presence of bilateral vestibular schwannomas, we focused on CN VIII and its associated functions. Histological analysis of *Postn-Cre; Nf2*$^{flox/flox}$ mice revealed aberrant Schwann cell growth in CN VIII proximal to its entry into the inner ear, including tumors observed in Scarpa's ganglion, the anatomic site of the afferent nerve cell bodies prior to their synapse with vestibular hair cells (**Figure 7A** and **7B**). *Postn-Cre; Nf2*$^{flox/flox}$ mice also demonstrated Schwann cell hyperplasia in the spiral ganglion (**Figure 7C**), a structure containing nerve cell bodies that transmit sound-derived nerve impulses from the cochlea to the brain. We observed none of these aberrations in *Cre*-negative littermates. Importantly, the cochlea did not display any other obvious structural differences between the two genotypes (**Figure 8**).

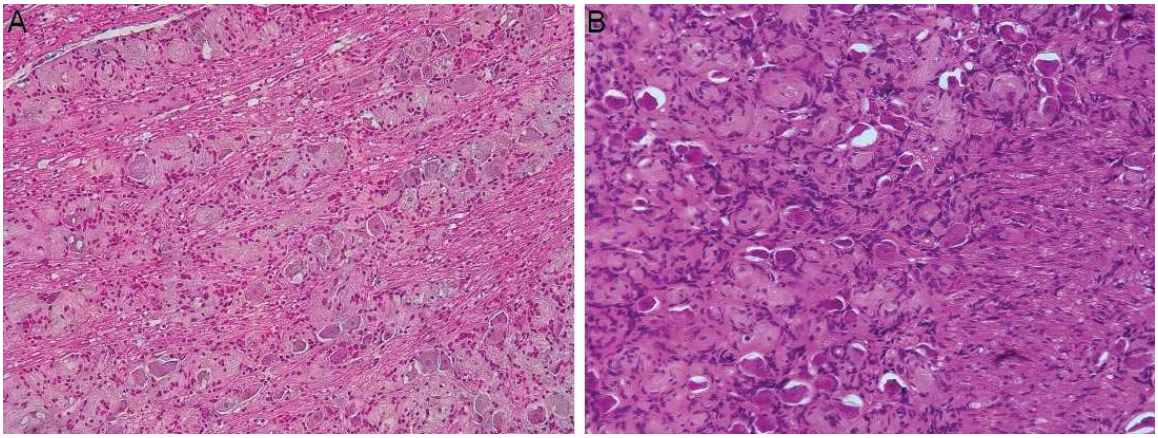

Figure 6. *Postn-Cre; Nf2*$^{flox/flox}$ mice develop schwannomas on CN V and CN VII. (**A** and **B**) Representative H&E stains of CN V (**A**) and CN VII (**B**) from *Postn-Cre; Nf2*$^{flox/flox}$ mice displaying schwannoma development in the cranial nerves. Original magnification x200.

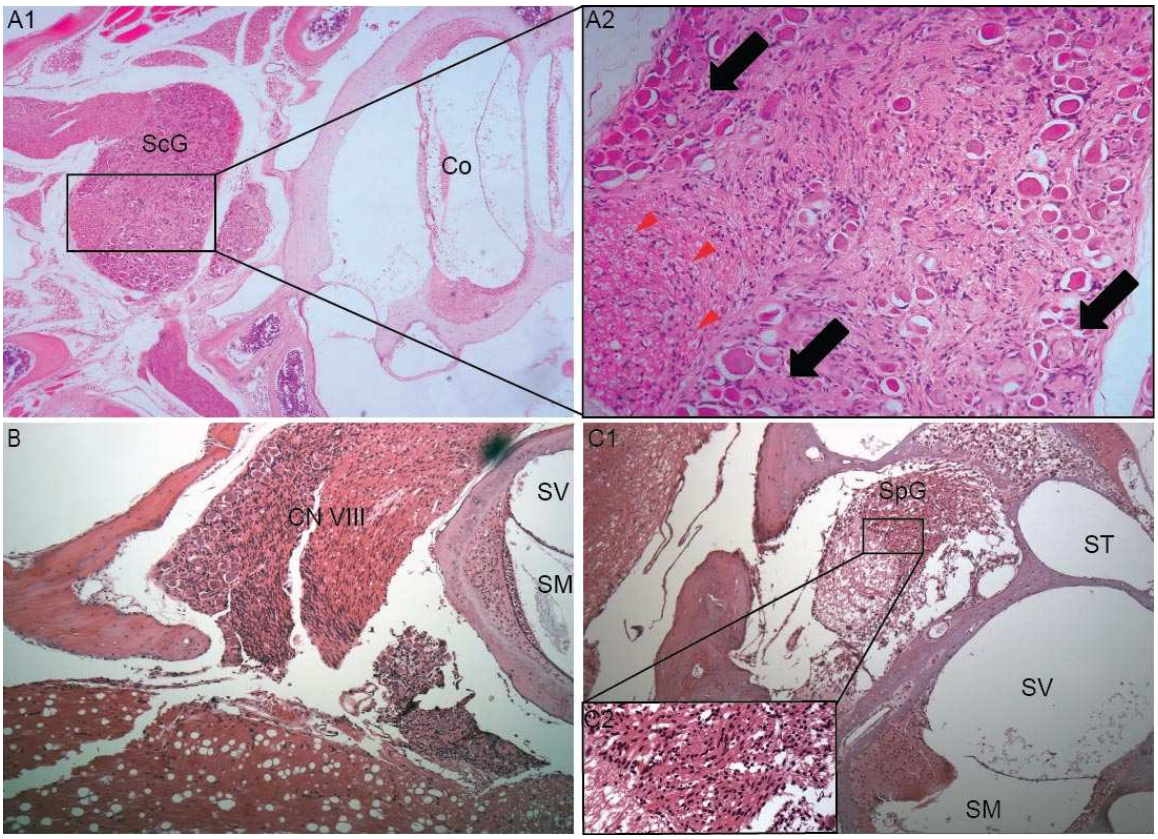

Figure 7. *Postn-Cre; Nf2$^{flox/flox}$* mice develop schwannomas on CN VIII. (**A1**) H&E stain of a vestibular schwannoma located in Scarpa's ganglion (ScG). Original magnification x100. In the 200x magnified inset image (**A2**), notice the Schwann cell proliferation displacing nerve cell bodies (black arrows) and pushing axons to the periphery of the nerve (red arrowheads). (**B**) Diffuse hypercellularity observed in CN VIII. Original magnification x100. (**C1**) Schwann cell proliferation in the spiral ganglion (SpG), expanding and disrupting the architecture of the ganglion. Original magnification x100. In the magnified (400x) inset **C2**, notice the dysplastic, irregularly spaced Schwann cells. Cochlea (Co), Scala Media (SM), Scala Vestibuli (SV), Scala Tympani (ST).

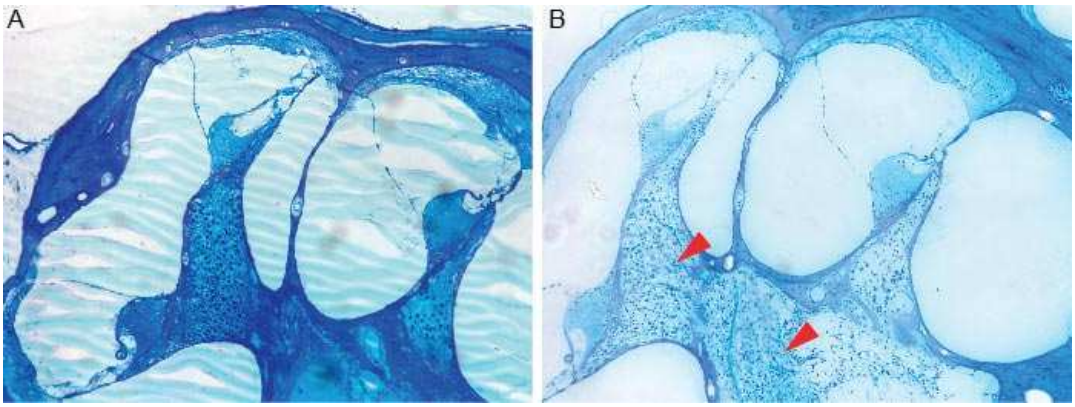

Figure 8. The cochleas in *Postn-Cre; Nf2*$^{flox/flox}$ mice are structurally similar to *Cre*-negative controls. (**A** and **B**) Toludene Blue stain of the spiral ganglion and cochlea showing that cochleas of *Postn-Cre;Nf2*$^{flox/flox}$ mice (**B**) are structurally comparable to their *Cre*-negative (**A**) age-matched counterparts (16 months), save for schwannoma/Schwann cell hyperplasia present in the spiral ganglion (red arrowheads). Original magnification x100.

Postn-Cre+ mice experience hearing loss and vestibular impariment

To correlate these CN VIII lesions with potential functional hearing deficits, we used click-evoked auditory brainstem response (ABR) testing, a standard method to assess hearing loss in humans and small animals [79]. ABRs are electrical potentials recorded from electrodes placed on the scalp and near the ear. In response to sound stimuli, a characteristic ABR waveform with a series of peaks and troughs is observed, where peaks correspond to different components of the ascending auditory pathway [80]. We tested cohorts of mice at three, six, eight, and ten months of age, finding a progressively increasing ABR threshold in *Postn-Cre; Nf2*$^{flox/flox}$ mice, while control mice maintained a relatively consistent hearing threshold throughout the study (**Figure 9A** and **9B**). Given that this click-ABR screening was limited to a stimulus range from 30 – 90 decibel sound pressure level (dB SPL), and that the majority of *Cre*-negative mice exhibited robust waveforms at 30 dB SPL, it is likely that the mean differences between the two groups are even larger than those depicted in **Figure 9B**. Thus, the present data indicate a hearing loss that is temporally correlated with tumorigenesis in this mouse model. Functionally, a sensorineural hearing loss of this type would negatively impact a patient's quality of life by limiting communication and social interaction in everyday listening environments with background noise.

To expand our analysis of the hearing impairment in *Postn-Cre; Nf2*$^{flox/flox}$ mice, we studied the individual peaks present in click-ABR waveforms (**Figure 9C** and

9E). The first ABR wave (W1) represents potentials generated from the cochlear nerve [81]. The summating potential (SP), which appears as a small shoulder preceding W1, is largely comprised of potentials originating from the inner hair cells of the cochlea, with some contributions from outer hair cells [82, 83]. No significant differences were observed between *Postn-Cre; Nf2*$^{flox/flox}$ mice and *Cre*-negative control SPs at both the six and eight month time points, but a significant reduction in SP amplitude was observed in the *Postn-Cre; Nf2*$^{flox/flox}$ mice at ten months (**Figure 9D**). W1 amplitude was significantly attenuated in the *Postn-Cre; Nf2*$^{flox/flox}$ mice compared with *Cre*-negative controls at all of the tested time points (**Figure 9F**). The reduction in W1 amplitude at the six and eight month time points, when contrasted with the non-significant differences in SP amplitude, specifically points to a functional disruption in the cochlear synapse and/or cochlear nerve in *Postn-Cre; Nf2*$^{flox/flox}$ mice. These data also indicate a more extensive disruption of auditory function at the ten month time point, with decreased SPs suggesting diminished hair-cell function in addition to deficits in the cochlear synapse and/or cochlear nerve. Altogether, these studies reveal that *Postn-Cre; Nf2*$^{flox/flox}$ mice acquire sensorineural hearing loss that, in consideration of the schwannoma histopathology described in Figure 3, likely originates in the cochlear nerve.

Vestibular schwannomas can also severely impair a patient's sense of normal balance and orientation, leading to vertigo, nausea, accidents related to falls, and, thus, substantially decreased quality of life. In our studies with *Postn-Cre;*

Nf2$^{flox/flox}$ mice, we observed that some mice acquired a phenotype suggestive of vestibular dysfunction, as they exhibited head tilting, head tossing, head bobbing, and locomotive circling behavior. This behavior is collectively referred to as shaker/waltzer behavior, and has been observed in mice possessing defects in their vestibular organs [84, 85]. To test for vestibular dysfunction, we conducted three different behavioral tests to examine the integrity of the vestibular system [86]. Each mouse underwent a trunk curl, contact righting, and swim test on three occasions over the course of three consecutive days, with the results scored by two independent observers experimentally blinded to the genotype of the mice. *Postn-Cre; Nf2*$^{flox/flox}$ mice demonstrated profound impairment in their ability to successfully complete each of the three tests when compared to their *Cre*-negative littermates (**Table 1**).

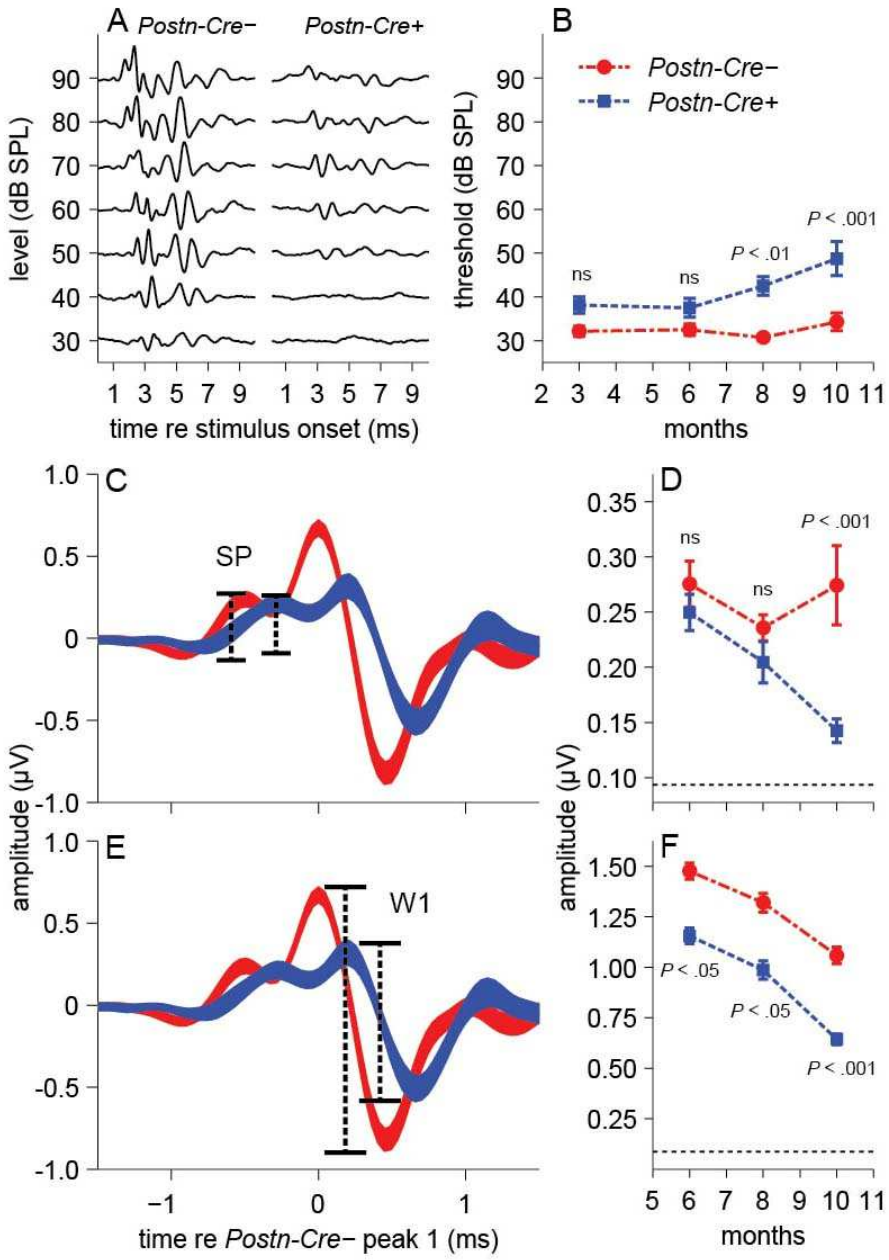

Figure 9. *Postn-Cre; Nf2$^{flox/flox}$* mice show deficits in both threshold and supra-threshold auditory brainstem responses (ABRs). (**A**) Representative ABR waveforms from individual *Cre*-negative (left) and *Postn-Cre; Nf2$^{flox/flox}$* mice (right) at 10 months of age. (**B**) Time-course click-ABR study quantitating differences between *Cre*-negative and *Postn-Cre; Nf2$^{flox/flox}$* mice. Significant threshold elevations were seen in *Postn-Cre; Nf2$^{flox/flox}$* mice at 8 ($P < .01$) and 10

($P < .001$) months of age (n = 15, 12, 15, and 19 mice for 3, 6, 8, and 10 months, respectively). Thresholds were averaged across animals (mean ± SEM). (**C** and **D**) The summating potential (SP) (**C**), dominated by inner-hair-cell receptor potentials and evident in the ABR waveform immediately preceding peak 1, is comparable in amplitude across groups at 6 and 8 months of age, but is reduced in *Postn-Cre; Nf2*$^{flox/flox}$ mice at 10 months ($P < .001$) (**D**). (**E** and **F**) ABR wave 1 (W1) (**E**), representing the summed response of the cochlear nerve, is reduced in *Postn-Cre; Nf2*$^{flox/flox}$ mice compared to *Cre*-negative controls at all ages ($P < .05$, $P < .05$, $P < .001$) (**F**), indicating deficits in pre- and/or post-synaptic cochlear nerve function. All statistical tests: two-way ANOVA with Bonferonni post-hoc analysis. Thickness of waveforms (**C** and **E**) represent mean ± SEM. Amplitudes (**D** and **F**) represent high-level responses (across 60-90 dB SPL) averaged across animals (mean ± SEM). Horizontal dotted lines (**D** and **F**) at the base of the y-axis indicate the noise floor measurement.

Test	Genotype	Number of mice	Successes	Failures	*P*
Trunk Curl					< .0001
	Postn-Cre-	7	19	2	
	Postn-Cre+	7	4	17	
Contact Righting					< .0001
	Postn-Cre-	6	18	0	
	Postn-Cre+	7	4	17	
Swimming					< .0001
	Postn-Cre-	7	21	0	
	Postn-Cre+	7	5	16	

Table 1: *Postn-Cre; Nf2$^{flox/flox}$* mice develop vestibular impairment.

Results of examination of the vestibular system in *Postn-Cre; Nf2$^{flox/flox}$* mice and *Cre*-negative controls. Tests were conducted on three consecutive days and scored by two independent scorers experimentally blinded to the animal's genotype. Mice were scored on a two-point scale, either succeeding or failing a particular test. A detailed description of the three tests can be found in the methods section. All mice were 13 months old at the time of testing. Fischer's Exact Test was used to test for statistically significant differences.

Embryonic analysis of *PostnCre*+ progenitor populations

To gain a more detailed understanding of the temporal, anatomical, and cellular origins of *Nf2*-associated schwannomas, we further characterized gene expression driven by the *3.9kbPeriostin* promoter element. First, recombination of *Nf2* was confirmed in the cranial and spinal nerves (**Figure 10**). Next, we performed embryologic studies with an intercross between *Postn-Cre* and *Rosa26 lox-stop-lox LacZ* reporter mice. By E12.5, robust β-galactosidase expression was observed in the DRG, facial ganglia, and the developing cranial, spinal, and peripheral nerves (**Figure 11A, 11B,** and **11C**). Approximately half of Schwann cells derived from the sciatic nerve of adult mice demonstrated positive X-gal staining with universal S100-positivity (**Figure 11D** and **11E**). In the DRG, nerve roots, and peripheral nerves of E14 and E14.5 tissue, β-galactosidase expression coincided with Brain Lipid-Binding Protein (*Blbp*) expression, an established immunological marker of Schwann cell precursors and immature Schwann cells (**Figure 11F** and **11G**) [60]. Schwann cell precursors and immature Schwann cells are multipotential embryonic Schwann cell lineages that descend from neural crest cells and represent the progenitor cell populations that give rise to mature Schwann cells. Importantly, the time points of the X-gal stained embryos in Supplemental Figure 6 represent the transition from Schwann cell precursors (E12-E13) to immature Schwann cells (E13-E15) [60]. These data indicate that *Postn-Cre* is expressed in early multipotent glial cell populations, likely representing the tumor cell of origin for this model.

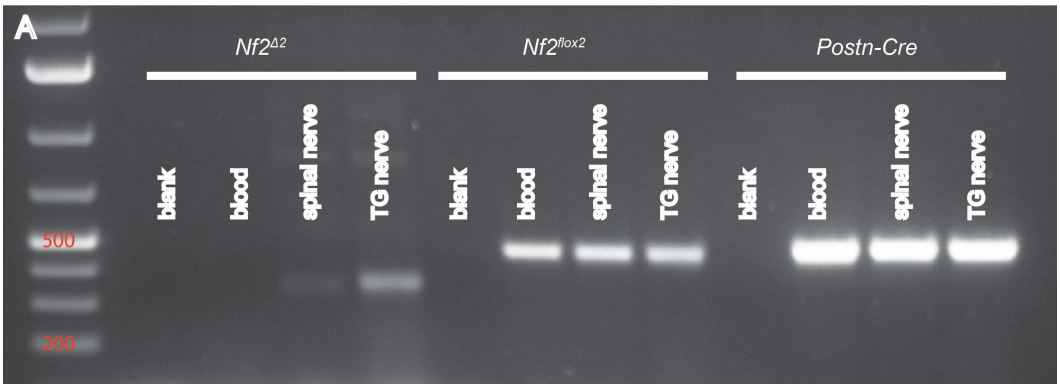

Figure 10: *Postn-Cre* induces recombination in neural crest-derived tissues. (**A**) PCR analysis demonstrating that *Postn-Cre* induces recombination in adult nerve tissues, but not the blood. Blood was taken from the tail vein of a *Postn-Cre; Nf2*$^{flox/flox}$ mouse prior to sacrifice. After sacrifice, spinal and Trigeminal nerve tissue were dissected from the same mouse. DNA was then isolated from these tissues and used for PCR analysis. The presence of the *Nf2*^{delta2} allele indicates recombination of the *Nf2*^{flox2} allele. This is representative data of PCR analysis in three different *Postn-Cre; Nf2*$^{flox/flox}$ mice. The *Nf2*^{flox2} allele is 440 base pairs (bp), *Nf2*^{delta2} allele is 338 bp, and *Postn-Cre* is 450 bp in length. Trigeminal Nerve (TG Nerve).

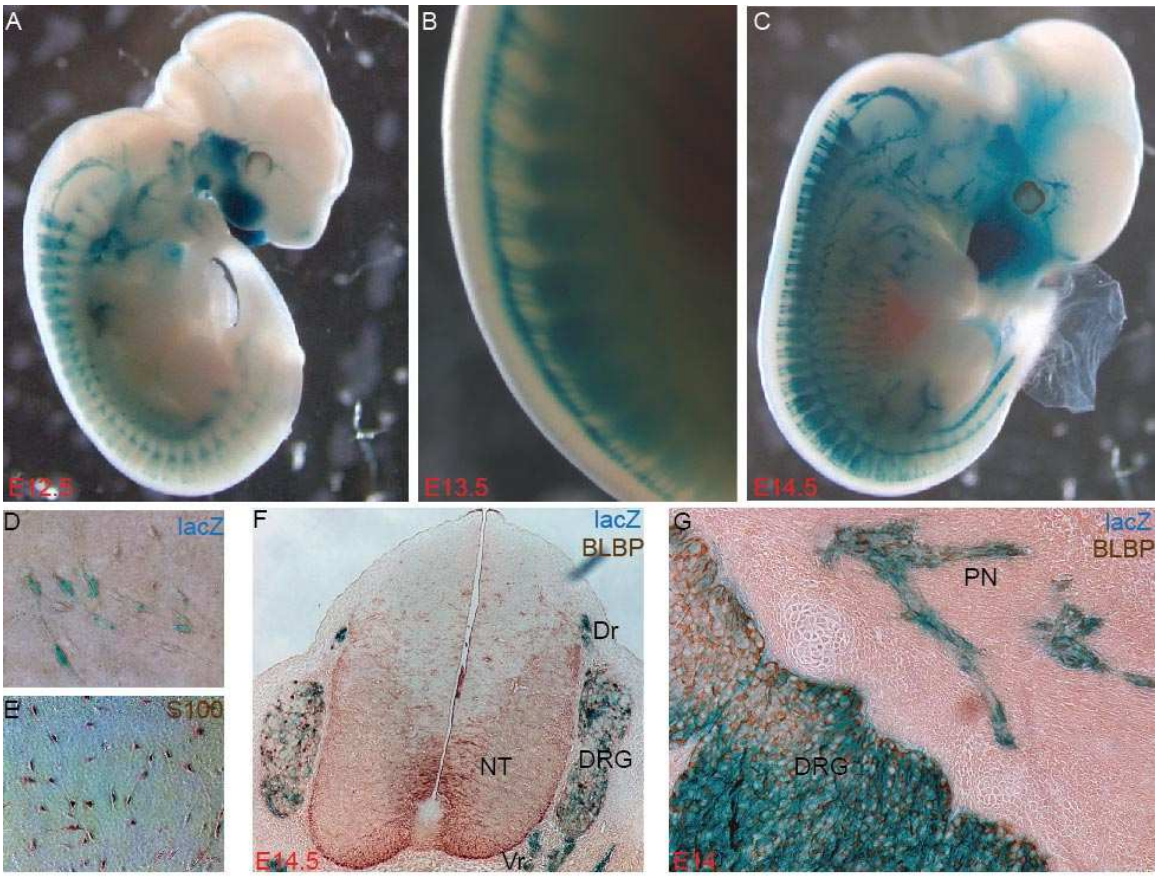

Figure 11. *Postn-Cre* is expressed in multipotent embryonic Schwann cell lineages. (**A** and **C**) Beta-Galactosidase activity in *Postn-Cre; Rosa26 lox-stop-lox Lacz* embryos at indicated embryonic time points (**A**, E12.5; **C**, E14.5). (**B**) Beta-Galactosidase activity in the DRG of an E13.5 embryo. (**D**) Beta-Galactosidase activity in cultured Schwann cells from the adult sciatic nerve of a *Postn-Cre; Rosa26 lox-stop-lox LacZ* mouse. Original magnification x400. **(E)** S100 stain of cultured Schwann cells from the adult sciatic nerve of a *Postn-Cre; Nf2*$^{flox/flox}$ mouse. All cells were found to be S100 positive. Original magnification x200. (**F** and **G**) Immunostaining of BLBP in X-gal stained E14.5 (**F**) and E14 (**G**) embryo sections. BLBP is a marker of Schwann cell precursors and immature

Schwann cells. **F**, Original magnification x100. **G**, Original magnification x200. Neural Tube (NT), Dorsal Root (Dr), Ventral Root (Vr), Peripheral Nerve (PN).

DISCUSSION

In this study, we describe a novel NF2 mouse model recapitulating schwannoma phenotypes found in human patients. NF2-associated schwannomas are most frequently located on CN VIII and/or the spinal roots, and these tumors are seen in nearly all NF2 patients [1]. The NF2 mouse model presented in this study develops tumors on both structures with complete penetrance, and it also demonstrates functional impairments in hearing and balance that are commonly associated with human vestibular schwannomas.

The characteristics of this model permit three broad areas of translational study. First, the genesis of genetically engineered models and the use of genetic intercrosses to provide *in vivo* proofs of concept have recently resulted in advances in the understanding of tumor suppressor genes and their roles in regulating specific signalling pathways, including other neurocutaneous disorders such as NF1 and tuberous sclerosis [87-92]. While the *NF2* gene product was identified as mutated in familial NF2 disease over 25 years ago, it remains unclear which pathways are critical to tumor development downstream of *NF2* [93]. This genetic model may provide the means for elucidating which signalling pathways downstream of NF2 are essential to schwannoma development.

Second, the utility of accurate preclinical models that allow physiologic testing of clinical phenotypes is particularly important for orphan genetic diseases such as NF2, where patient numbers limit the ability to conduct multiple meaningful trials. In the entire United States, it is estimated that there are 12,000 individuals that have NF2. Though nearly all patients acquire vestibular schwannomas, at any given time only a small number of patients are available for clinical trials. Thus, preclinical models that can effectively screen for pharmaceutical agents that have meaningful therapeutic benefit for schwannomas are essential for the advancement of NF2 therapies. Functional ABR assessment of hearing during studies utilizing this model provides a unique, non-invasive, and physiologically relevant measure for determining therapeutic efficacy of compounds.

Finally, a preclinical model can assist in understanding the basic biology of the hearing loss associated with vestibular schwannomas, which is incompletely understood. Tumor size resulting in local compression of CN VIII does not appear to account completely for the onset and progression of hearing loss in NF2 patients [33]. Interestingly, the recent short-term improvements in hearing with Bevacizumab treatment of vestibular schwannomas in NF2 patients are not consistently associated with a reduction in tumor size [94]. It has also been suggested that biochemical disturbance of the inner-ear fluids could be the underlying cause of hearing loss related to these tumors [95]. Otoacoustic-emission studies in patients with vestibular schwannomas support the hypothesis that some degree of hearing loss is cochlear in origin [96, 97]. Altogether, the

degree to which hearing loss in these patients is retrocochlear (thus likely originating in the cochlear nerve) or cochlear in origin remains an open question.

Our studies suggest functional impairment of cochlear-nerve activity in *Postn-Cre; Nf2*$^{flox/flox}$ mice at both early (six and eight months) and later (ten months) stages of disease progression. In contrast, *Postn-Cre; Nf2*$^{flox/flox}$ mice have significantly reduced summating potentials only at ten months, suggesting that the structures required for mechanoelectric transduction of sound prior to the inner hair cell-cochlear nerve synapse are not significantly impaired earlier in the disease process. These findings, in association with the neoplastic Schwann-cell accumulation and extensive morphologic changes seen in the spiral ganglion, strongly suggest that a significant component of the hearing loss in this model originates in the cochlear nerve. Evidence for an additional, later-onset dysfunction of cochlear origin comes from the combination of increased thresholds at ten months with further decreased wave 1 amplitude and decreased summating potential. In summary, these data suggest an early retrocochlear form of hearing loss beginning in the cochlear nerve, and, at later time points, a more extensive form of hearing loss incorporating both the cochlear nerve and cochlea. Further studies utilizing the *Postn-Cre*-based NF2 mouse model may allow additional insights into this clinical question regarding the mechanisms of hearing loss present in vestibular schwannoma patients.

INTRODUCTION TO CHAPTER TWO

NF-κB signaling pathway

The NF-κB (nuclear factor kappa-light-chain enhancer of activated B cells) family of DNA-binding protein complexes was first identified as a B-cell specific transcription factor in 1986 [98]. Subsequent work by the same group discovered that this family of proteins possessed inducible DNA-binding activity and was expressed in a wide-variety of cell types [99, 100]. In the nearly 30 years since, NF-κB has emerged as a major regulator of immunity and inflammation, among a host of other basic functions in cellular physiology [101, 102].

The NF-κB family of transcription factors is comprised of NF-κB1/p105, NF-κB2/p100, RELA, RELB, and c-REL. All of these transcription factors possess an N-terminal Rel homology domain (RHD), which is known to mediate both the homo-/heterodimerization characteristic of NF-κB proteins as well as their DNA-binding sequence specificity. *NFκB1* and *NFκB2* encode the precursor proteins p105 and p100, respectively, which are subsequently processed to their transcription factor counterparts, p50 and p52. RELA, RELB, and c-REL contain a C-terminal transcriptional activation domain (TAD) which distinguishes them from p50 and p52. Thus, p50 and p52 rely on dimerization with other Rel family members to promote the transcription of target genes[103]. RELA and c-REL preferentially interact with p50 [104], while RELB is predominantly found with p100 or p52 [105-107].

Dimers of NF-κB transcription factors are largely regulated by nucleo-cytoplasmic shuttling. The principal mediators of this regulation are the IκB proteins, also known as the inhibitors of NF-κB [104]. IκB proteins possess multiple ankyrin repeats that are responsible for the binding of NF-κB transcription factors. Their ability to sequester NF-κB proteins in the cytoplasm depends on their ability to obscure the nuclear localization signal present in the NF-κB proteins. Though there are a number of IκB proteins, this introduction will only focus on IκBα, a classical IκB, and p100, an atypical IκB. RELA:p50 heterodimers are primarily held in the cytoplasm by IκBα [104]. p100 is thought to predominantly bind RELB in the cytoplasm, while not having a substantial effect on other NF-κB proteins [105-107]. Some have reported that p100 may also play a role in regulating RELA localization, however [108]. p105 contains C-terminal ankyrin repeats and does possess IκB activity for p50, RELA, and c-REL, but it is constitutively processed to p50 in unstimulated cells and primary function is believed to reside in the production of p50 [109-111]. In response to a broad set of stimuli that result in upstream NF-κB pathway activation, IκB proteins are degraded by the proteasome [101]. For example, IκBα is rapidly degraded in response to TNF-α and LPS, two well-studied activators of NF-κB. NF-κB pathway activation also promotes the transcription of the gene encoding IκBα, which is one of the many examples of feedback regulation present in this particular pathway [112, 113].

The most well-studied arm of NF-κB signaling, the canonical pathway, primarily results in the nuclear accumulation of p50:RELA and p50:c-REL heterodimers. The degradation of IκBα and nuclear translocation of NF-κB proteins depends on activation of the upstream IKK complex. The IKK complex consists of the catalytically active IKKα and IKKβ subunits and the regulatory subunit NEMO (also referred to as IKKγ). The activation of the IKK complex is intricate and quite different depending on the particular ligand/cognate receptor interaction, and as such is beyond the scope of this introduction. Once activated, the IKK complex phosphorylates IκBα at Serine 32 and 36, promoting its K48-polyubiquitination and degradation by the proteasome [104]. IKKβ is believed to be the major IκB kinase in most cell types [114].

The alternative or non-canonical NF-κB signaling pathway is not as well-studied as the canonical pathway. In response to non-canonical NF-κB stimuli, NF-κB inducing kinase (NIK) is stabilized, resulting the phosphorylation and activation of its preferred substrate, IKKα [106, 115]. Activated IKKα homodimers phosphorylate p100 in its C-terminal ankyrin repeat domain, resulting in its polyubiquitination and partial processing by the proteasome. This partial processing of p100 to p52 results in the accumulation of p52:RELB heterodimers that are free to translocate to the nucleus and induce target gene expression. A diagram depicting the major proteins in both the canonical and non-canonical NF-κB signaling pathways is seen in **Figure 12**.

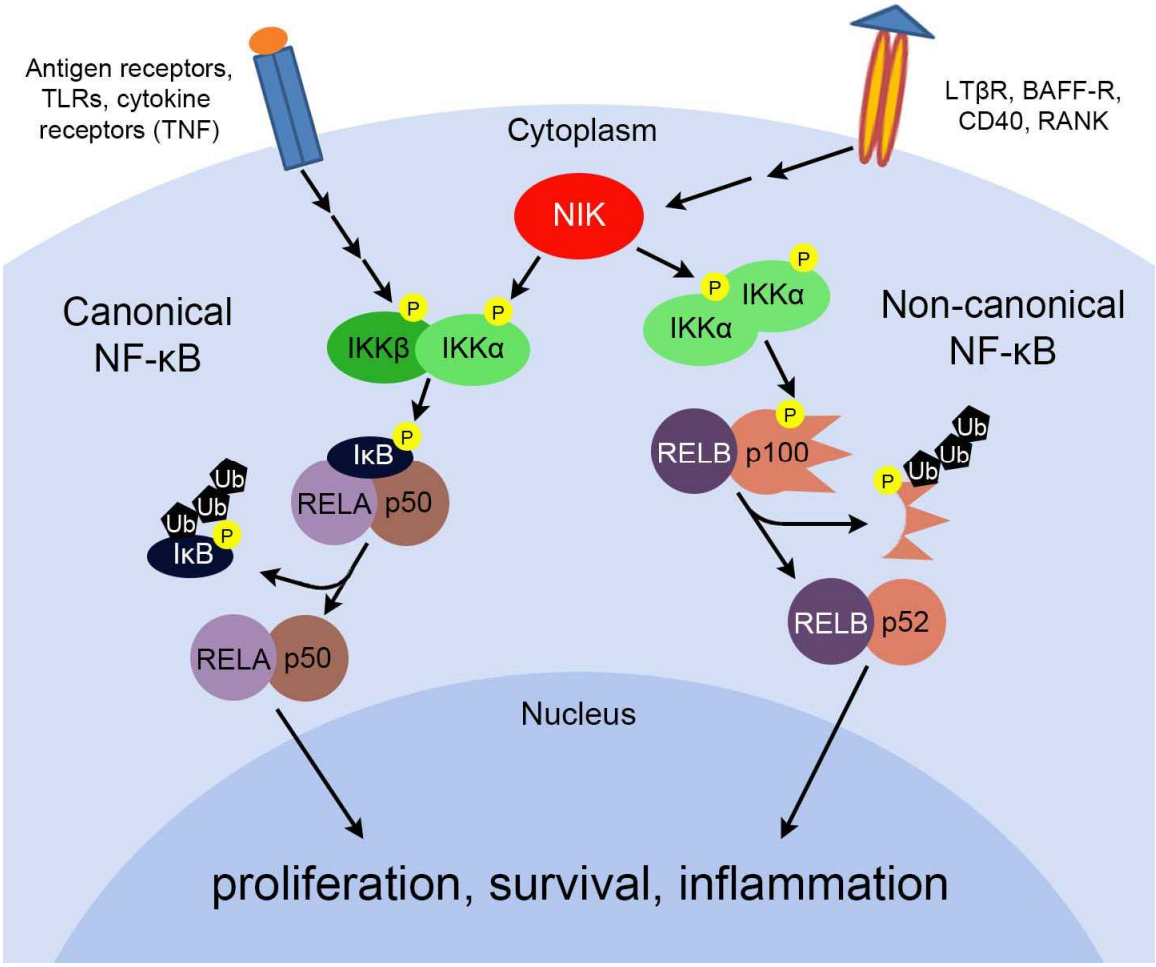

Figure 12. Schematic representation of the NF-κB signaling pathway. Diagram depicting a selected group of the critical proteins involved with canonical and non-canonical NF-κB signaling. In the canonical pathway, upstream signals including cytokines and TNF ligands result in activation of an IKK complex comprised of IKKα and IKKβ. IκB phosphorylation by IKKβ leads to proteosomal degradation of IκB, freeing p50:RELA dimers to translocate to the nucleus and transactivate target genes. In the non-canonical pathway, ligands such as BAFF/LTβ induce NIK stabilization. NIK stabilization is sufficient to activate an IKKα homodimeric complex, which phosphorylates p100, leading to its

proteosomal processing to p52. The degradation of p100 allows p52:RELB complexes formerly sequestered in the cytoplasm to translocate to the nucleus and induce the expression of target genes. NF-κB target genes include those known to promote survival, proliferation, and inflammation. Notice that NIK is placed upstream of both pathways, as it is sufficient to activate both canonical and non-canonical NF-κB signaling.

Interestingly, canonical NF-κB pathway activation can also feed into the non-canonical pathway. *NFκB2,* the gene encoding p100 is a known target gene of the canonical pathway [116]. This suggests the possibility of synergistic crosstalk between the canonical and non-canonical NF-κB pathways. An observation supporting this theory is that basal RELA NF-kB activity is required for LTβ-induced RELB:p52 dimer generation [117]. Given that four of the five RHD containing NF-κB transcription factors are encoded by canonical NF-κB target genes [116, 118-121], the pathway as a whole has been suggested to be dynamic in its ability to amplify and/or alter target gene expression [122].

NIK, NF-κB, and cancer

Previous studies of mice carrying a point mutation or knockout of NIK indicated its requirement in regulating the non-canonical NF-κB pathway [123, 124]. Further study of NIK revealed it to be a tremendously unstable protein that is rapidly degraded in cells under basal conditions [125]. In response to certain ligands including CD40L, LTβ, and RANKL, NIK is stabilized, phosphorylating IKKα and inducing downstream p100 processing [125, 126]. NIK degradation is regulated by an E3 ligase complex comprised of TRAF2, TRAF3, c-IAP1, and c-IAP2 [127, 128]. TRAF3 functions as a molecular tether to a complex of TRAF2 and c-IAP1/2, in which c-IAP1/2 actually mediate the K48-polyubiquitination of NIK, targeting it to the proteasome for degradation (**Figure 13**).

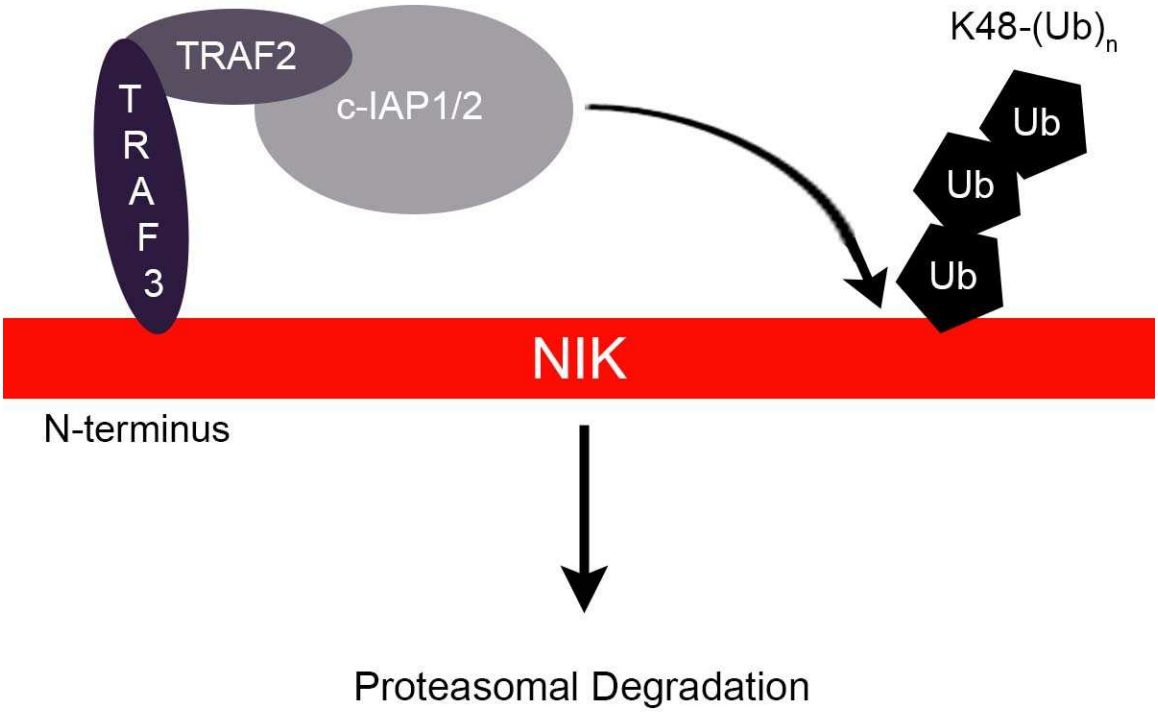

Figure 13. Schematic representation of NIK degradation by an E3 Ligase protein complex including TRAF2, TRAF3, and c-IAP1/2. NIK is a protein maintained at low basal levels due to constitutive turnover by the proteasome. TRAF3 interacts with NIK in its TRAF3 binding domain in the N-terminus, tethering it to an E3 complex containing TRAF2 and c-IAP1/2. Once formed, c-IAP1/2 mediates the K48-polyubiquitination of NIK, leading to its proteasomal degradation.

Recent Multiple Myeloma (MM) studies have provided additional insights into the mechanism of NIK degradation. Many MM cell lines possess mutations/deletions in *TRAF3* or *NIK* that preclude their interaction at the protein level, resulting in stabilization of NIK [129, 130]. Additional MM cell lines were found to have large deletions of the locus including *BIRC2* and *BIRC3*, the genes encoding c-IAP1 and c-IAP2, respectively [130]. A subset of MALT Lymphomas harboring an oncogenic fusion resulting in a c-IAP2-MALT1 fusion protein are also driven by stabilization of NIK signaling [131]. The resultant fusion protein is a protease with unique specificity for NIK, cleaving the N-terminus and removing the TRAF3 binding domain. The remaining NIK C-terminal fragment is resistant to proteasomal degradation and is now free to drive downstream oncogenic signaling. Importantly, NIK stabilization is also capable of inducing canonical NF-κB signaling through activation of IKKα\β heterodimers [129, 132]. It has previously been suggested that NIK's ability to activate both pathways is a possible explanation for the multitude of genetic alterations observed in MM that all result in stabilization of NIK [133]. A trenchant explanation for the tight regulation of NIK at the protein level is that studies have shown NIK to be a constitutively activated kinase independent of additional post-translational modifications [134]. Overall, these studies implicate NIK as a potent oncogene and regulator of NF-κB signaling.

The first direct connection between NF-κB activation and cancer came from the characterization of the viral homolog to c-REL, v-REL. v-REL was shown to be a

driver of avian leukemias and lymphomas [135]. Further support of NF-κB's role in oncogenesis is demonstrated by the observation of constitutive NF-κB activity in cancer cells derived from patients with MM, Acute Lymphocytic Luekemia (ALL), and Chronic Myelogenous Leukemia (CML) [136]. NF-κB is a well-established regulator of normal lymphocyte development and physiology, and as such is capable of activating genes involved with cellular proliferation and survival [137]. Deregulation of NF-kB, which is seen in most cancers [138], can result in the expression of proteins regulating cell cycle progression and survival, including Cyclin D1, Cyclin D2, CDK6, c-Myc, c-Myb, BCL2, ERBB2, and MET [139-145]. Given the central role of NF-κB in integrating signals from a diverse array of stimuli and transducing these signals into vital basic cellular functions, one can begin to understand why many cancers co-opt this pathway for selective advantage.

NF-κB and NF2 in the nervous system

Since its initial discovery as an important regulator of hematopoietic cell function, the bulk of studies investigating pathologic roles for NF-κB focus on hematopoietic cell types. Because of this bias, there exists a relative dearth of knowledge on the role NF-κB plays in non-hematopoetic cell types and solid tumor biology. Due to the focus of this manuscript on schwannomas, a peripheral nerve tumor, we now review what is known of NF-κB in cell types and tumors of the nervous system, with a particular focus on glial cells.

NF-κB signaling in glial cells is believed to be heavily inducible but possess low basal activity [146, 147]. Because of this inducible nature of NF-κB in glial cells, it has been suggested that NF-κB activity may be linked to pathologic events [148]. Spinal cord injury studies in a transgenic mouse conditionally overexpressing a non-phosphorylatable form of IκBα in astrocytes, a glial cell of the CNS, support this hypothesis [149]. The authors concluded that NF-κB does not play a substantial role in regulating normal astrocyte homeostatic function but it does clearly contribute to astrocyte chemokine secretion in response to spinal cord injury. These studies demonstrated that by blocking NF-κB signaling in activated astrocytes, mice had fewer healing defects post-injury and glial scarring was reduced.

Canonical NF-κB activity involving RELA is required for peripheral myelination of axons by Schwann cells, indicating this developmental program is regulated by NF-κB [68] . In the sciatic nerves of rats, increased NF-κB activation was observed in pre-myelinating Schwann cells *in vivo* and *in vitro*. Further evidence of this relationship was seen in *Rela* knockout mice, which failed to properly myelinate peripheral nerves. Blocking NF-κB activity in Schwann cell and neuron co-cultures significantly attenuated myelination and, additionally, prevented the induction of OCT6, a transcription factor required for proper myelination. These data suggest that NF-κB signaling is an essential mediator of the pre-myelinating Schwann cell developmental stage. Additional studies support the notion that NF-κB is a regulator of Schwann cell differentiation [150, 151].

Previous studies have indicated that, at the molecular level, schwannomas resemble Schwann cells at the pre-myelinating stage of differentiation. In one immunohistochemical study, the investigators found that the schwannoma cells had lost expression of markers of a mature myelinated phenotype, including P0 and MBP. Rather, the schwannoma cells now expressed markers of embryonic Schwann cell lineages, including NGFR, NCAM, L1CAM, and OCT6 [152]. In a recent microarray study of schwannomas, the investigators also found that schwannomas possessed a molecular phenotype similar to that of pre-myelinating Schwann cells [153]. This study made the observation that schwannomas overexpressed *L1CAM*, *ITGA4*, *TFAP2A*, *CDH2*, and *CDH19*, which are all molecular markers of developing Schwann cell lineages prior to a mature myelinated phenotype [60].

Given that loss of *NF2* is the rate-limiting step in schwannoma formation [74, 75, 154], the above studies suggest a fascinating potential link between schwannomas, NF2, and NF-κB signaling. Indeed, NF2 has been previously identified as a negative regulator of canonical NF-κB activation [155]. In a more recent study using human schwannoma cells, Cyclin-D1 and Survivin were found to be expressed in an NF-κB dependent manner *in vitro* [156]. Further, the authors observed that total RELA and Phosphorylated S536-RELA, a marker of canonical NF-κB activation and RELA nuclear localization, are increased in schwannoma cells when compared to normal nerves.

Another interesting potential link between NF2 and NF-κB comes from a study examining a different tumor in the nervous system called ependymoma. Ependymomas are observed in up to 50% of NF2 patients, and are the 3rd most common tumor observed in these patients behind schwannoma and meningioma [1]. In this study, the authors identified a recurring *C11orf95-RELA* oncogenic translocation in sporadic supratentorial ependymomas [157]. The resulting RELA fusion protein, which also contains the C11orf95 zinc-finger domain, spontaneously translocates to the nucleus to transactivate target genes. Transplantation of neural stem cells expressing this fusion protein into mice resulted in ependymoma formation and dramatically reduced survival when compared to mice transplanted with stem cells expressing WT RELA or a control vector. These studies demonstrate that constitutive NF-κB signaling is sufficient to drive ependymoma development, a tumor NF2 patients are genetically predisposed to acquire.

In summary, there exist several studies connecting NF2, NF-κB, and schwannoma formation. The studies herein employ broad genomic analyses to further implicate NF-κB activation in schwannomas, and then examine NF-κB signaling in murine and human schwannoma. Finally, we show activation of this pathway through an upstream regulator, NIK, is sufficient to increase the proliferation, survival, and adhesion of primary Schwann cells and, additionally,

induce a transcriptional profile that is remarkably similar to that observed in murine and human schwannomas.

MATERIALS AND METHODS

Microarray and Ingenuity Pathway Analysis

Previously published schwannoma microarray data [153] (http://www.ncbi.nlm.nih.gov/geo/query/acc.cgi?acc=GSE39645) were downloaded from the Gene Expression Omnibus (GEO) and loaded into Partek Genomics Suite (Partek, Inc.). In our analysis, we included 31 schwannoma samples and 8 control samples (the human Schwann cell group was excluded from the controls). The data were then quantile-normalized and differentially-expressed genes (DEGs) were identified by ANOVA as those having P-values less than .05. The Bejamini and Hochberg method was used to correct for multiple testing. Further filtering of DEGs was completed to remove genes with fold changes between -2 and 2. Network analysis was then completed with this DEG set with Ingenuity Pathway Analysis (IPA, QIAGEN Redwood City, www.qiagen.com/ingenuity). Microarray analysis and IPA were completed by the Indiana University School of Medicine Center for Computational Biology and Bioinformatics.

Statistical methods

Statistical analyses were performed with GraphPad Prism 6.0. As noted in the text, ANOVA or Student's T-test was used to test for differences between samples. Specific tests and significance levels can be found in the figures and figure legends.

Preparation of mouse Trigeminal nerves for RNA and protein studies

Mice were sacrificed and Trigeminal nerve tissue was freshly dissected, minced with a scalpel, and washed 3 times with cold PBS, pelleting the tissue in between washes using a tabletop centrifuge (Eppendorf) at 4C. Tissue was then prepared for protein or RNA studies. For whole lysate protein studies, xTractor Lysis buffer (Clontech) with cOmplete Protease inhibitor cocktail (Roche) and PhosSTOP Phosphatase inhibitor cocktail (Roche) was incubated with the tissues. This mixture was then sonicated on ice, spun down at max speed on a tabletop centrifuge for 10 minutes at 4C, and the supernatant was collected and stored at -80 for future use. Trigeminal nerve tissue was fractionated into cytoplasmic and nuclear protein fractions using the NE-PER Subcellular fractionation kit (Thermo Pierce). For subsequent RNA extraction, tissues were suspended in RNALater (Life Technologies) and stored at -20.

RNA extraction from Trigeminal Nerves and primary Schwann cells

RNA extraction, cDNA synthesis, qRT-PCR, data acquisition, analysis, and QC of mouse Trigeminal nerve samples were completed by Genome Explorations USA (Memphis, TN). All other RNA work was completed at Indiana University School of Medicine. RNA was extracted from primary Schwann cells with Trizol (Life technologies). QuantiTect Reverse Transcription kit (Qiagen) and Fast SYBR Green Real-Time PCR Master Mix (Life Technologies) were then used for two-step qRT-PCR with an ABI 7500 Fast Thermal Cycler.

qRT-PCR Primer list (all are targeted to genes in mice)

gene/primer name	Sequence
Bcl2 For	aagctgtcacagaggggcta
Bcl2 Rev	ctctcaggctggaaggagaa
Birc2 For	tgtggcctgatgttggataac
Birc2 Rev	ggtgacgaatgtgcaaatctact
Birc3 For	acgcagcaatcgtgcattttg
Birc3 Rev	cctataacgaggtcactgacgg
Casp8 For	tgcttggactacatcccacac
Casp8 Rev	tgcagtctaggaagttgacca
Ccnd1 For	tctttccagagtcatcaagtgtg
Ccnd1 Rev	gactccagaagggcttcaat
Ccnd2 For	gctgtgcatttacaccgaca
Ccnd2 Rev	acactaccagttcccactcca
Erbb2 For	gagacagagctaaggaagctga
Erbb2 Rev	acggggattttcacgttctcc
Gapdh For	aggtcggtgtgaacggatttg
Gapdh Rev	tgtagaccatgtagttgaggtca
Met For	gtgaacatgaagtatcagctccc
Met Rev	tgtagtttgtggctccgagat
Nfkb1 For	tcaggtgcagtgtcttgagc
Nfkb1 Rev	ggagggacagcagtaacaaca
Nfkb2 For	agtgtgcgctgtgtctgtag
Nfkb2 Rev	gttcttcttggttacatgcagga
Rela For	tgcccagaccgcagtatc
Rela Rev	ggattcgctggctaatgg
Relb For	gtgacctctcttccctgtcact
Relb Rev	tgtattcgtcgatgatttccaa
Rel For	agaggggaatgcggtttagat
Rel Rev	ttctggtccaaattctgcttcat

Procurement and preparation of human vestibular schwannoma tissue for protein and histological studies

Freshly excised tumor specimen was snap frozen and stored in liquid nitrogen. Tissue was then prepared for protein studies similar to the procedure outlined above for murine nerve tissue. Preparation of tissues for histological studies was completed as per the fixation and embedding protocol outlined in **Chapter One** for murine nerve tissues. All studies were conducted under IRB approval (IRB# 1107006213, "Genotype, Phenotype, and Treatment of Human Vestibular Schwannomas.").

Primary antibody list

The following antibodies were used for Western Blotting experiments: RELA (Cell Signaling #8242), RELB (Cell Signaling #4954), p100/p52 (Cell Signaling #4882), c-REL (Cell Signaling #12707), GAPDH (Cell Signaling #5174), NIK (Cell Signaling #4994), IKKα (Cell Signaling #2682), IκBα (Cell Signaling #4814), Myc (Cell Signaling #2278), HA (Cell Signaling #3724), FLAG (Cell Signaling #8146), NF2 (Abcam ab30329), and Caspase 8 (Santa Cruz sc-6136). The custom polyclonal NIK antibody targeting murine NIK residues 311:328 was generated by Thermo Pierce custom antibody services. For IHC/IF, the following antibodies were used: RELA (Santa Cruz sc-109), RELB (Santa Cruz sc-226), NIK (Santa Cruz sc-7211), GFP (Abcam ab1218), and S100 (Dako IS504).

Western Blot densitometry

Western blot film was scanned into a digital format and intensity values were determined using the Image Studio Lite Version 3.1 (LI-COR Biosciences).

Histology and immunohistochemistry

Immunohistochemistry for RELA (Santa Cruz, sc-109), RELB (Santa Cruz, sc-226), and NIK (Santa Cruz, sc-7211) using formalin-fixed, paraffin-embedded mouse and human samples was completed by the Indiana University School of Medicine Immunohistochemistry core. RELA and RELB were visualized using the Dako EnVision+ Rabbit system and NIK was visualized with the DAKO Flex HRP system. Schwannoma tissue microarrays (US Biomax) stained for RELA and NIK were also completed by the Indiana University School of Medicine Immunohistochemistry core.

Cell culture and transfection

HEK-293T cells (American Type Culture Collection, ATCC) were used for transfection experiments with polyethyleneimine (PEI, Sigma). Unless otherwise noted, Dulbecco's Modified Eagle Medium (DMEM, Gibco/Invitrogen) containing 10% Fetal Bovine Serum(Sigma), 50 U/mL penicillin, 50 ug/mL streptomycin, and 2mM L-Glutamine(Lonza) was used for cell culture. For creation of a stable NF-κB reporter cell line, 293T cells were transduced with Cignal NF-κB GFP Reporter Lentivirus (Qiagen) and selected with puromycin (Sigma). The Cignal NFκB GFP Lentivirus stably inserts a modified form of the *GFP* gene under the

control of a minimal CMV promoter with tandem repeats of the canonical NF-κB transcriptional response element.

Plasmids and site-directed mutagenesis

C-terminal Myc/FLAG-tagged full-length (FL) NIK and Caspase-8 cDNAs in the PCMV6-Entry vector were purchased from Origene. The Caspase-8 cDNA was then shuttled into the PCMV6-AC-HA backbone (Origene) using the Sgf1 and Mlu1 restriction sites. N-Myc FL NIK, N-Myc and C-FLAG 309-801 NIK were PCR-amplified (adding epitope tag sequences and cloning sites) using Phusion Hi-Fidelity polymerase (New England Biolabs) from a vector containing FL NIK, subcloned into a TOPO-TA cloning vector (Life Technologies), and then cloned into the PCMV6-XL5 backbone (Origene) using the EcoRI and SalI cloning sites. The pCR-FLAG-IKKalpha-KM, pFlag-CrmA, and pcDNA-CrmA plasmids were acquired from Addgene. Site-directed mutagenesis of FL NIK was completed using the New England Biolabs Q5 QuickChange Site-Directed Mutagenesis kit and validated by Sanger sequencing. The NEBaseChanger web application was used for primer design.

Virus generation and titration

The puc2CL6IEGwo Lentiviral IRES-EGFP construct was a kind gift of Helmut Hannenberg at Indiana University School of Medicine. Using standard molecular cloning techniques, we cloned C-FLAG 309-801 NIK into the puc2CL6IEGwo construct using the EcoRI and BamHI cloning sites. The puc2CL6IEGwo

construct contains an IRES-EGFP cassette and multiple cloning site downstream of the spleen focus-forming virus (SFFV) promoter, which robustly drives transcription in Eukaryotic cells. To generate virus, 293T cells grown to 70% confluence were transfected with 10 ug each of C-FLAG 309-801 NIK puc2CL6IEGwo (Lenti 309-801 NIK) or empty vector puc2CL6IEGwo (Lenti IRES EGFP), 5 ug of gag-pol expressing plasmid, and 1 ug of foamyviral envelope containing plasmid (PCOPE01) in 6 mL of Dulbecco's Modified Eagle Medium (DMEM, Gibco/Invitrogen) containing 10% FBS and 0.0075 mg/mL polyethyleneimine (PEI, Sigma). After roughly 16 hours of transfection at 37C, transfection media was replaced with 6 mL fresh DMEM containing 10% FBS, 50 U/mL penicillin, 50 ug/mL streptomycin, 2mM L-Glutamine(Lonza). After 24 hours, cultures were collected and filtered through a .22 um polyethersulfone (PES) membrane Stericup unit (Millipore) and centrifuged at 30,000 x g at 4C for 2 hours in a polycarbonate Oak Ridge centrifuge tube (Nalgene). Supernatant was then decanted, bleached, and placed in biohazard waste. The viral pellet was then resuspended in 1 mL of DMEM containing 10% FBS. Virus was then stored in aliquots at -80C. Titration of virus to calculate effective infectious particles per unit volume (Transduction Units, or TU, per mL) was determined by percent GFP-positivity (as measured by flow cytometry) of serially transduced HT1080 cells plated at 100,000 per well on a six-well plate in 1 mL of DMEM/10% FBS. Serial dilutions started at 10^{-3} and ended with 10^{-8} dilution.

Primary Schwann cell procurement and culture

Wild type (WT) embryonic day 13.5 (E13.5) embryos were harvested from pregnant dams after sacrifice. The dorsal root ganglion (DRG) was then dissected from each embryo with the aid of a dissecting microscope. The DRGs were then digested in Trypsin and dissociated with syringes. Individual DRGs (a collection from a single embryo) were then plated on Poly-D-Lysine (PDL, .1mg/mL)/Laminin (.25mg/mL, Sigma) coated 12-well plates at one embryo per well in Schwann Cell Media I (SCM-I) comprised of DMEM with 50 U/mL penicillin, 50 ug/mL streptomycin, 2mM L-Glutamine(Lonza), 1X N2 supplement (Life Technologies), and 250 ng/mL Nerve Growth Factor (NGF, Sigma). The following day, the media was changed to Schwann Cell Media II (SCM-II), which was identical to SCM-I except for the substitution of 2 uM Forskolin and 10 ng/mL Neuregulin (Sigma) for NGF.

Transduction of primary Schwann cells

Three days after harvesting and plating WT Schwann cells on 12-well plates, cells were then transduced with Lentivirus in 1 mL of SCM-II at a MOI of 20 (based on an approximate cell number of 200,000 cells per well). Cells were incubated in SCM-II with virus for 72 hours before replating. All experiments utilized passage 1 Schwann cells.

Schwann cell proliferation assays

Hemacytometer-based: 200,000 Schwann cells of each genotype were seeded in triplicate on a PDL/Laminin-coated 12-well plate and allowed to adhere overnight. The following morning, the media was changed to fresh SCM-II, and 72 hours later the cell number in each well was calculated by Trypan Blue exclusion with a hemacytometer.

EdU with fluorescent microscopy: 200,000 Schwann cells of each genotype were plated on coated coverslips in 12-well plates. The following morning, the media was changed to fresh SCM-II with 10 uM EdU. Cells were pulsed for 8 hours and fixed. Life Technologies Alexa 594 EdU Imaging kit was used to complete the staining of the cells. Coverslips were then imaged on the deconvolution microscope.

Schwann cell survival assay

In a PDL/Laminin-coated 12-well plate, 200,000 Schwann cells of each genotype were seeded in triplicate and allowed to adhere overnight. The following day, the media was removed, cells washed 1X with PBS, and growth-factor free DMEM with 50 U/mL penicillin, 50 ug/mL streptomycin, and 2mM L-Glutamine was added. The number of living cells in each well was counted 48 hours later by Trypan Blue exclusion with a hemacytometer.

Schwann cell adhesion assay

For measurement of cell adhesion, the ACEA iCelligence system was used. The iCelligence system uses an impedance calculation that allows for real-time monitoring of diverse cellular processes, including cellular adhesion. First, E-plates (ACEA) were coated with PDL/Laminin and 250 uL of SCM-II was added to the plates to take an initial impedance reading. Next, IRES-EGFP and 309-801 NIK Schwann cells were added to the wells at 25,000 cells/well with a final volume of 500 uL. Impedance values were measured every second for the following three hours.

Cycloheximide NIK protein stability assay

293T cells at 70% confluency in 10 cm dishes (BD Falcon) were transfected with 4 ug/dish of FL N-Myc NIK or N-Myc 309-801 NIK for 36 hours prior to addition of media containing 10 ug/mL Cycloheximide (Sigma). Cells were then lysed at the indicated conditions/time points and the protein visualized by SDS-PAGE.

Immunoprecipitation experiments in 293T cells

Immunoprecipitation experiments were completed in 293T cells transfected with the indicated plasmids/concentrations at 70% confluency in 10 cm dishes. Two days after transfection, cells were lysed with RIPA Buffer (50 mM Tris-HCl pH 8.0, 150 mM NaCl, 1% Triton X-100, .5% Sodium Deoxycholate, .1% SDS, protease and phosphatase inhibitors), sonicated, and samples were standardized by BCA (Thermo Pierce). Samples were then incubated overnight with M2 Flag

Affinity Gel (Sigma). Immunoprecipitated proteins were then visualized with SDS-PAGE.

In vitro Caspase-8 cleavage assay

Purification of FLAG-NIK: FLAG-NIK was transfected at 20 ug/dish in 70% confluent 15 cm dishes and harvested 48 hours later in Lysis Buffer (25 mM HEPES pH 7.4, 150 mM NaCl, 1 mM EDTA, 1% Triton X-100, protease and phosphatase inhibitors) and sonicated. These samples were then incubated overnight with M2 Flag Affinity Gel. Flag NIK was then eluted from the resin with 100 uL of Flag peptide elution solution (200 ug/mL in TBS, Sigma).

In vitro Caspase-8 cleavage of NIK: 200 ng of activated Caspase-8(BD) was added to 200 ng of purified NIK protein in a 50 uL volume of reaction buffer (20 mM HEPES pH 7.4, 20 mM NaCl, 1 mM EDTA, 1 mM EGTA, 1.5 mM $MgCL_2$, 10 mM DTT) for 1 hour at 37C. Q-VD-Oph, an irreversible pan-caspase inhibitor, was purchased from ApexBio.

Prediction of Caspase-8 cleavage sites and orthologous cleavage site analysis

Caspase-8 cleavage sites were predicted for human NIK using two different applications, Cascleave 2.0 [158, 159] and SitePrediction [160]. Cascleave 2.0 was set to a medium stringency threshold for prediction of cleavage sites. The

NCBI homologene application was used to identify orthologous cleavage sites in chimpanzee, macaque, mouse, rat, dog, and cow.

Deconvolution microscopy

Cells were fixed in 4% Paraformaldehyde on coverslips in 12-well plates (BD Falcon). Following fixation, coverslips were washed 2X in PBS and permeabilized in .2% Triton X-100 in PBS and Blocked in .2% Triton X-100, 2% BSA in PBS. Coverslips were then incubated with primary antibody in 1% BSA in PBS overnight at 4C, washed three times in PBS, and subsequently incubated for one hour at room temperature with fluorophore-conjugated anti-mouse or anti-rabbit antibodies (Molecular Probes, Invitrogen). After washing in PBS three times, coverslips were then incubated in PBS containing Hoescht and Phalloidin (Life Technologies) to stain the nuclei and actin cytoskeleton, respectively. Coverslips were then sealed on microscope slides (Fischer Scientific) with lacquer and allowed to dry overnight. Data were acquired on a DeltaVision deconvoloving microscopy system (Applied Precision). Typical controls included cells incubated with secondary (fluorophore-conjugated) antibody but not primary antibody.

RESULTS

Genomic studies indicate NF-κB is activated in schwannomas

In an effort to better understand the signaling pathways deregulated in human schwannomas, we retrieved and re-analyzed published microarray data [153] from a recent study on the Gene Expression Omnibus [161, 162]. In this study, 31 human vestibular schwannomas were compared to normal nerve samples. After generating a set of differentially expressed genes (DEGs), we input this gene set into Ingenuity Pathway Analysis (IPA) to identify activated transcriptional modules and signaling pathways. IPA canonical pathway and upstream regulator analyses both identified the NF-κB pathway as deregulated in schwannomas (**Figure 14A**). A number of genes formerly identified as either regulated by NF2 or overexpressed in schwannomas are NF-κB target genes, including *CCND1*, *ERBB2*, and *MET*, and were also overexpressed in this dataset (**Figure 14B**) [139, 143, 145, 163-167]. To validate these deregulated genes, we performed qRT-PCR on primary nerve tissue from WT (*Postn-Cre-;Nf2*$^{flox/flox}$) and NF2-KO mice (*Postn-Cre+;Nf2*$^{flox/flox}$, **Figure 14C**). All genes listed in **Figure 14B** with the exception of *Bcl2* (P = .073) were also overexpressed in murine schwannomas.

A

IPA Gene set	Gene Overlap	*P*-value
NF-κB signaling pathway	32/173	9.05×10^{-3}
NF-κB transcriptional targets	61/301	2.75×10^{-5}

B

Gene	Fold Increase
BCL2	2.15
BIRC2	2.85
BIRC3	2.92
CCND1	2.72
CCND2	2.53
ERBB2	2.12
MET	5.77

C

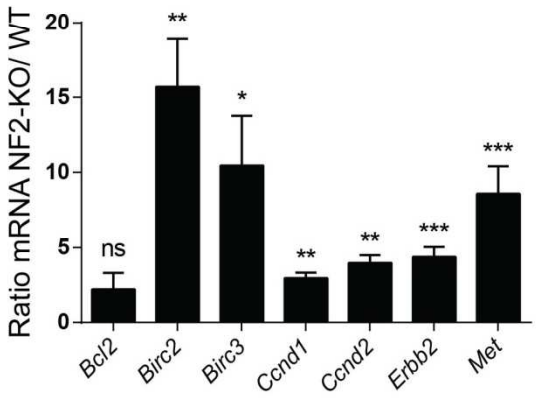

Figure 14. Ingenuity Pathway Analysis and qRT-PCR in schwannomas suggests activation of the NF-κB pathway. (**A**) Ingenuity Pathway Analysis (IPA) of human schwannoma microarray data. IPA Canonical Pathway analysis indicated significant deregulation of NF-κB signaling, with 32 genes in the human schwannoma differentially expressed gene (DEG) group annotated as NF-κB signaling pathway members. Similarly, IPA Upstream analysis indicated 61 DEGs as NF-κB target genes. (**B**) Selected NF-κB target genes deregulated in human schwannomas, some of which have been previously identified as genes regulated by NF2. (**C**) Validation of the deregulated genes in **B** by qRT-PCR in primary nerve tissues derived from eight month old WT and NF2-KO mice. The experiment testing *Birc2* and *Birc3* included three WT and four NF2-KO mice. All other genes tested included four WT and four NF2-KO mice. ns = not significant,

* = $P < .05$, ** = $P < .01$, *** = $P < .001$; unpaired Student's T test. Error bars represent SEM.

Increased expression of REL proteins in schwannomas

Equipped with the knowledge that schwannomas from the NF2 mouse model resemble human schwannomas at the molecular level, we decided to examine these tumors for NF-κB activation. qRT-PCR from age-matched primary nerve tissues revealed that all Rel family transcription factors were overexpressed at the RNA level (**Figure 15A**). To see if this was also the case at the protein level, we analyzed whole lysate nerve tissues by SDS-PAGE. Western blotting revealed increases in p100, RELA, RELB, and c-REL in NF2-KO tissues when compared to WT (**Figure 15B**). p100, RELA, RELB, and c-REL are encoded by *Nfkb2*, *Rela*, *Relb*, and *Rel* genes, respectively. We also observed an increase in p52 levels in NF2-KO nerve tissue. The accumulation of p52 is an indicator of non-canonical NF-κB activation in murine schwannomas. IκBα was increased in NF2-KO tissue at the protein level, and it appeared to migrate as a doublet in both WT and NF2-KO tissues (**Figure 15B**). The upper band of IκBα was especially robust in the NF2-KO tissues, suggesting that a large fraction of the increased pool of IκBα was possibly phosphorylated and inactivated. Overall, the increase in p100 and IκBα, IκB proteins, makes the net effect of the increase in RELA, c-REL, RELB, and p52 unclear, as it is possible that the increase in REL proteins is countered by the increase in IκB activity. To address this question, we used Immunohistochemisty (IHC) and subcellular fractionation to localize the increase in REL proteins to the cytoplasm and nucleus. By IHC, we noted a diffuse increase in both cytoplasmic and nuclear accumulation of RELA in both mouse and human schwannoma (**Figure 16**). Additional examples of the

increase in nuclear RELA staining in human schwannomas can be seen in **Figure 17**. A diffuse increase in cytoplasmic and nuclear RELB staining was also seen by IHC in human schwannomas (**Figure 18**). Finally, by subcellular fractionation, we further identified the increase in RELA and RELB in murine schwannomas to be both in cytoplasm and nucleus (**Figure 19**). Altogether, these data indicate activation of both canonical and non-canonical NF-κB in schwannomas.

The simultaneous increase in REL proteins and IκB proteins in schwannomas seemed unusual, as activation of NF-κB is typically paired with a decrease in IκB proteins. We reasoned that chronic activation of NF-κB could result in upregulation of both REL family members and IκB proteins since they are encoded by genes upregulated by NF-κB, with the exception of RELA. Indeed, similar observations have been made in Cylindromatosis, a disease exhibiting chronic activation of NF-κB. In B-cells expressing a mutant form of *CYLD*, a gene encoding a NF-κB negative regulator and deubiquitinase, an increase in both IκBα and p100 was observed [168]. Yet *CYLD* mutant B cells still exhibited an increase in NF-κB DNA binding by Electrophoretic Mobility Shift Assays (EMSA) and, additionally, an increase in both cytoplasmic and nuclear RELB. Interestingly, human patients with germline mutations in *CYLD* develop multiple benign tumors of skin appendages.

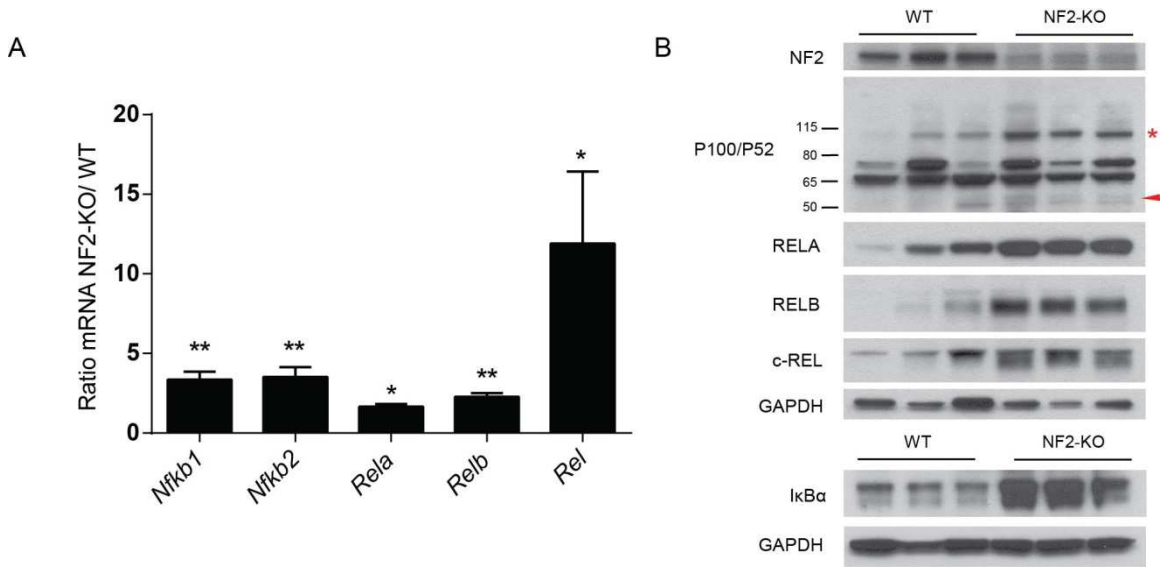

Figure 15. Murine schwannomas exhibit increased levels of Rel transcription factors at the RNA and protein level. (**A**) qRT-PCR of NF-κB transcription factors in primary nerve tissue from WT and NF2-KO mice showing an increase in all Rel family members at the RNA level. All experiments involved four WT and four NF2-KO mice, except for *Rel*, which included three WT and four NF2-KO mice. ns = not significant, * = $P < .05$, ** = $P < .01$; unpaired Student's T test. Error bars represent SEM. (**B**) Whole Lysate SDS-PAGE Western blot demonstrating an increase in NF-κB transcription factor and signaling pathway members at the protein level in NF2-KO nerve tissue. Note the red asterisk next to p100, the protein encoded by the *Nfkb2* gene and the red arrowhead next to p52, the resulting protein from p100 processing by the proteasome. p52 accumulation, as seen in this blot, indicates activation of the non-canonical arm of NF-κB. Increased IκBα was observed in murine schwannomas, which is an NF-κB target gene and a negative regulator of the canonical pathway. IκBα also migrated as a doublet in WT and NF2-KO tissues,

with an especially robust upper band in NF2-KO tissues. All tissues are derived from eight month old mice.

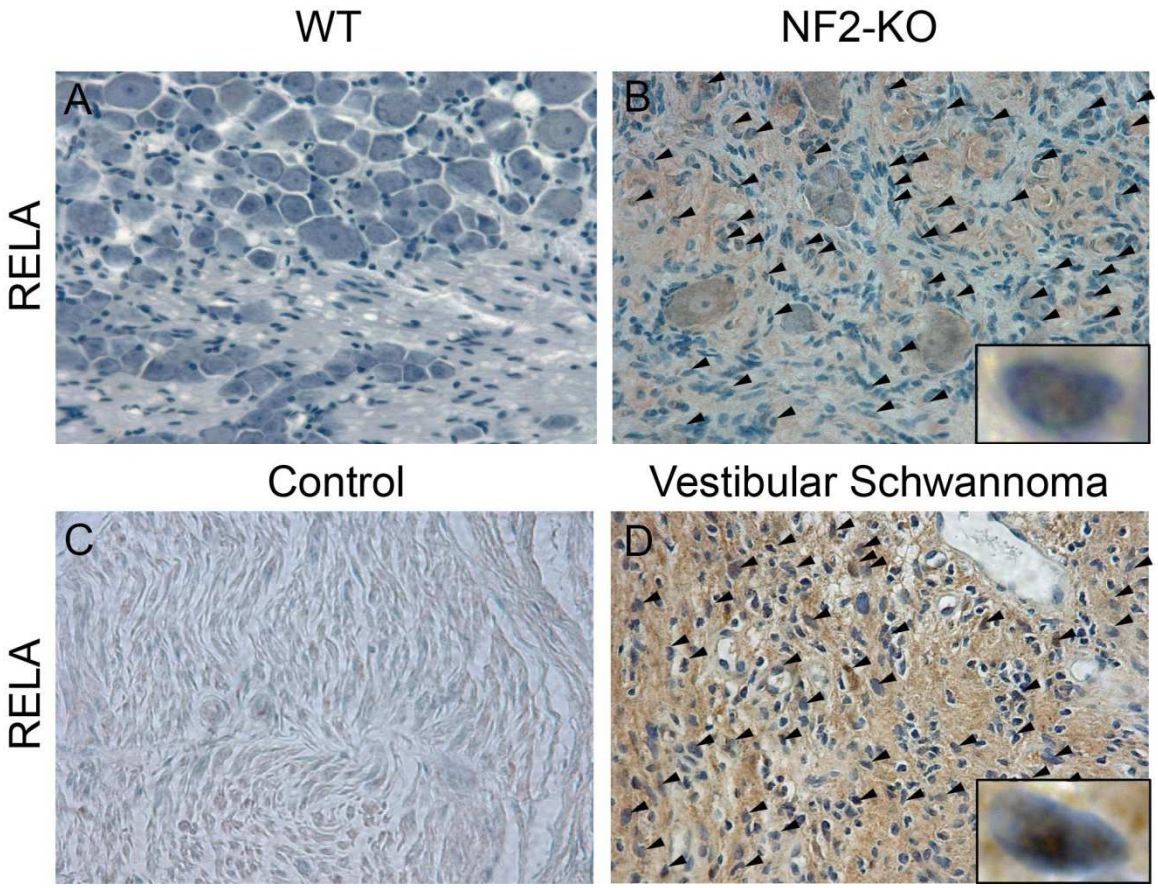

Figure 16. Increased cytoplasmic and nuclear RELA reactivity observed by immunohistochemistry in murine and human schwannomas. (**A** and **B**) IHC of RELA in age-matched 12 month old murine WT (**A**) and NF2-KO DRG (**B**). Similarly, **C** and **D** present RELA IHC of control human nerve (**C**) and human vestibular schwannoma tissue (**D**), respectively. Original magnification x400. Arrows in **B** and **D** point to nuclei with positive staining for RELA. The magnified (1000x) images in the bottom right corner of **B** and **D** are examples of positive nuclear staining.

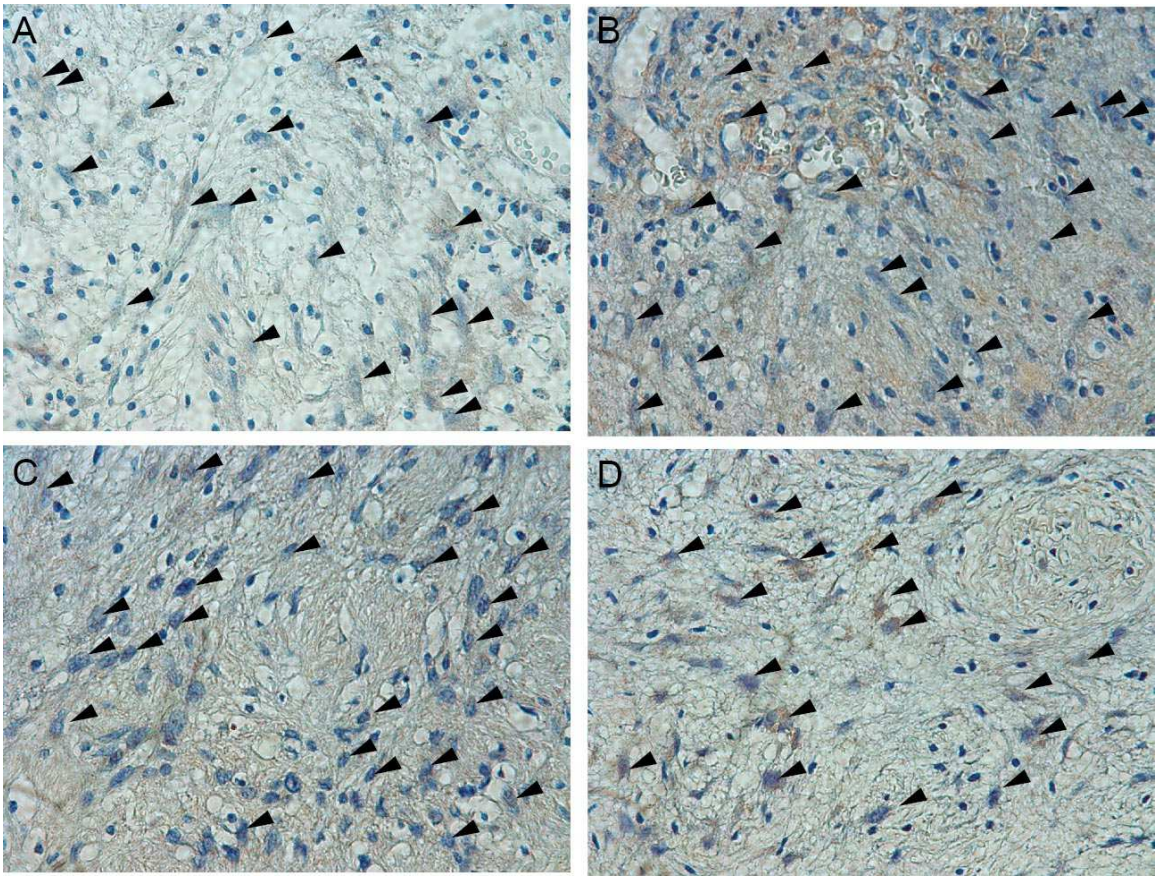

Figure 17. Expanded immunohistochemical panel of RELA in human schwannomas. (**A**-**D**) IHC of RELA in four different human schwannomas. Note that these tumors are not vestibular schwannomas. Arrows point to nuclei with positive staining for RELA. Original magnification x400.

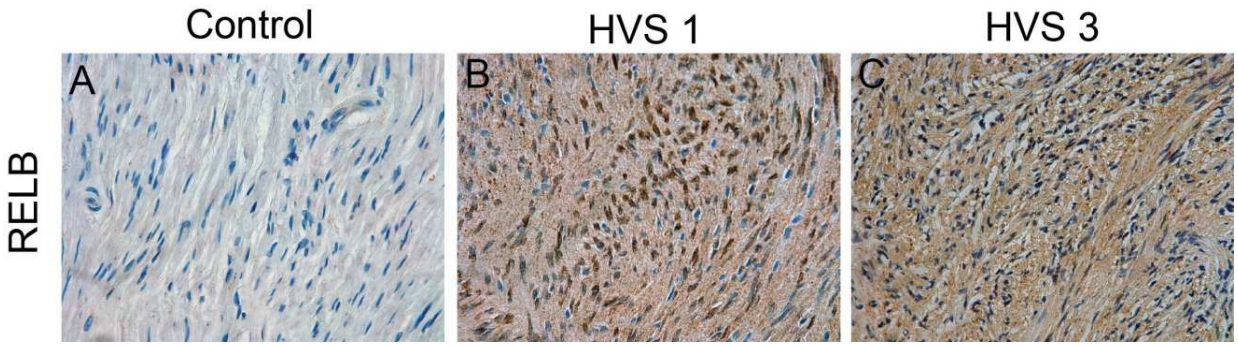

Figure 18. Increased cytoplasmic and nuclear RELB reactivity observed by immunohistochemistry in human schwannomas. (**A**,**B**, and **C**) IHC of RELB in control human nerve tissue (**A**) and human vestibular schwannomas (HVS,**B** and **C**). Note the intense nuclear signal of RELB in vestibular schwannomas, in particular the tumor shown in **B**. Original magnification x400.

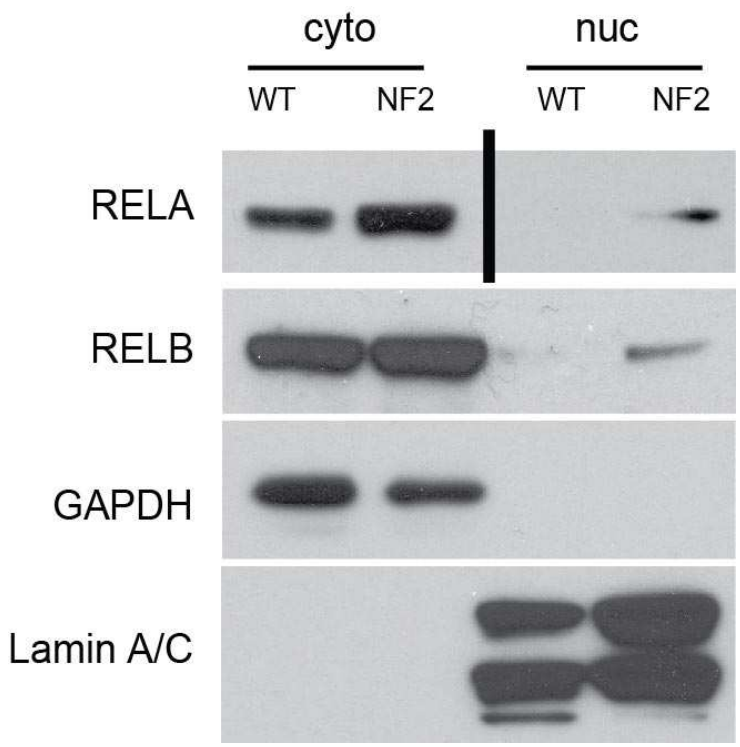

Figure 19. Increased cytoplasmic and nuclear RELA and RELB seen by subcellular fractionation in murine schwannomas. Subcellular fractionation and subsequent SDS-PAGE Western Blot of primary Trigeminal nerve tissue from age-matched eight month old WT and NF2-KO mice demonstrating a relative increase in cytoplasmic and nuclear levels of RELA and RELB proteins. The black line separating cytoplasmic and nuclear fractions in the RELA blots indicate different exposures of the cytoplasmic and nuclear fractions. cyto = cytoplasmic fraction, nuc = nuclear fraction.

Schwannomas exhibit an increase in NIK and fragments of the NIK kinase domain

Considering that our data indicated both the canonical and non-canonical NF-κB pathways were activated, we decided to look for upstream NF-κB regulators that are known to activate both pathways. MAP3K14/NIK, a protein kinase, was first identified as an activator of the canonical pathway but is now better known as an essential regulator of the non-canonical pathway [126, 132, 169]. NIK-deficient human patients have been described, and isolated cells from these patients were deficient in both canonical and non-canonical NF-κB activation [170]. Further implication of NIK comes from previous studies utilizing NIK mutant and knockout mice, which exhibit decreased basal levels of Rel family proteins, suggesting that NIK signaling influences the overall levels of NF-κB transcription factors present in cells [171, 172]. If NIK does indeed regulate the level of Rel family proteins present in cells, then an increase in NIK signaling could explain the overall increase seen schwannomas. Whole lysate SDS-PAGE analysis of primary nerve tissues from WT and NF2-KO mice for NIK revealed accumulation of fragments of the kinase domain of NIK the NF2-KO nerves, in particular a band that migrated around 55 kilodaltons (**Figure 20A**). We also observed the presence of this 55 kD fragment of the kinase domain (p55 NIK) in three of three analyzed human vestibular schwannomas (**Figure 20B**). In addition to this fragment, we saw a remarkable increase in full length (FL) NIK in the human tumors, which typically migrates around 120 kD. In an expanded panel of murine tissues analyzed by SDS-PAGE, we saw a roughly three fold increase in FL NIK

in NF2-KO nerves (**Figure 21**). IHC localized the increase in NIK to the tumorigenic cells in both human and murine schwannoma (**Figure 22 and 23**). Since NIK is a constitutively activated kinase [134], the relative increase in NIK between WT and NF2-KO tissues as measured by our Western Blotting studies could possibly explain the downstream activation of NF-κB. Additionally, since cleavage of NIK to generate a stable, proteasome resistant fragment of the kinase domain has already been observed as a driver of cancer [131], we were intrigued to study the 55 kD fragment accumulating in both human and mouse schwannoma samples.

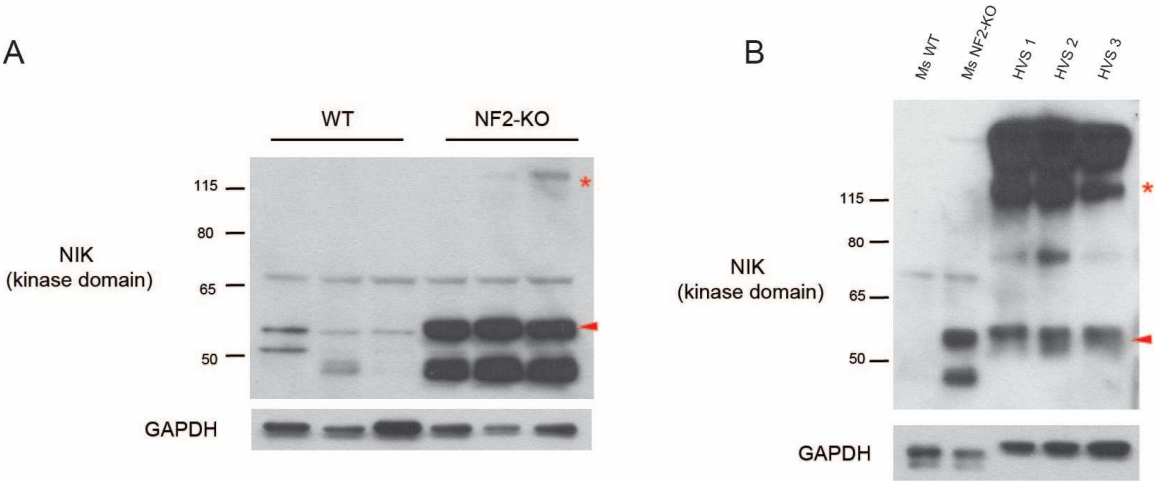

Figure 20. Accumulation of NIK and fragments of the NIK kinase domain in murine and human schwannomas. (**A**) Whole lysate SDS-PAGE Western blot demonstrating the accumulation of multiple fragments of the kinase domain of NIK in NF2-KO nerve tissue, including a 55 kD fragment indicated by the red arrowhead. FL NIK can be identified by the red asterisk. All tissues are derived from eight month old mice. (**B**) Similar to **A**, Western blot showing accumulation of a 55 kD fragment of the NIK kinase domain in three human vestibular schwannomas (HVS). Note the increase in FL NIK seen in human tumors, indicated by the red asterisk. The far two left lanes are mouse WT and NF2-KO tissues, respectively.

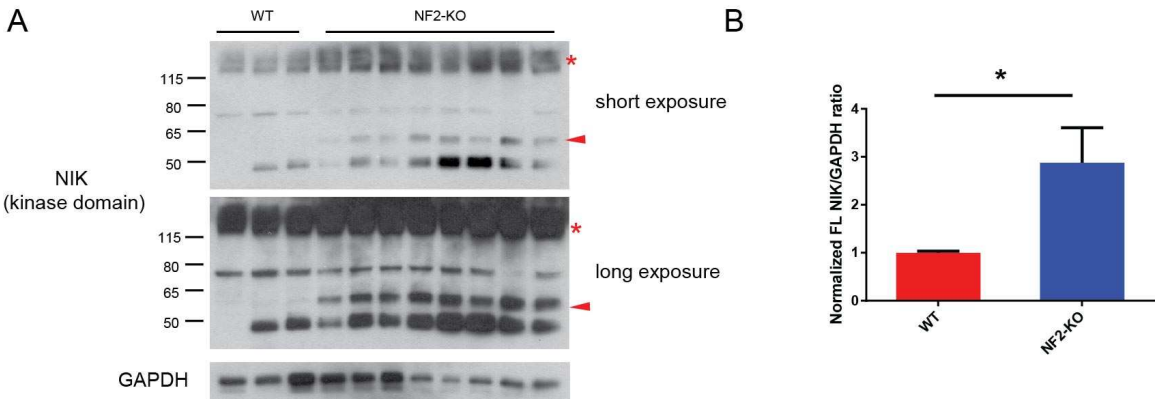

Figure 21. Accumulation of FL NIK and p55 NIK in murine schwannomas. Whole lysate SDS-PAGE Western blot of mouse primary nerve tissue showing accumulation of both the 55 kD fragment of the NIK kinase domain (red arrowhead) as well as FL NIK (red asterisk). All tissues shown are from eight month old mice, save for the far two right lanes, which are from 12 month old mice. (**B**) Densitometry of FL NIK (red asterisk) in **A**. ns = not significant, * = $P < .05$, ** = $P < .01$, *** = $P < .001$; unpaired Student's T test. Error bars represent SEM.

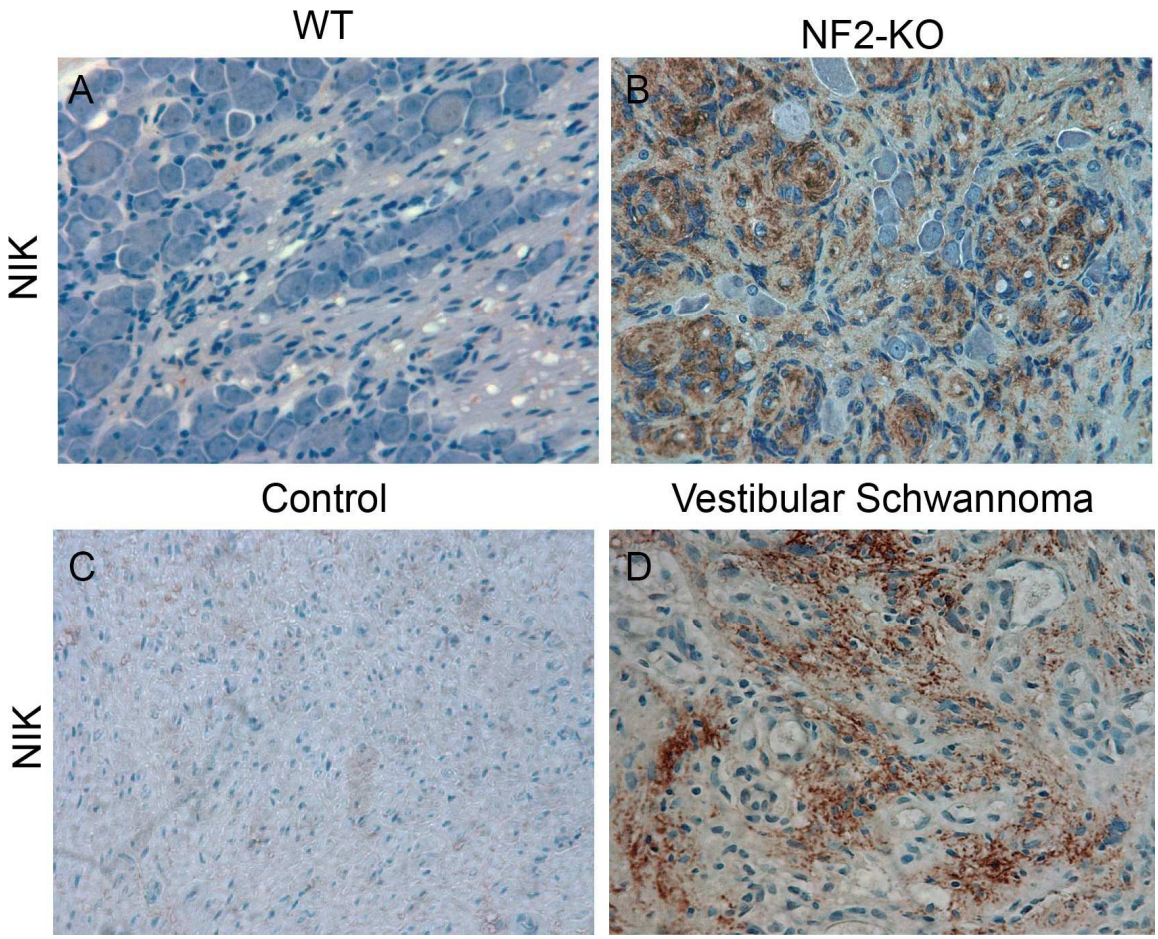

Figure 22. Immunohistochemistry localizes NIK accumulation to tumorigenic cells in schwannomas. (**A** and **B**) IHC of NIK in age-matched 12 month old murine WT (**A**) and NF2-KO DRG (**B**). (**C** and **D**) NIK IHC of control human nerve (**C**) and human vestibular schwannoma tissue (**D**). Original magnification x400.

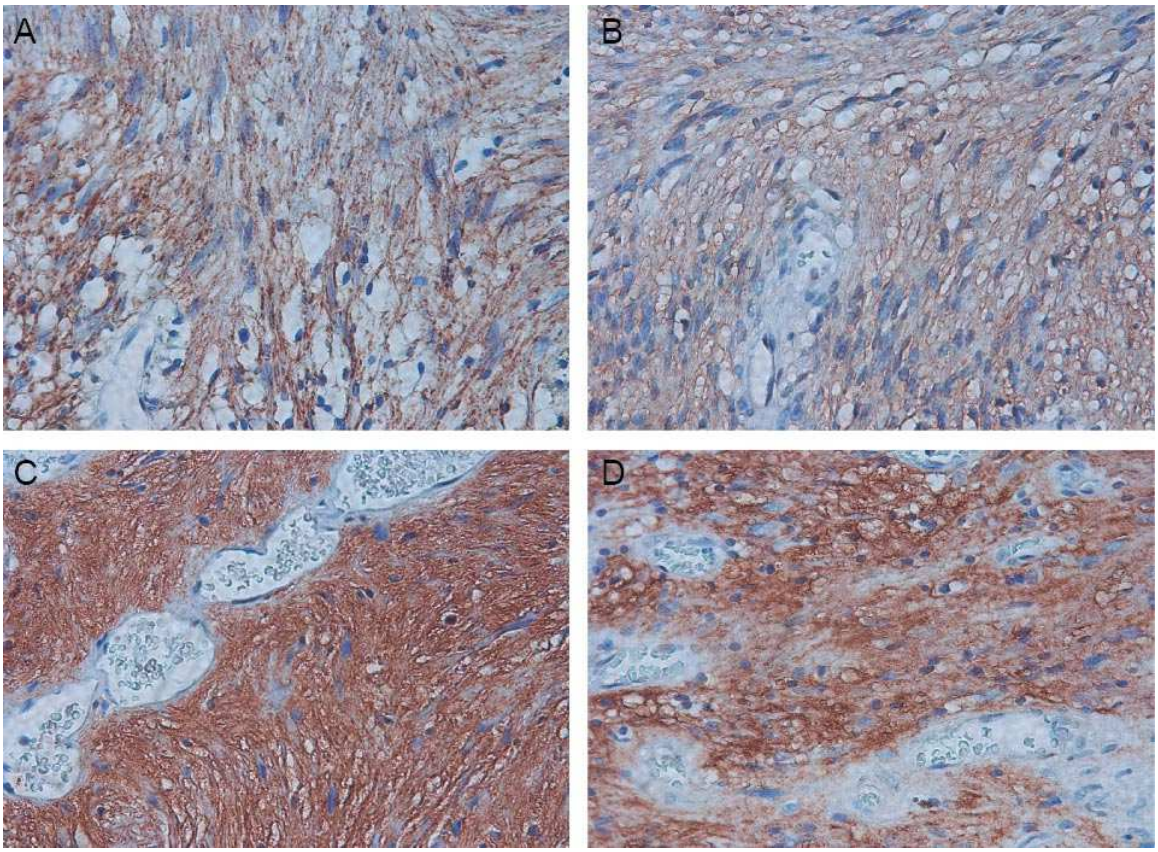

Figure 23. Expanded immunohistochemical panel of NIK-positive human schwannomas. (**A**-**D**) IHC of NIK in four different human schwannomas. Original magnification x400.

Caspase-8 cleaves NIK to generate a fragment of the kinase domain

To our knowledge, only two previous studies have identified fragments of NIK and the proteases responsible for the cleavage event. In the study mentioned previously [131], the authors found that a fusion cIAP2-MALT1 protease cleaved NIK at Arg-325, removing NIK's TRAF3 binding domain. Importantly, this study showed that wild type (WT) MALT1 does not demonstrate any protease activity on NIK. Another study found that the cysteine-protease Caspase-8 was capable of cleaving NIK, generating fragments of the N and C-terminus [173]. The authors inferred from the migration of the fragments the actual sites of cleavage, and went on to build constructs that they used in overexpression studies. No 55 kD fragment of the kinase domain was observed, and none of the predicted NIK fragments were capable of activating NF-κB. In this study, however, antibodies were used against the N and C-terminus of NIK, but no antibodies directed to internal regions of NIK were used. Our Western Blotting experiments in schwannomas employed an antibody targeting an internal region of NIK surrounding Gly-659 of the kinase domain. Thus, it remains an open question whether Caspase-8 cleavage of NIK can generate an internal fragment of NIK. We found that co-transfection of NIK and Caspase-8 in 293T cells resulted in the cleavage of NIK, generating a 55 kD fragment of the kinase domain (**Figure 24**). CrmA, a caspase inhibitor with high affinity for Caspase-1 and Caspase-8, inhibited Caspase-8 activation as seen by the abolishment of p43 and p18 Caspase-8 fragments. Procaspase-8 monomers are activated by dimerization and subsequent interchain proteolysis [174, 175]. CrmA inhibition of caspase

activity also prevented cleavage of NIK. To confirm this cleavage event was specific to Caspase-8, we performed an *in vitro* cleavage assay with purified NIK and activated Caspase-8 (**Figure 25**), demonstrating that Caspase-8 does indeed cleave NIK, producing a 55 kD fragment of the kinase domain. We did not detect any differences in Caspase-8 at the RNA level in NF2-KO tissues, but we did observe a decrease in Procaspase-8, which could mean increased processing of Procaspase-8 into its activated form in schwannoma samples (**Figure 26**).

Caspase cleavage-mediated regulation of kinase function is a known phenomenon, with the bulk of studies focusing on this event in a pro-apoptotic context [176]. Importantly, NIK is a member of the STE family of kinases, in which there are many examples of caspase cleavage removing a negative regulatory region of the kinase, rendering the kinase constitutively active. HPK1, MST1, MST2, MST3, PAK2, and MEKK1 are all STE family kinases that are cleaved and activated by caspases (**Figure 27**) [177-188]. This supports the notion of caspase cleavage activating NIK and subsequent downstream signaling.

Despite its well-established role as an initiator of apoptosis, multiple studies have identified Caspase-8 as an activator of NF-κB [173, 189, 190]. Two of these studies identified a physical interaction between Caspase-8 and NIK, and went

on to show that NF-κB activation by Caspase-8 required NIK. Through a co-immunoprecipitation experiment in 293T cells, we also confirmed that NIK and Caspase-8 are found in together in a protein complex (**Figure 28**). Interestingly, both Caspase-8 and NIK-deficient human patients have been described, and both manifest as a primary immunodeficiency with substantially impaired lymphocyte and Natural Killer (NK) cell function [170, 191]. Basic studies of Caspase-8 and NIK deficient cells support these observations, indicating that the impaired immunity seen in these patients results from defective activation of NF-κB [124, 192-194].

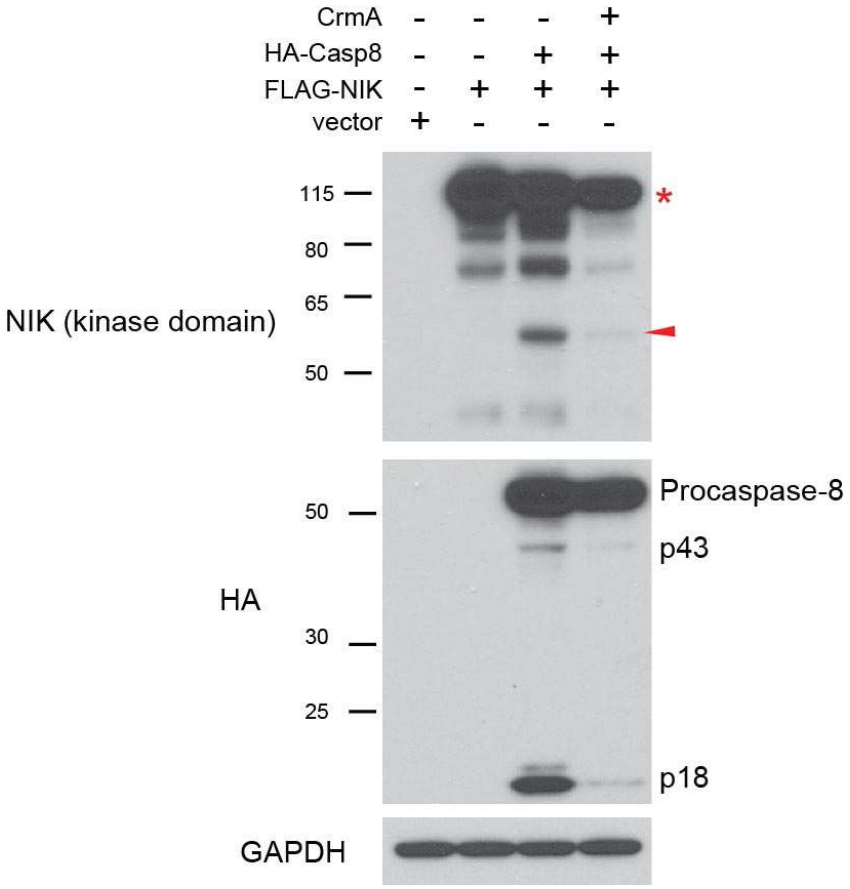

Figure 24. Caspase-8 is sufficient to induce cleavage of NIK, resulting in a 55 kD fragment of the kinase domain. Transfection experiment in 293T cells demonstrating that caspase-8 activity is sufficient to induce the cleavage of NIK, resulting in a 55 kD fragment of the kinase domain. CrmA, a protein isolated from smallpox, is a caspase inhibitor that preferentially inhibits Caspase-8 and Caspase-1. The red asterisk indicates FL NIK, while the red arrowhead points to the 55 kD fragment of the kinase domain.

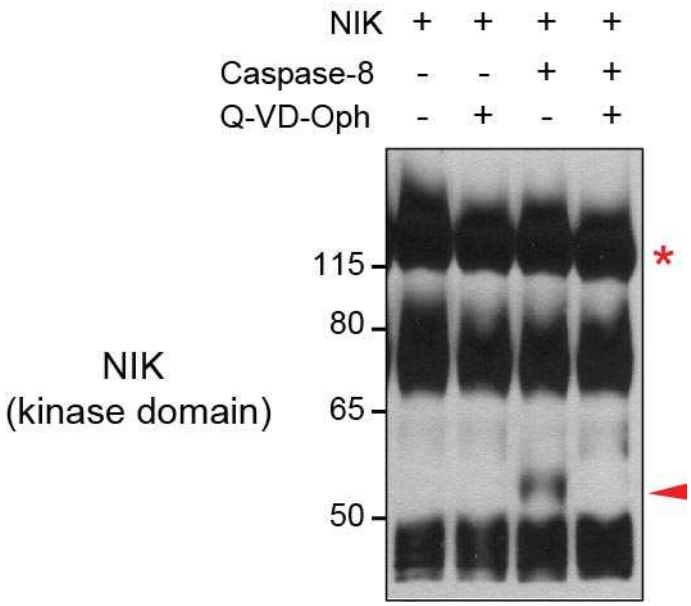

Figure 25. Caspase-8 is sufficient to cleave NIK *in vitro.* Purified NIK protein was incubated in the presence activated Caspase-8, 10 uM of Q-VD-Oph (a pan-Caspase inhibitor), or both for 1 hour. Incubation of NIK with activated Caspase-8 was capable of producing a 55 kD fragment of the NIK kinase domain. The red asterisk indicates FL NIK, while the red arrowhead points to the 55 kD fragment of the kinase domain.

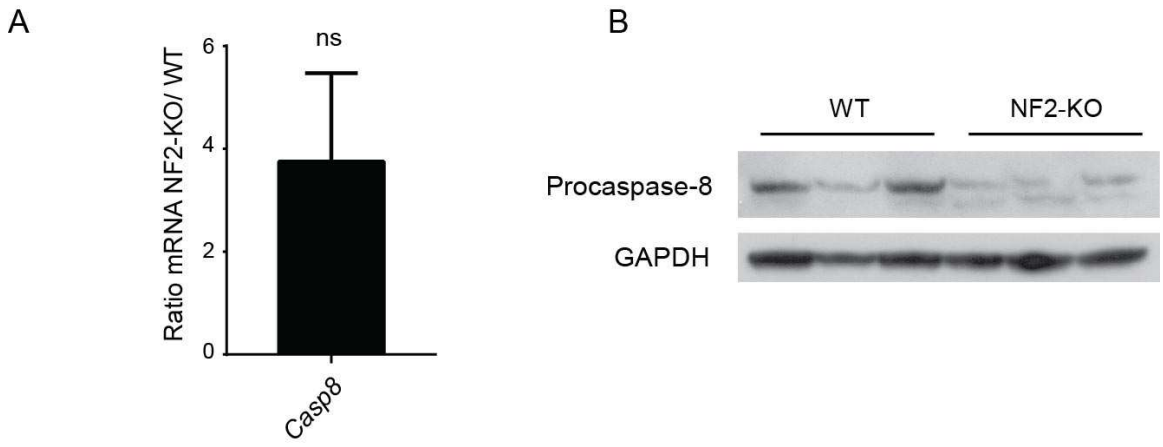

Figure 26. Decreased levels of Procaspase-8 seen at the protein level in schwannomas. (**A**) qRT-PCR of 8 month old WT and NF2-KO primary nerve tissues (seven mice total, 3 WT, 4 NF2-KO). Caspase-8 mRNA trended higher in NF2-KO tissues but no significant difference was seen between genotypes. ns = not significant, unpaired Student's T-test. Error bars represent SEM. (**B**) Western Blotting of whole lysate SDS-PAGE samples revealed a decrease in Procaspase-8 at the protein level in NF2-KO tissues, suggestive of possible Caspase-8 activation.

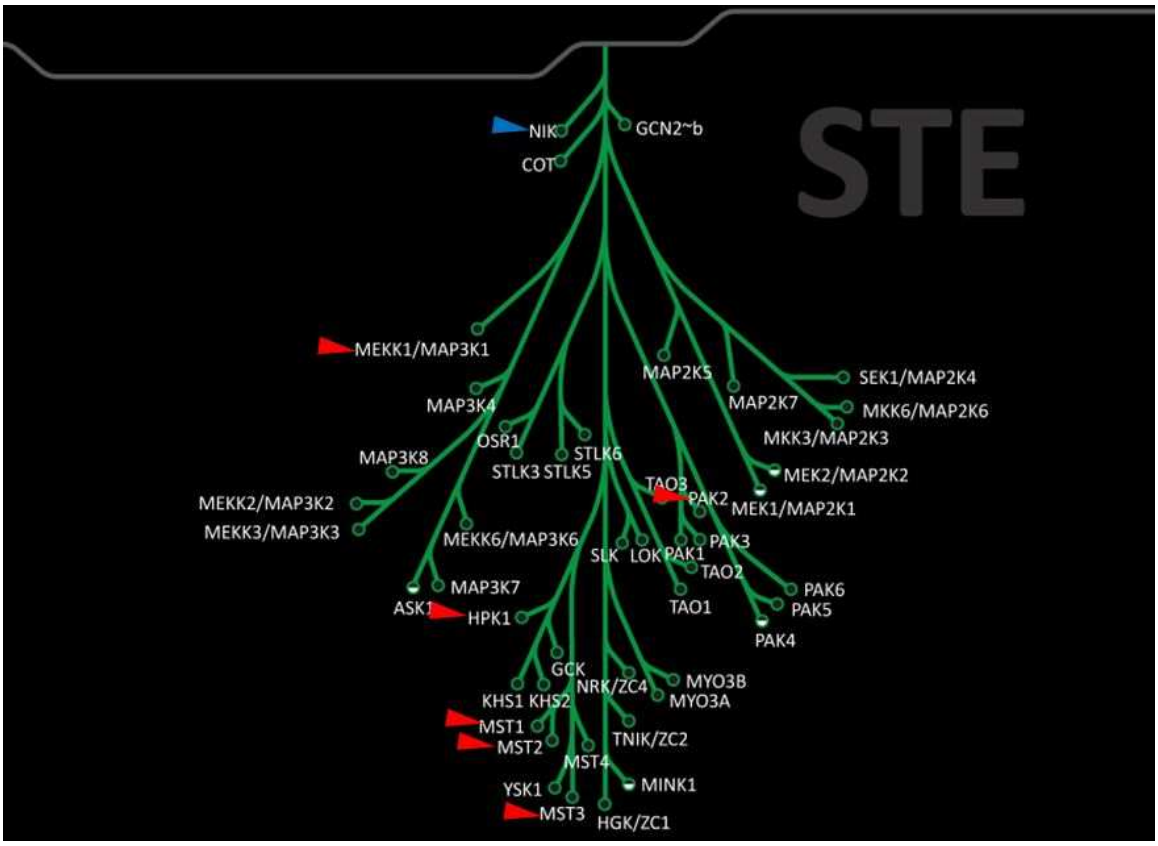

Figure 27. Diagram indicating which STE family kinases are cleaved by caspases. Phylogenetic tree of STE family kinases indicating which members are cleaved and activated by caspases. NIK is identified by the blue arrowhead, while other STE family kinases regulated by caspase cleavage are identified with red arrowheads. This image has been modified from the Promega website (available at the URL http://www.promega.com/a/kinase/).

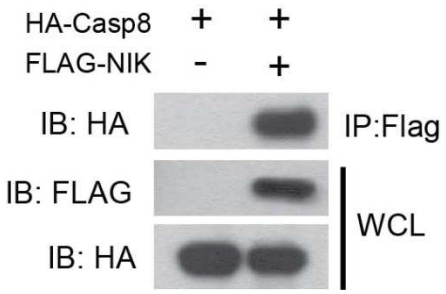

Figure 28. Caspase-8 co-immunoprecipitates with NIK in 293T cells. Co-Immunoprecipitation experiment in 293T cells. FLAG-NIK (10 ug/10 cm dish) was co-transfected with HA-Casp8 (1 ug/10 cm dish) in 293T cells. FLAG-NIK was immunoprecipitated with FLAG antibody-conjugated agarose beads and samples were then separated by SDS-PAGE for subsequent Western Blotting. IB = Immunoblot, IP = Immunoprecipitation, WCL = Whole cell lysate.

Bioinformatics analysis identifies clusters of Caspase-8 cleavage sites in NIK

Since we established that Caspase-8 does indeed cleave NIK to generate a 55 kD fragment of the kinase domain, we then used Bioinformatics tools to identify putative sites of cleavage in NIK. To this end, we employed two different software programs, Cascleave 2.0 [158, 159] and SitePrediction [160]. Both programs utilize features that are important to known caspase cleavage motifs, such as amino acid preference, secondary structure, and solvent accessibility, for the prediction of novel motifs. Caspases recognize and cleave scissile bonds featuring a P4-P3-P2-P1-P1'-P2'-P3'-P4' motif, with the P1 residue being an Aspartic acid (Asp, D) or, in certain cases, a Glutamic Acid (Glu, E) residue. Caspase-8 prefers an P4-P1 motif matching the pattern of IETD, but it is important to note that all caspases possess overlapping specificities and there are no absolute rules governing their cleavage, save for the D or E residue in the P1 position [195]. Unexpectedly, the output from both software programs predicted clusters of N and C-terminal Caspase-8 cleavage sites that give rise to an approximately 55 kD fragment of the kinase domain, with each cluster possessing multiple sites within roughly 20 residues of one another. Specifically, both programs predicted the cleavage of D291 and D308, as well as D801, D807, D808, and D822 (**Figure 29**). The D298 site was predicted by Cascleave 2.0 but not by SitePrediction.

Clusters of cleavage sites have been observed in caspase substrates before, and their presence would likely increase the probability of a cleavage event for the substrate in that region of the protein [196]. We looked at the conservation of these cleavage sites across other mammalian species, as conservation would suggest that these sites may subserve some critical function in NIK biology. In the N-terminal cluster, cleavage sites homologous to D308 in human NIK were present in chimp, macaque, rat, mouse, dog, and cow NIK (**Figure 30 A**). The additional cleavage site corresponding to D291 in human NIK was also present in chimp and macaque NIK. Virtually all residues included in and around the C-terminal cleavage motifs were conserved in all tested species (**Figure 30 B**).

To further characterize the regions of NIK present in our 55 kD fragment in murine schwannomas, we probed these samples with a peptide antibody targeting murine NIK 311:328 (**Figure 31**). The corresponding human residue to murine NIK amino acid (AA) 311 is AA 309, which would represent the hypothesized extreme N-terminus of our 55 kD cleavage fragment. At least two fragments appeared to migrate around 55 kD in the NF2-KO tissues, providing additional evidence that the fragments appearing in schwannomas are the result of cleavages occurring in the N and C-terminal Caspase-8 cleavage site clusters located at roughly AA 300 and 800, respectively.

After mapping the location of these cleavage sites onto the structure of human NIK, we made the observation that cleavage at the N and C-terminus would

liberate NIK from all known mechanisms of negative regulation and destabilization (**Figure 32**). In the N-terminus of NIK, a fragment at the proposed cleavage sites would lose the TRAF3 binding domain (approximately residues 30-120) as well as the overwhelming majority of the negative regulatory domain (NRD, approximately residues 121-317) [125, 134, 197]. Recently, an Inhibitor of Apoptosis (IAP) binding motif was discovered in the extreme N-terminus of NIK that increases the c-IAP1-mediated destabilization of NIK [198]. This motif would also be removed by a cleavage occurring near residue 300 in the N-terminus of NIK. Structural studies of deletion mutants of NIK indicate that deletions proximal to residues 348 would be expected to have competent NIK kinase function, with residues 348-377 in the N-terminus of NIK appearing to be critical to the kinase function of NIK [134]. In the C-terminus of NIK, IKKα phosphorylates NIK at residues 809, 812, and 815, constituting a negative feedback mechanism that destabilizes NIK and attenuates non-canonical signaling [199]. In this case, cleavage at residues 801, 807, and 808 would fully relieve the NIK fragment of IKKα-mediated negative feedback. The NRD of NIK has been shown to include a cis-acting element that disrupts the association of NIK with IKKα [197]. Again, a fragment at the proposed sites of cleavage would no longer be subject to this regulation, as this cis-acting element would be lost in an N-terminal cleavage event.

A

	residue	P4-P4' Site	Cascleave 2.0	SitePrediction
N-terminus	291	ACVD-SQKP	yes	yes
	298	PLPD-PHLS	yes	no
	308	ACVD-SPKP	yes	yes
C-terminus	801	LSID-SLSL	yes	yes
	807	SLSD-DSEK	yes	yes
	808	LSDD-SEKN	yes	yes
	822	SSRD-TLSS	yes	yes

B

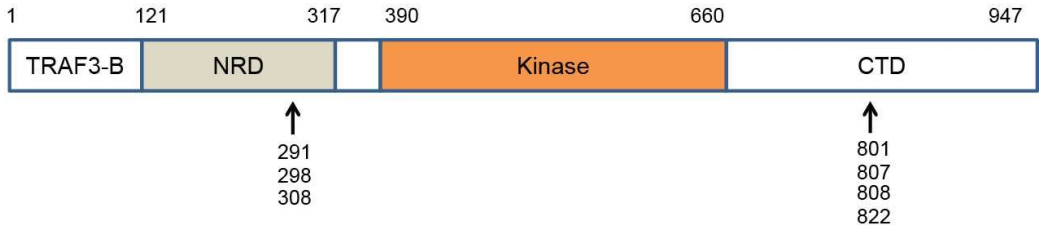

Figure 29. Computational prediction of caspase-8 cleavage sites. (**A**) Table displaying the prediction of human NIK cleavage by Caspase-8 in two different software programs, Cascleave 2.0 and SitePrediction. The combination of any of the N-terminal cleavage site cluster (D291, D298, D308) and C-terminal cleavage site cluster (D801, D807, D808, and D822) results in a roughly 55 kD fragment of the kinase domain. (**B**) Mapping of cleavage sites onto the structure of human NIK. Abbreviations are as follows: TRAF3-B = TRAF3 binding domain, NRD = Negative Regulatory domain, Kinase = Kinase domain, and CTD = C-terminal domain.

A

(H. sapiens)	285	GKLA-CVDSQKPLPD-PHLSKLACVDSPKPLPGPHLEPSCLSRGAHE	329
(P. troglodytes)	285	GKLA-CVDSQQPLPD-PHLSKLACVDSPKPLPGPHLEPSCLSRGAHE	329
(M. mulatta)	285	GKLA-CVDSQQPLPH-PHLSKLACVDSPKPLPGPHLEPSCPSRGAHE	329
(M. musculus)	286	DKLA-GVSGQRPLPGPPHLSQLAHGDSQKPLPGPHLESSCPSRGALE	331
(R. norvegicus)	286	DKLA-AVSGQRPLPGPPHLSKPAYRDSQKPLPGPHLESSCLSREALE	331
(C. lupus)	286	NKLT-CIDSQQPLSG-PHLGKLACVDSQKPVPGPCLEPRCPSRGTRE	330
(B. Taurus)	283	GKLTNCVDDQQPLPG-PHLGRLACADSQKPLPSPHLKPSFPSRGSRD	328

B

(H. sapiens)	794	ILSCLSIDSLSLSDDSEKNPSKASQSSRDTLSSGVHSWSSQA	835
(P. troglodytes)	794	ILSCLSIDSLSLSDDSEKNPSKASQSSRDTLSSGVHSWSSQA	835
(M. mulatta)	794	ILSCLSIDSLSLSDDSEKNPSKASQSSRDTLSSGVHSWSSQA	835
(M. musculus)	789	ILSCLSIDSLSLSDDSEKNPSKASQSSRDTLSSGVHSWNSQA	830
(R. norvegicus)	789	ILSCLSIDSLSLSEDSEKNPSKASQSSRDTLSSGVHSWSSQA	830
(C. lupus)	802	ILSCLSIDSLSLSDDSEKNPSKASQSSRDTLSSGVHSWSSQA	843
(B. Taurus)	800	ILSCLSVDSLSLSDDSEKNPSKASQSSRDTLSSGVHSWSSQA	841

Figure 30. Caspase cleavage sites on human NIK are conserved across mammalian species. (A and **B)** Multiple sequence alignment of human NIK N-terminal cleavage cluster (**A**) and C-terminal cleavage cluster (**B**). Note that the cleavage site corresponding to human NIK residue D308 is conserved across all species, while all the cleavage sites in the C-terminal cleavage cluster are conserved. Blue highlighting indicates the cleaved Aspartic Acid residue, while yellow highlighting indicates the eight amino acid caspase cleavage motif.

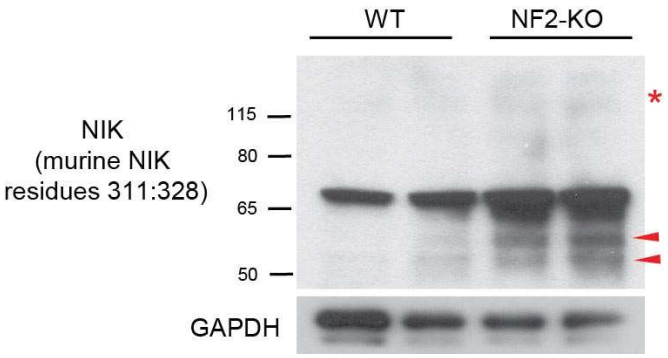

Figure 31. Further characterization of the 55 kilodalton fragment of the NIK kinase domain in murine schwannomas using a peptide antibody targeting internal NIK residues. Whole lysate SDS-PAGE Western Blot of primary murine Trigeminal nerve tissue. A custom antibody targeting a peptide corresponding to residues 311:328 of murine NIK was used. Residue 311 in murine NIK corresponds to residue 309 in human NIK. The antibody detected at least two fragments ~55 kD in NF2-KO mice. All tissues are derived from eight month old mice. The red asterisk indicates FL NIK, while the red arrowhead points to the 55 kD fragment of the kinase domain.

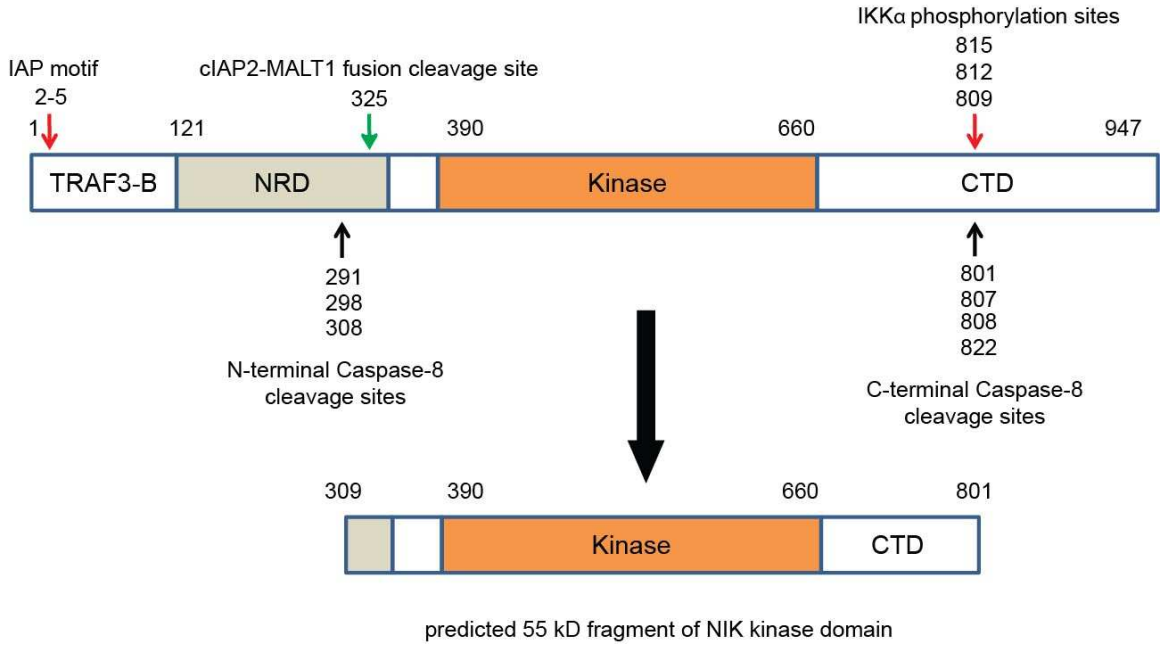

Figure 32. Caspase-8 cleavage of NIK renders the resulting kinase fragment resistant to known mechanisms of regulation of wild type NIK. Caspase-8 cleavage sites mapped onto the structure of human NIK. The c-IAP2/MALT1 fusion protein cleavage site is also mapped onto the structure of NIK to demonstrate the location of another known cleavage site giving rise to a proteome-resistant fragment of NIK lacking the N-terminal TRAF3 binding domain. Loss of the IAP binding motif in the N-terminus would render NIK more resistant to c-IAP1-mediated destabilization. IKKα phosphorylation sites are included since they also are known to regulate NIK stability. The phosphorylation of these sites by IKKα serves as a negative feedback loop, destabilizing NIK. Finally, loss of the NRD would remove a cis-acting element previously identified to disrupt NIK's association with IKKα. Cleavage at the proposed sites would give rise to a fragment of the NIK kinase domain absent any known negative regulatory region present in NIK. Abbreviations are as follows: TRAF3-B =

TRAF3 binding domain, NRD = Negative Regulatory domain, Kinase = Kinase domain, and CTD = C-terminal domain.

p55 NIK demonstrates increased protein stability and activates NF-κB

To test the hypothesis that cleavages in the N and C-terminal clusters result in enhanced NIK stability, we generated a construct encoding residues 309-801 NIK and transfected this construct or one encoding FL NIK into 293T cells. We then pulsed cells in Cyloheximide (CHX), a protein translation inhibitor, for time points up to 24 hours. The inhibition of protein translation enables us to view NIK protein levels purely as a function of protein degradation. The first observation we made was that 309-801 NIK does indeed migrate at 55 kD, as predicted (**Figure 33**). We also noticed increased basal stability over FL NIK. By four hours of incubation with CHX, FL NIK levels had substantially decreased, and went on to decrease more at the ten and 24 hour time points. 309-801 NIK protein levels, however, did not appear to significantly change over the course of 24 hours. These data indicate that 309-801 NIK encodes a 55 kD fragment of the kinase domain with a remarkable increase in stability at the protein level when compared to FL NIK.

Previous studies utilizing fragments of the NIK kinase domain suggest that a fragment encoding AA 309-801 of NIK would retain strong kinase activity toward IKKα, as a smaller fragment comprised of AA 329-667 was sufficient to phosphorylate IKKα *in vitro* [134]. In fact, their data demonstrates that fragments of 329-667 NIK and 329-747 both possess increased kinase activity toward IKKα compared to FL NIK, which is consistent with our reasoning outlined above. To confirm that the 309-801 NIK fragment does activate downstream NF-κB

signaling, we transfected the 309-801 NIK construct into 293T cells. 309-801 NIK, along with FL NIK, was sufficient to activate canonical NF-κB as measured by induction of phospho-S536 RELA, an IKKβ dependent site [200], and an increase in RELB (**Figure 34A**). Both constructs also activated non-canonical signaling, indicated by the processing of p100 to p52. To further assess canonical pathway activation, we transfected constructs into 293T cells that have stably integrated a consensus NF-κB responsive promoter upstream of a GFP reporter. Both FL NIK and 309-801 NIK robustly activated GFP expression (**Figure 34B**). Finally, we also validated an interaction of 309-801 NIK with IKKα through a co-immunoprecipitation experiment in 293T cells (**Figure 35**).

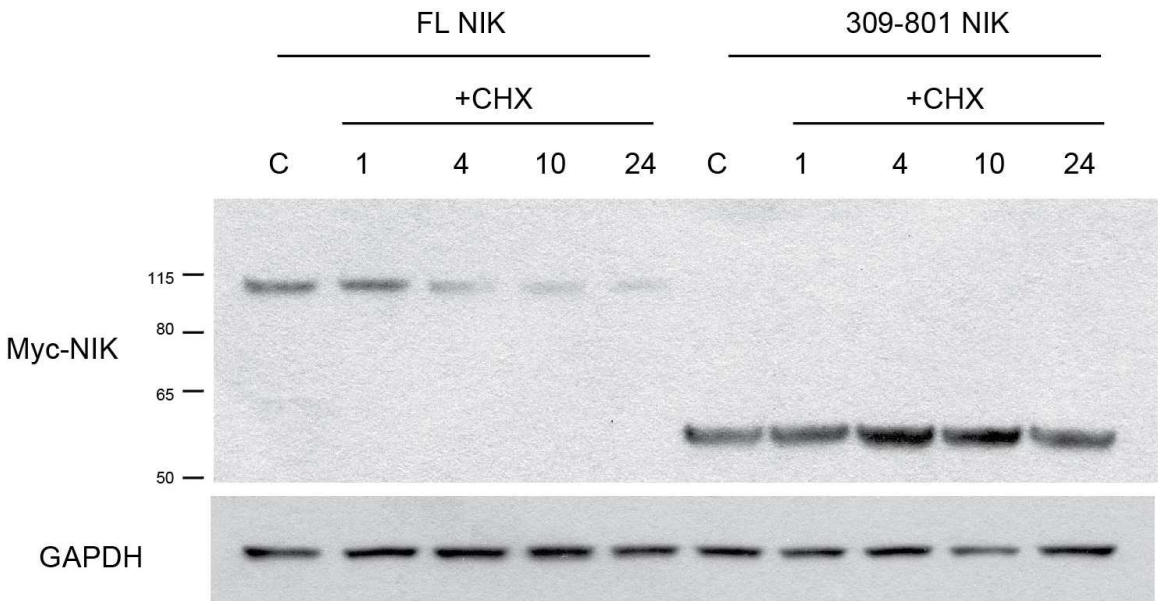

Figure 33. 309-801 NIK demonstrates increased stability over FL NIK. Transfection of 293Ts with the indicated plasmids. Cycloheximide, a protein translation inhibitor, was added to cell culture medium and the protein levels of FL NIK or 309-801 NIK were monitored over a time course (labeled numbers above blots are hour time points). The addition of Cycloheximide allows for the observation of differences in rates of protein degradation. 309-801 NIK is significantly more stable than FL NIK, owing to the lack of negative regulatory regions present in the wild type protein.

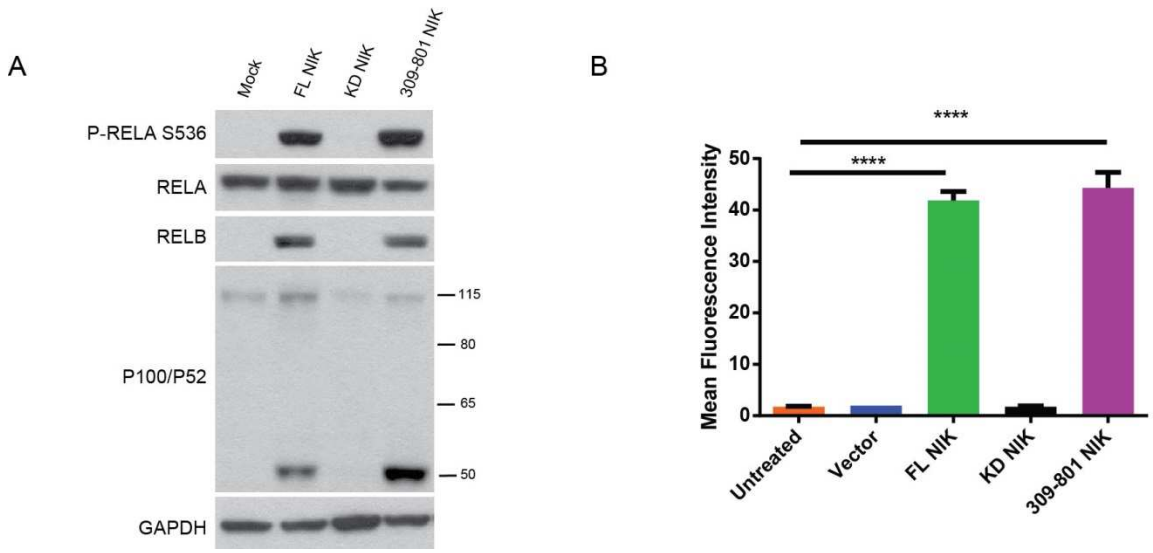

Figure 34. 309-801 NIK is sufficient to activate canonical and non-canonical NF-κB signaling. (**A**) Transfection of 293T cells with the indicated plasmids. The S536 phosphorylation of RELA and accumulation of RELB are indicative of activation of the canonical arm of NF-κB, while processing of p100 to p52 demonstrate activation of the non-canonical arm of NF-κB. (**B**) Transfection of Cignal-293T cells possessing an NF-κB responsive promoter upstream of a GFP reporter. FL NIK and 309-801 NIK robustly transactivate canonical NF-κB gene expression. FL NIK = Full Length NIK, KD NIK = Kinase Dead NIK. **** = $P < .0001$; ANOVA with Bonferonni post-hoc analysis. Error bars represent SEM.

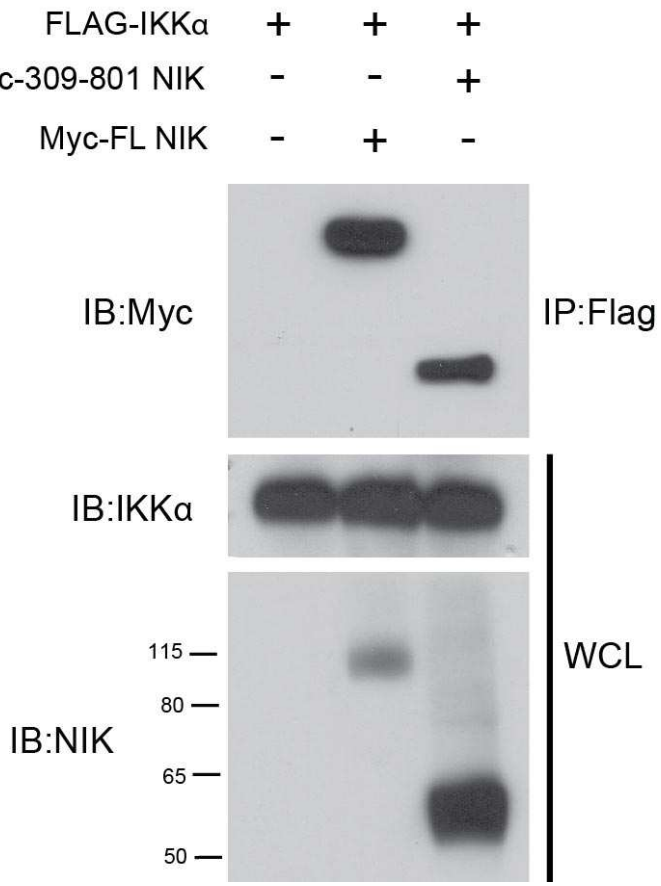

Figure 35. 309-801 NIK co-immunoprecipitates with IKKα in 293T cells. Co-Immunoprecipitation experiment in 293T cells. FLAG-IKKα (8 ug/10 cm dish) was co-transfected with Myc-FL NIK/Myc 309-801 NIK (3 ug/10 cm dish) in 293T cells. FLAG-IKKα was immunoprecipitated with FLAG antibody-conjugated agarose beads and samples were then separated by SDS-PAGE and proteins detected through Western Blotting. IB = Immunoblot, IP = Immunoprecipitation, WCL = Whole cell lysate.

NIK signaling regulates Schwann cell function and gene expression

NF2-deficient cell types have previously been described to demonstrate abnormalities in cell proliferation, survival, and adhesion [50, 54, 201, 202]. Now that we identified 309-801 NIK as a kinase-competent fragment of NIK with enhanced stability, we examined what functional effects it has on primary Schwann cells. We first confirmed that, in our culture conditions, passage one (P1) murine Schwann Cells are a homogenous population of mature S100+ Schwann cells (**Figure 36A**). We then transduced P1 Schwann cells with a Lentivirus stably inserting either an IRES-EGFP control or 309-801 NIK IRES-EGFP cassette. To observe for differences in cell cycle progression into or through S-phase, we pulsed both populations with the Thymidine analog EdU. Quantitation of Immunofluorescence staining revealed over a two-fold increase in EdU-positive nuclei in 309-801 NIK transduced Schwann cells, suggestive of an increase in cell proliferation (**Figure 36B** and **C**). To address this question a different way, we performed manual cell counting of both genotypes three days after initial seeding. This experiment revealed nearly a 1.5 fold increase in overall cell number in the 309-801 NIK transduced cells (**Figure 36D**). We next assessed 309-801 NIK transduced Schwann Cells for an increase in survival in response to growth factor starvation. After two days in starve media, nearly 50% of the 309-801 NIK transduced cells were still alive, whereas only 17% were alive in the IRES-EGFP control population (**Figure 36E**). In addition to its more appreciated role governing cell proliferation and survival, NIK/NF-κB signaling has also been shown to regulate cell adhesion [131]. We tested if 309-801 NIK

transduced Schwann cells display increased adhesion relative to IRES-EGFP controls on Poly-D-Lysine/Laminin coated plates. Using the iCelligence realtime cell monitoring assay, we noted a remarkable increase in cell adhesion through the first three hours after plating both populations of cells (**Figure 36F**).

Having established that 309-801 NIK does increase Schwann cell proliferation, survival, and adhesion, we now used qRT-PCR to see if 309-801 NIK was sufficient to induce a gene expression profile similar to that observed in human and murine schwannomas. As seen in **Figure 37A**, 309-801 NIK induces the transcription of four of the five Rel family transcription factors, all of which are NF-κB target genes, save for *Rela*. Since previous studies suggest that NIK signaling may regulate overall levels of Rel family transcription factors [171, 172], this experiment presents strong supporting data that NIK signaling could be responsible the increased expression of Rel family proteins in schwannomas.

We next examined the set of NF-κB target genes shown in **Figure 12** to be increased in both human and murine schwannomas. 309-801 NIK positively regulated the expression of all analyzed genes, save for *Ccnd1* (**Figure 37B**). Though 309-801 NIK only modestly increased the expression of *Bcl2*, a 2 fold or greater increase was seen in *Birc2*, *Birc3*, *Ccnd2*, *Erbb2*, and *Met*. In fact, the overall levels of induction by 309-801 NIK mirror those seen in **Figure 12C**, with *Birc2*, *Birc3*, and *Met* increasing in expression the most in NF2-KO tissues relative to controls.

A

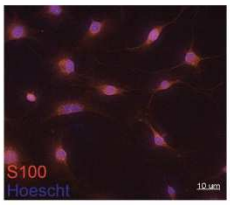

B

	IRES-EGFP	309-801 NIK	*P*-value
% EdU+ nuclei	16.5	33.5	< .0001

C

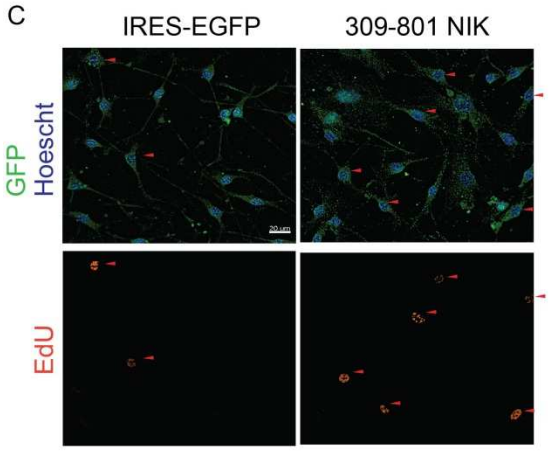

D

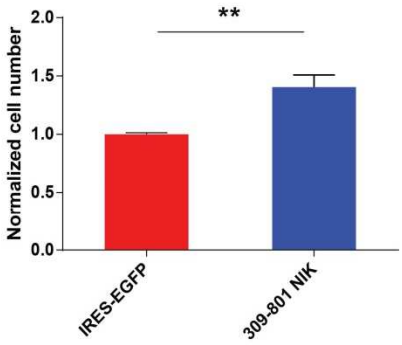

E

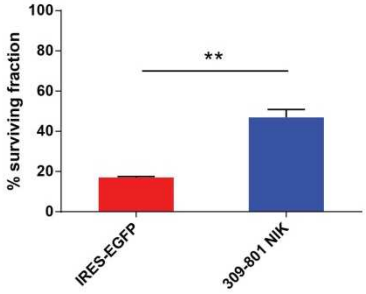

F

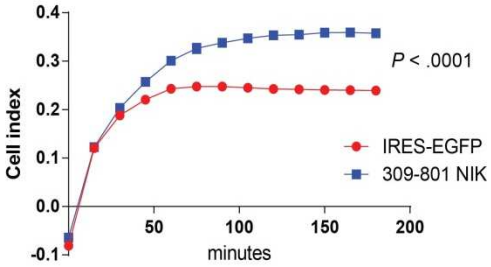

Figure 36. 309-801 NIK increases primary Schwann cell proliferation, survival, and adhesion. (**A**) S100 staining of Passage one WT Schwann cells, confirming they are a homogenous population of mature Schwann cells in our culture conditions. Hoescht is a nuclear stain. Original magnification x200. (**B**) Table quantitating EdU positive nuclei in both populations of Schwann cells. P1 primary Schwann cells were stably transduced with an IRES-EGFP control Lentivirus or 309-801 NIK IRES-EGFP Lentivirus. Cells labeled with EdU are those that have progressed into or through S-phase of the cell cycle, which is indicator of cell cycle progression. Over 400 cells were counted from three

biological replicates per genotype. $P < .0001$, Fischer's Exact test. (**C**) Representative images of EdU Immunofluorescence experiment with IRES-EGFP and 309-801 NIK transduced Schwann cells. Red arrowheads point to EdU positive nuclei. Original magnification x200. (**D**) Cell counting experiment over the course of three days demonstrating a nearly 50 percent increase in the 309-801 NIK transduced cell population. ** = $P < .01$, unpaired Student's T-test. (**E**) Cells transduced with 309-801 NIK demonstrate increased survival. Cells were plated in the evening and the following morning the media was changed to starve media absent growth factors for 48 hours. Over a 2.5 fold increase in cell survival was observed in the 309-801 NIK transduced population. ** = $P < .01$, unpaired Student's T-test. In **D** and **E**, the unpaired Student's T-test was used on raw cell counts to test for differences in the two populations. For presentation purposes, the data were then re-scaled and plotted as seen in the Figure. (**F**) iCelligence cell adhesion assay showing increased adhesion in 309-801 NIK transduced Schwann cells. The unpaired Student's T-test was used to test for a significance difference at the three hour time point. *** = $P < .001$. Error bars represent SEM.

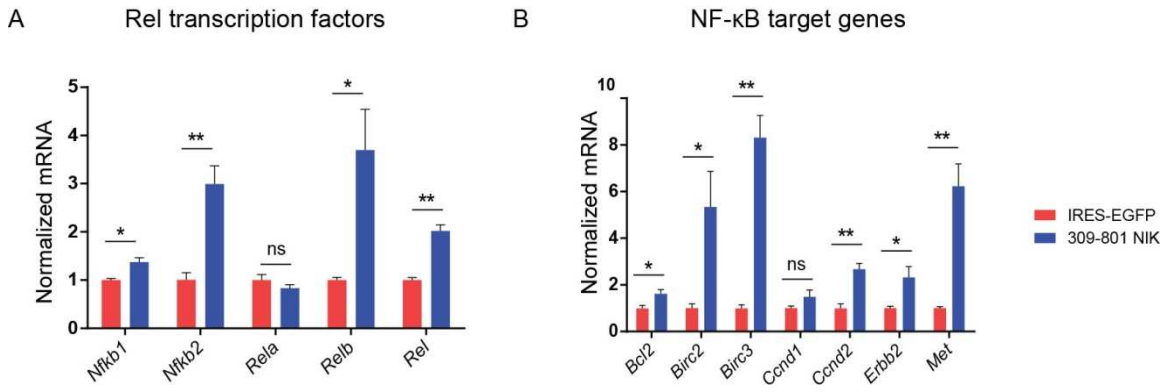

Figure 37. 309-801 NIK induces expression of Rel family transcription factors and NF-κB target genes that are deregulated in human and murine schwannomas. (**A**) qRT-PCR in primary Schwann cells showing that NIK induces the expression of NF-κB transcription factors. Note that with the exception of *Rela*, NIK induces the transcription of all Rel family transcription factors. (**B**) qRT-PCR experiment demonstrating that 309-801 NIK induces NF-κB target gene expression similar to that observed in human and murine schwannomas. ns = not significant, * = $P < .05$, ** = $P < .01$, *** = $P < .001$, unpaired Student's T-test. Each experiment included three biological replicates per genotype, per gene tested. Error bars represent SEM.

Evidence of persistent NIK signaling in schwannomas

NIK has previously been shown to direct its own expression, as well as its negative regulators TRAF2 and TRAF3 [203-205]. We demonstrate that NIK strongly induces the NF-κB target genes *Birc2* and *Birc3*, which encode c-IAP1 and c-IAP2, the other two members of the four-part E3 complex that degrades NIK (**Figure 37B**). qRT-PCR of primary murine nerve tissues demonstrated that the genes encoding NIK, TRAF2, and TRAF3 are also overexpressed in NF2-KO tissues (**Figure 38**). Thus, all four genes encoding the negative regulatory complex of NIK, as well as NIK itself, are found to be overexpressed in schwannomas. From these results we conclude that there appears to be persistent NIK signaling present in schwannomas that is no longer subject to negative regulation by the E3 complex comprised of TRAF2, TRAF3, and c-IAP1/2.

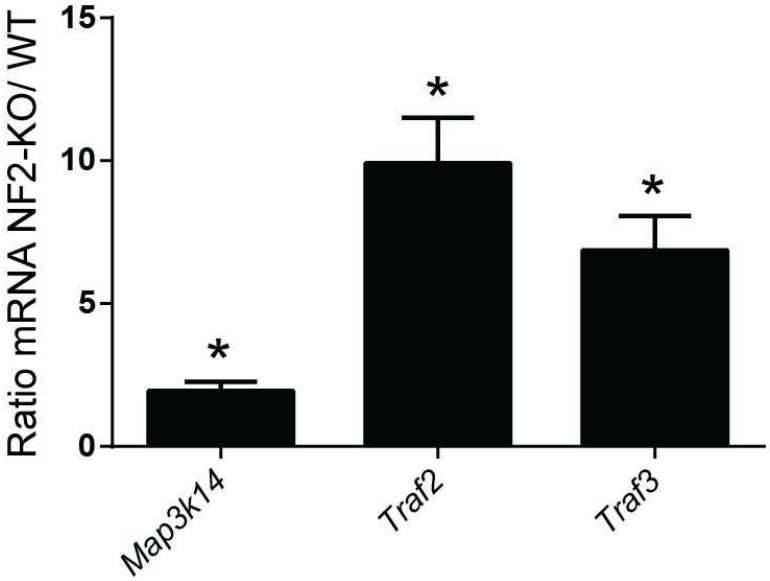

Figure 38. The genes encoding NIK, TRAF2, and TRAF3 are overexpressed in murine schwannomas. (A) qRT-PCR of *Map3k14*, *Traf2*, and *Traf3* in primary nerve tissues derived from eight month old WT and NF2-KO mice. The experiments testing *Traf2* and *Traf3* included three WT and four NF2-KO mice, while the experiment testing *Map3k14* included five WT and five NF2-KO mice. ns = not significant, * = $P < .05$; unpaired Student's T test. Error bars represent SEM.

DISCUSSION

In order to identify pathways deregulated in human schwannomas, we completed an unbiased genomics study of published microarray data. Through our analysis, we discovered activation of the NF-κB signaling pathway, with members of the signaling pathway and target genes seen at increased levels in schwannomas. We then validated these observations in both human tumors and our novel mouse model of NF2, described in **Chapter One**. As we examined these tumors for proteins that could possibly explain the apparent chronic activation NF-κB, we discovered that the tumors had accumulated NIK, as well as fragments of the NIK kinase domain. By combining bioinformatics and biochemical studies to support our observations, we characterized N and C-terminal clusters of Caspase-8 cleavage sites in NIK that give rise to roughly 55 kD fragments of the kinase domain that are absent any known NIK regulatory domains. Importantly, the single genetic manipulation of transducing primary, untransformed Schwann cells with an expression cassette encoding this 55 kD fragment of the kinase domain was sufficient to induce a transcriptional profile that is strikingly similar to those we identified in both human and murine schwannomas.

Though we have identified a number of genes regulated by NIK/NF-κB in schwannomas, of special interest are the receptor tyrosine kinases ERBB2 and MET. Both ERBB2 and MET have previously been identified as oncogenes and

drivers of cancer [206-209]. ERBB2 signaling is critical for Schwann cell development, proliferation, and survival, and its hyperactivation is believed to be a contributor to schwannoma formation [165, 210, 211]. Indeed, the ErbB family of receptors is viewed as a possible therapeutic target for schwannomas, with clinical trials currently in progress [212]. MET receptor expression has been shown to regulate schwannoma cell proliferation *in vitro* and, additionally, has been implicated in the angiogenesis observed in vestibular schwannomas [167]. The identification of NIK as the putative driver behind the expression of both ERBB2 and MET has tremendous implications for therapeutic strategies to treat these tumors, as it provides an additional approach to preventing the increased expression and activation of these oncogenes in schwannomas.

Through our studies in Schwann cells, we demonstrated that persistent NIK signaling is sufficient to explain the much of the NF-κB activation that we observed in schwannomas. The single exception is RELA, whose expression is not induced by 309-801 NIK in Schwann cells but is increased at the RNA and protein level in schwannomas. From this result we conclude that the increase in RELA is likely either through signaling promoted by the schwannoma microenvironment, or possibly a different pathway under control of NF2. Since RELA is the only Rel protein that is not encoded by a known NF-κB target gene, it makes sense that NIK activation in Schwann cells *in vitro* is insufficient to induce its expression. Further support of NIK regulating the increase in other REL proteins is seen in previous studies utilizing NIK mutant and knockout mice,

which have decreased levels of p100, p52, p50, RELB, and c-REL [171, 172]. One of these studies found no difference in RELA levels [172], while another did see a decrease in RELA [171]. Thus, there exists some conflicting data over whether NIK does regulate levels of RELA, and, if so, through what pathway, since *Rela* is not a known NF-κB target.

Schwann cells possess some unique characteristics among terminally differentiated cell types, especially in the context of nerve repair. In response to nerve injury, Schwann cells drive the process of Wallerian degeneration. Wallerian degeneration is a physiologic process preceding peripheral nerve regeneration where the axon distal to the site of injury is degenerated. In this process, Schwann cells de-differentiate and re-enter the cell cycle [213, 214]. Further, they increase TLR expression, become phagocytic, and release inflammatory mediators like IL-6 and MCP-1 to attract inflammatory cells to the site of injury [215-219]. Schwannomas appear to share many features of Schwann cells undergoing Wallerian degeneration. Studies have indicated that schwannomas resemble embryonic Schwann cell lineages at the molecular level, indicating de-differentiation [152, 153]. NF2-null cells are also deficient in the ability to growth arrest, implicating deregulation of their cell cycle [54, 201]. We also have data demonstrating murine schwannomas overexpress TLRs, IL-6, and MCP-1 (data not shown).

Interestingly, NIK/NF-κB activation is sufficient to explain aspects of the phenotypes seen in both schwannomas and Wallerian degeneration. Our data in primary Schwann cells demonstrate that NF-κB activation through NIK upregulates the expression of genes known to promote cell proliferation and survival. One study identified Met to be overexpressed in regenerating nerves when compared to naïve nerve samples [220]. We provide clear evidence of *Met* overexpression in schwannomas, and, further, that NIK is sufficient to induce its expression in primary Schwann cells. Additionally, a number of studies implicate NF-κB as a crucial regulator of both Schwann cell differentiation and myelination [68, 150, 151, 221]. The strongest support for this relationship comes from a study using transgenic mice expressing a non-phosphorylatable mutant of IκBα, which showed a direct role for NF-κB in nerve regeneration and re-myelination [222]. In the regenerating nerve, Schwann cells must transiently suppress the genes involved in myelination and then, later in the repair process, markedly upregulate their expression [223]. A similar process of temporal modulation of myelination gene expression is seen in the developing nerve, which significantly upregulates myelinating gene expression until adulthood, where steady-state expression is achieved [60]. Though clearly this relationship between NF-κB, Wallerian degeneration, and schwannomas is speculative, it does provide a compelling explanation for the similar phenotypes observed in both the physiologic (Wallerian degeneration) and pathologic (schwannoma) Schwann cell states.

Recently, a surprising relationship was observed between patients taking aspirin and VS growth. In a retrospective study, the authors noted that a substantial fraction of those who took aspirin did not experience an increase in VS size (Odds Ratio: .5, Confidence interval: .29-85) [224]. In a follow up study, the same group showed that non-steroidal anti-inflammatory drugs (NSAIDs) had a cytostatic effect on VS *in vitro*, and that COX-2 expression was elevated in VS samples compared to normal nerve[225]. An independent group has noted a correlation between COX-2 expression and VS growth rate [226]. Though NSAIDs are widely-appreciated to mediate their effects by knocking down COX-2 function, they are also known to inhibit NF-κB activity at doses attainable in human patients [227]. Further, COX-2, encoded by the *PTSG2* gene, is a well-established NF-κB target [228-230]. Thus, it is possible that the cytostatic effects observed in these studies are due inhibition of NF-κB activation. The observation of increased COX-2 levels also supports our hypothesis of aberrant NF-κB activation driving oncogenic signaling in schwannomas.

Our data indicates that schwannomas exhibit a simultaneous increase in the mRNA of the gene encoding NIK as well as all four genes encoding the E3 complex required to degrade NIK. All five genes have been described to be induced by either NIK or NF-κB [203-205, 231]. However, one would expect an increase in the expression of the E3 complex to negatively regulate FL NIK levels and, as a result, attenuate the increased levels of NIK mRNA. The presence of a stabilized, proteasome-resistant fragment of the NIK kinase domain provides a

cogent explanation for these apparently antagonistic molecular states. p55 NIK, lacking a TRAF3 binding domain, is no longer recognizable by the E3 complex targeting it for degradation. Thus, p55 NIK is free to activate downstream canonical and non-canonical signaling and its presence in NF2-KO tissues is sufficient to explain the chronic NF-κB activation observed in schwannomas, with persistent upregulation of genes encoding Rel family proteins, IκB proteins, and NF-κB targets (**Figure 39**).

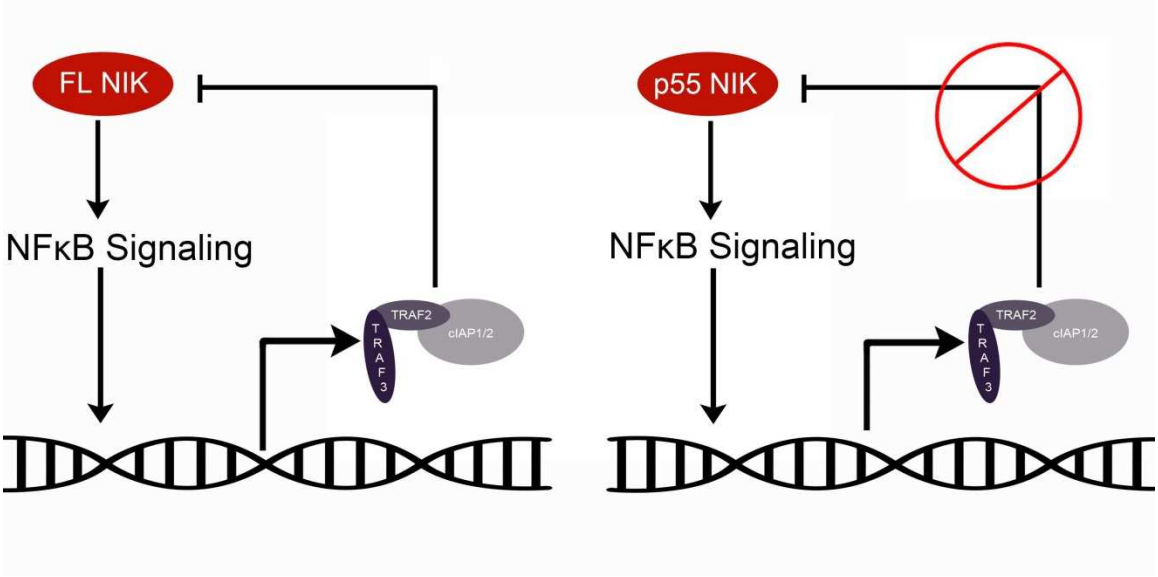

Figure 39. Schematic representation of hypothesized persistent NIK signaling present in schwannomas. NIK induces the expression of its negative regulators TRAF2, TRAF3, and c-IAP1/2. This serves as a negative feedback mechanism to prevent sustained activation of NIK. p55 NIK, however, no longer possesses a TRAF3 binding domain, and thus continues to drive downstream NF-κB signaling since it is no longer degraded by the proteasome.

It is plausible that an increase in stability is not the only gain in function for p55 NIK. Previous studies using fragments of the NIK kinase domain indicate similar truncations result in a remarkable increase in kinase activity toward IKKα when compared to FL NIK [134]. There are at least two possible explanations for this. First, the loss of the C-terminal IKKα phosphorylation sites would prevent the destabilization mediated by IKKα phosphorylation [199]. However, since this was an *in vitro* kinase assay performed in the absence of protein degradation machinery, this explanation is less likely to be the case. An alternate explanation comes from the knowledge that NIK forms dimers and transautophoshorylates itself as it initiates downstream signaling through IKKα [232]. The NRD of NIK is known to negatively regulate NIK signaling by interfering with NIK's interaction with IKKα through binding a region in the C-terminus of NIK, where IKKα also binds[197, 232]. Though this regulation would be expected to be present in *cis*, since NIK dimerizes to activate IKKα one would also expect this regulation to be relevant in *trans* as well. p55 NIK, however, lacks both the NRD as well as a portion of its C-terminus. Thus, p55 NIK no longer possesses the NRD that binds to the C-terminus, but it is also possible that p55 NIK can no longer be targeted by the NRD present in other FL NIK molecules because of its truncated C-terminus. If this is indeed the case, p55 NIK would no longer exert a negative regulatory influence on itself or other NIK molecules, but it would also be impervious to the *trans* regulation imparted by the NRD in other NIK molecules. Though we did not work up this aspect of p55 NIK and rather focused on protein stability, support for the hypothesized increase in activity toward IKKα is seen in

Figure 34A, where transfection of 309-801 NIK results in increased processing of p100 to p52 when compared to FL NIK.

To our knowledge, there is no known link between NF2 and caspase activity. Thus, how direct the relationship is between loss of NF2 and altered caspase function in schwannomas is unclear. PAK1, which is negatively regulated by NF2, is known to phosphorylate and activate Caspase-1 [233]. Additionally, there are other examples of PAK family proteins interacting with caspases [234-236]. It is possible that NF2 regulates caspase function through interactions with PAK proteins. The negative regulation of PAK activation by NF2 prevents PAK localization to focal adhesions, where Caspase-8 has also been found to localize and enhance tumor cell migration [53, 237]. Importantly, PAK1 is also known to activate NF-κB signaling through phosphorylation of NIK, thereby supporting the notion of PAK proteins linking NF2, caspases, and NIK in a protein complex [238, 239]. Though we demonstrate that Caspase-8 is sufficient to induce cleavage of NIK and the resulting p55 fragment of the kinase domain, we do not claim that it is the only caspase capable of cleaving NIK. Caspases possess overlapping substrate specificities such that protein localization as well as protein levels also likely dictate cleavage events, in addition to the preferred motifs within a substrate [195].

While these studies have tremendous relevance to schwannoma and Schwann cell biology, the identification of caspase-regulated NIK/NF-κB signaling in

schwannomas is also a significant contribution to basic caspase and NF-κB biology. The conservation of N and C-terminal cleavage sites in NIK across species suggests that these sites may be important sites of NIK regulation (**Figure 30**). Since being first identified in 2000, caspase activation of NF-κB remains poorly understood [173, 189]. Our studies provide a possible explanation of this event through cleavage of NIK rendering a fragment of the NIK kinase domain that is free to promote downstream NF-κB signaling independent of its normal mode(s) of regulation. They also provide an explanation for the interesting similarities seen between Caspase-8 and NIK-deficient patient phenotypes, as well as the abnormalities observed in isolated cells from these patients.

FUTURE DIRECTIONS

There are many fascinating directions emanating from the studies described in this manuscript. Of chief interest to our group is the determination if NIK signaling is necessary and sufficient for the development of schwannomas. We are currently approaching this question by conducting two rigorous *in vivo* proof of concept experiments. First, we seek to address the question of whether NIK signaling is necessary for NF2-deficient schwannoma formation by intercrossing our NF2-KO conditional knockout mouse with a constitutive NIK knockout (NIK-KO) mouse. NIK-KO mice are viable but do have lymphoid tissue abnormalities and display poor antibody responses [124]. We will examine these mice to see if loss of NIK signaling rescues NF2-KO mice from the tumor phenotype described in **Chapter One**. To test whether NIK activation in Schwann cells is sufficient to induce schwannoma formation, we again turn to an *in vivo* system. We are working with SAGE labs in St. Louis to generate injectable Crispr mRNA encoding a donor for a conditional knock-in of 309-801 NIK into the ROSA locus. This donor also includes an EGFP reporter, and the cassette is under control of the robust CAG promoter. Thus, when intercrossing the resulting transgenic mouse with a tissue specific Cre recombinase mouse, such as *Postn-Cre*, we can conditionally overexpress our NIK kinase fragment specifically in the developing Schwann cell lineages. We can then characterize this mouse and determine if it possesses a decrease in survival and/or develops schwannomas.

We are also excited to study the inflammatory cytokines elaborated from schwannomas. Given that NF-κB is a central regulator of cytokine and immunomodulatory gene expression, we would expect schwannomas to elaborate of number of inflammatory mediators that could possibly serve as autocrine and paracrine signaling factors. We already possess some preliminary cytokine data through multiplex analysis of IRES-EGFP and 309-801 NIK transduced Schwann cell conditioned medium. Of interest, 309-801 NIK transduced Schwann cells secreted 5-fold more IL-6, 18-fold more TNF-α, 149-fold more MIP-1β (CCL4), 163-fold more RANTES (CCL5), and over 1200-fold more GM-CSF. Given the paracrine signaling loop that our lab has previously studied between NF1-deficient Schwann cells and mast cells in the microenvironment, we are well-poised to further examine the interplay between NF2-null Schwann cells and potential cooperating inflammatory cell types [87, 240].

REFERENCES

1. Asthagiri, A.R., et al., *Neurofibromatosis type 2.* Lancet, 2009. **373**(9679): p. 1974-86.
2. Evans, D.G., et al., *A genetic study of type 2 neurofibromatosis in the United Kingdom. I. Prevalence, mutation rate, fitness, and confirmation of maternal transmission effect on severity.* Journal of medical genetics, 1992. **29**(12): p. 841-6.
3. Evans, D.G., et al., *Incidence of vestibular schwannoma and neurofibromatosis 2 in the North West of England over a 10-year period: higher incidence than previously thought.* Otol Neurotol, 2005. **26**(1): p. 93-7.
4. Evans, D.G., et al., *A clinical study of type 2 neurofibromatosis.* The Quarterly journal of medicine, 1992. **84**(304): p. 603-18.
5. Parry, D.M., et al., *Neurofibromatosis 2 (NF2): clinical characteristics of 63 affected individuals and clinical evidence for heterogeneity.* Am J Med Genet, 1994. **52**(4): p. 450-61.
6. Baser, M.E., et al., *Genotype-phenotype correlations for nervous system tumors in neurofibromatosis 2: a population-based study.* American journal of human genetics, 2004. **75**(2): p. 231-9.
7. Mautner, V.F., et al., *The neuroimaging and clinical spectrum of neurofibromatosis 2.* Neurosurgery, 1996. **38**(5): p. 880-5; discussion 885-6.

8. Samii, M., C. Matthies, and M. Tatagiba, *Management of vestibular schwannomas (acoustic neuromas): auditory and facial nerve function after resection of 120 vestibular schwannomas in patients with neurofibromatosis 2.* Neurosurgery, 1997. **40**(4): p. 696-705; discussion 705-6.

9. Fisher, L.M., et al., *Distribution of nonvestibular cranial nerve schwannomas in neurofibromatosis 2.* Otol Neurotol, 2007. **28**(8): p. 1083-90.

10. Otsuka, G., et al., *Age at symptom onset and long-term survival in patients with neurofibromatosis Type 2.* Journal of neurosurgery, 2003. **99**(3): p. 480-3.

11. Patronas, N.J., et al., *Intramedullary and spinal canal tumors in patients with neurofibromatosis 2: MR imaging findings and correlation with genotype.* Radiology, 2001. **218**(2): p. 434-42.

12. Dow, G., et al., *Spinal tumors in neurofibromatosis type 2. Is emerging knowledge of genotype predictive of natural history?* J Neurosurg Spine, 2005. **2**(5): p. 574-9.

13. Mautner, V.F., et al., *Spinal tumors in patients with neurofibromatosis type 2: MR imaging study of frequency, multiplicity, and variety.* AJR Am J Roentgenol, 1995. **165**(4): p. 951-5.

14. Rennie, A.T., et al., *Intramedullary tumours in patients with neurofibromatosis type 2: MRI features associated with a favourable prognosis.* Clin Radiol, 2008. **63**(2): p. 193-200.

15. MacCollin, M. and V.F. Mautner, *The diagnosis and management of neurofibromatosis 2 in childhood.* Semin Pediatr Neurol, 1998. **5**(4): p. 243-52.

16. Mautner, V.F., et al., *Skin abnormalities in neurofibromatosis 2.* Archives of dermatology, 1997. **133**(12): p. 1539-43.

17. Evans, D.G., et al., *Management of the patient and family with neurofibromatosis 2: a consensus conference statement.* Br J Neurosurg, 2005. **19**(1): p. 5-12.

18. Baser, M.E., et al., *Evaluation of clinical diagnostic criteria for neurofibromatosis 2.* Neurology, 2002. **59**(11): p. 1759-65.

19. Nunes, F. and M. MacCollin, *Neurofibromatosis 2 in the pediatric population.* Journal of child neurology, 2003. **18**(10): p. 718-24.

20. Ruggieri, M., et al., *Earliest clinical manifestations and natural history of neurofibromatosis type 2 (NF2) in childhood: a study of 24 patients.* Neuropediatrics, 2005. **36**(1): p. 21-34.

21. Evans, D.G., J.M. Birch, and R.T. Ramsden, *Paediatric presentation of type 2 neurofibromatosis.* Archives of disease in childhood, 1999. **81**(6): p. 496-9.

22. J.H., W., *Case of tumours in the skull, dura mater and brain.* Edinburgh Med Surg J, 1822(18): p. 393-97.

23. Feiling, A. and E. Ward, *A Familial Form of Acoustic Tumour.* Br Med J, 1920. **1**(3093): p. 496-7.

24. Gardner W.J., F.C.H., *Bilateral acoustic neurofibromas: a clinical study and field survery of a family of five generations with bilateral deafness in thirty-eight members. .* Arch Neurol Psychiatr, 1930(23): p. 266-302.

25. Seizinger, B.R., et al., *Linkage analysis in von Recklinghausen neurofibromatosis (NF1) with DNA markers for chromosome 17.* Genomics, 1987. **1**(4): p. 346-8.

26. Rouleau, G.A., et al., *Genetic linkage of bilateral acoustic neurofibromatosis to a DNA marker on chromosome 22.* Nature, 1987. **329**(6136): p. 246-8.

27. Parry, D.M., et al., *Germ-line mutations in the neurofibromatosis 2 gene: correlations with disease severity and retinal abnormalities.* American journal of human genetics, 1996. **59**(3): p. 529-39.

28. Evans, D.G., et al., *Genotype/phenotype correlations in type 2 neurofibromatosis (NF2): evidence for more severe disease associated with truncating mutations.* Journal of medical genetics, 1998. **35**(6): p. 450-5.

29. Baser, M.E., et al., *The location of constitutional neurofibromatosis 2 (NF2) splice site mutations is associated with the severity of NF2.* Journal of medical genetics, 2005. **42**(7): p. 540-6.

30. Baser, M.E., et al., *Predictors of the risk of mortality in neurofibromatosis 2.* American journal of human genetics, 2002. **71**(4): p. 715-23.

31. Betka, J., et al., *Complications of microsurgery of vestibular schwannoma.* Biomed Res Int, 2014. **2014**: p. 315952.

32. Brackmann, D.E., et al., *Early proactive management of vestibular schwannomas in neurofibromatosis type 2.* Neurosurgery, 2001. **49**(2): p. 274-80; discussion 280-3.

33. Fisher, L.M., et al., *Concordance of bilateral vestibular schwannoma growth and hearing changes in neurofibromatosis 2: neurofibromatosis 2 natural history consortium.* Otol Neurotol, 2009. **30**(6): p. 835-41.

34. Stemmer-Rachamimov, A.O., et al., *Comparative pathology of nerve sheath tumors in mouse models and humans.* Cancer research, 2004. **64**(10): p. 3718-24.

35. Sherman, L., et al., *Interdomain binding mediates tumor growth suppression by the NF2 gene product.* Oncogene, 1997. **15**(20): p. 2505-9.

36. Bashour, A.M., et al., *The neurofibromatosis type 2 gene product, merlin, reverses the F-actin cytoskeletal defects in primary human Schwannoma cells.* Molecular and cellular biology, 2002. **22**(4): p. 1150-7.

37. Bretscher, A., K. Edwards, and R.G. Fehon, *ERM proteins and merlin: integrators at the cell cortex.* Nat Rev Mol Cell Biol, 2002. **3**(8): p. 586-99.

38. Fehon, R.G., A.I. McClatchey, and A. Bretscher, *Organizing the cell cortex: the role of ERM proteins.* Nat Rev Mol Cell Biol, 2010. **11**(4): p. 276-87.

39. Shimizu, T., et al., *Structural basis for neurofibromatosis type 2. Crystal structure of the merlin FERM domain.* The Journal of biological chemistry, 2002. **277**(12): p. 10332-6.

40. Gary, R. and A. Bretscher, *Ezrin self-association involves binding of an N-terminal domain to a normally masked C-terminal domain that includes the F-actin binding site.* Mol Biol Cell, 1995. **6**(8): p. 1061-75.

41. Pearson, M.A., et al., *Structure of the ERM protein moesin reveals the FERM domain fold masked by an extended actin binding tail domain.* Cell, 2000. **101**(3): p. 259-70.

42. Heiska, L., et al., *Association of ezrin with intercellular adhesion molecule-1 and -2 (ICAM-1 and ICAM-2). Regulation by phosphatidylinositol 4, 5-bisphosphate.* The Journal of biological chemistry, 1998. **273**(34): p. 21893-900.

43. Tsukita, S., et al., *ERM family members as molecular linkers between the cell surface glycoprotein CD44 and actin-based cytoskeletons.* The Journal of cell biology, 1994. **126**(2): p. 391-401.

44. Rong, R., et al., *Serine 518 phosphorylation modulates merlin intramolecular association and binding to critical effectors important for NF2 growth suppression.* Oncogene, 2004. **23**(52): p. 8447-54.

45. Surace, E.I., C.A. Haipek, and D.H. Gutmann, *Effect of merlin phosphorylation on neurofibromatosis 2 (NF2) gene function.* Oncogene, 2004. **23**(2): p. 580-7.

46. Kissil, J.L., et al., *Merlin phosphorylation by p21-activated kinase 2 and effects of phosphorylation on merlin localization.* The Journal of biological chemistry, 2002. **277**(12): p. 10394-9.

47. Xiao, G.H., et al., *p21-activated kinase links Rac/Cdc42 signaling to merlin.* The Journal of biological chemistry, 2002. **277**(2): p. 883-6.

48. Johnson, K.C., et al., *Cellular transformation by a FERM domain mutant of the Nf2 tumor suppressor gene.* Oncogene, 2002. **21**(39): p. 5990-7.

49. LaJeunesse, D.R., B.M. McCartney, and R.G. Fehon, *Structural analysis of Drosophila merlin reveals functional domains important for growth control and subcellular localization.* The Journal of cell biology, 1998. **141**(7): p. 1589-99.

50. Shaw, R.J., A.I. McClatchey, and T. Jacks, *Regulation of the neurofibromatosis type 2 tumor suppressor protein, merlin, by adhesion and growth arrest stimuli.* The Journal of biological chemistry, 1998. **273**(13): p. 7757-64.

51. Okada, T., M. Lopez-Lago, and F.G. Giancotti, *Merlin/NF-2 mediates contact inhibition of growth by suppressing recruitment of Rac to the plasma membrane.* The Journal of cell biology, 2005. **171**(2): p. 361-71.

52. Shaw, R.J., et al., *The Nf2 tumor suppressor, merlin, functions in Rac-dependent signaling.* Developmental cell, 2001. **1**(1): p. 63-72.

53. Kissil, J.L., et al., *Merlin, the product of the Nf2 tumor suppressor gene, is an inhibitor of the p21-activated kinase, Pak1.* Mol Cell, 2003. **12**(4): p. 841-9.

54. Lallemand, D., et al., *NF2 deficiency promotes tumorigenesis and metastasis by destabilizing adherens junctions.* Genes & development, 2003. **17**(9): p. 1090-100.

55. Yi, C., et al., *A tight junction-associated Merlin-angiomotin complex mediates Merlin's regulation of mitogenic signaling and tumor suppressive functions.* Cancer cell, 2011. **19**(4): p. 527-40.

56. Lopez-Lago, M.A., et al., *Loss of the tumor suppressor gene NF2, encoding merlin, constitutively activates integrin-dependent mTORC1 signaling.* Molecular and cellular biology, 2009. **29**(15): p. 4235-49.

57. James, M.F., et al., *NF2/merlin is a novel negative regulator of mTOR complex 1, and activation of mTORC1 is associated with meningioma and schwannoma growth.* Molecular and cellular biology, 2009. **29**(15): p. 4250-61.

58. Jessen, K.R., et al., *The Schwann cell precursor and its fate: a study of cell death and differentiation during gliogenesis in rat embryonic nerves.* Neuron, 1994. **12**(3): p. 509-27.

59. Dong, Z., et al., *Neu differentiation factor is a neuron-glia signal and regulates survival, proliferation, and maturation of rat Schwann cell precursors.* Neuron, 1995. **15**(3): p. 585-96.

60. Jessen, K.R. and R. Mirsky, *The origin and development of glial cells in peripheral nerves.* Nat Rev Neurosci, 2005. **6**(9): p. 671-82.

61. Britsch, S., et al., *The transcription factor Sox10 is a key regulator of peripheral glial development.* Genes & development, 2001. **15**(1): p. 66-78.

62. Wolpowitz, D., et al., *Cysteine-rich domain isoforms of the neuregulin-1 gene are required for maintenance of peripheral synapses.* Neuron, 2000. **25**(1): p. 79-91.

63. Meier, C., et al., *Developing Schwann cells acquire the ability to survive without axons by establishing an autocrine circuit involving insulin-like growth factor, neurotrophin-3, and platelet-derived growth factor-BB.* J Neurosci, 1999. **19**(10): p. 3847-59.

64. Trachtenberg, J.T. and W.J. Thompson, *Schwann cell apoptosis at developing neuromuscular junctions is regulated by glial growth factor.* Nature, 1996. **379**(6561): p. 174-7.

65. Yu, W.M., et al., *Schwann cell-specific ablation of laminin gamma1 causes apoptosis and prevents proliferation.* J Neurosci, 2005. **25**(18): p. 4463-72.

66. Syroid, D.E., et al., *Cell death in the Schwann cell lineage and its regulation by neuregulin.* Proceedings of the National Academy of Sciences of the United States of America, 1996. **93**(17): p. 9229-34.

67. Le, N., et al., *Analysis of congenital hypomyelinating Egr2Lo/Lo nerves identifies Sox2 as an inhibitor of Schwann cell differentiation and myelination.* Proceedings of the National Academy of Sciences of the United States of America, 2005. **102**(7): p. 2596-601.

68. Nickols, J.C., et al., *Activation of the transcription factor NF-kappaB in Schwann cells is required for peripheral myelin formation.* Nat Neurosci, 2003. **6**(2): p. 161-7.

69. Mirsky, R., et al., *Regulation of genes involved in Schwann cell development and differentiation.* Prog Brain Res, 2001. **132**: p. 3-11.

70. Jaegle, M., et al., *The POU proteins Brn-2 and Oct-6 share important functions in Schwann cell development.* Genes & development, 2003. **17**(11): p. 1380-91.

71. Sharpless, N.E. and R.A. Depinho, *The mighty mouse: genetically engineered mouse models in cancer drug development.* Nature reviews. Drug discovery, 2006. **5**(9): p. 741-54.

72. McClatchey, A.I., et al., *The Nf2 tumor suppressor gene product is essential for extraembryonic development immediately prior to gastrulation.* Genes & development, 1997. **11**(10): p. 1253-65.

73. McClatchey, A.I., et al., *Mice heterozygous for a mutation at the Nf2 tumor suppressor locus develop a range of highly metastatic tumors.* Genes & development, 1998. **12**(8): p. 1121-33.

74. Giovannini, M., et al., *Schwann cell hyperplasia and tumors in transgenic mice expressing a naturally occurring mutant NF2 protein.* Genes & development, 1999. **13**(8): p. 978-86.

75. Giovannini, M., et al., *Conditional biallelic Nf2 mutation in the mouse promotes manifestations of human neurofibromatosis type 2.* Genes & development, 2000. **14**(13): p. 1617-30.

76. Lindsley, A., et al., *Identification and characterization of a novel Schwann and outflow tract endocardial cushion lineage-restricted periostin enhancer.* Developmental biology, 2007. **307**(2): p. 340-55.

77. Stemmer-Rachamimov, A.O., et al., *Loss of the NF2 gene and merlin occur by the tumorlet stage of schwannoma development in neurofibromatosis 2.* J Neuropathol Exp Neurol, 1998. **57**(12): p. 1164-7.

78. Sperfeld, A.D., et al., *Occurrence and characterization of peripheral nerve involvement in neurofibromatosis type 2.* Brain : a journal of neurology, 2002. **125**(Pt 5): p. 996-1004.

79. Zheng, Q.Y., K.R. Johnson, and L.C. Erway, *Assessment of hearing in 80 inbred strains of mice by ABR threshold analyses.* Hear Res, 1999. **130**(1-2): p. 94-107.

80. Henry, K.R., *Auditory brainstem volume-conducted responses: origins in the laboratory mouse.* J Am Aud Soc, 1979. **4**(5): p. 173-8.

81. Melcher, J.R. and N.Y. Kiang, *Generators of the brainstem auditory evoked potential in cat. III: Identified cell populations.* Hear Res, 1996. **93**(1-2): p. 52-71.

82. Santarelli, R., et al., *Abnormal cochlear potentials from deaf patients with mutations in the otoferlin gene.* J Assoc Res Otolaryngol, 2009. **10**(4): p. 545-56.

83. Durrant, J.D., et al., *Are inner or outer hair cells the source of summating potentials recorded from the round window?* J Acoust Soc Am, 1998. **104**(1): p. 370-7.

84. Vidal, P.P., et al., *Postural and locomotor control in normal and vestibularly deficient mice.* J Physiol, 2004. **559**(Pt 2): p. 625-38.

85. Tsai, H., et al., *The mouse slalom mutant demonstrates a role for Jagged1 in neuroepithelial patterning in the organ of Corti.* Human molecular genetics, 2001. **10**(5): p. 507-12.

86. Hardisty-Hughes, R.E., A. Parker, and S.D. Brown, *A hearing and vestibular phenotyping pipeline to identify mouse mutants with hearing impairment.* Nat Protoc, 2010. **5**(1): p. 177-90.

87. Yang, F.C., et al., *Nf1-dependent tumors require a microenvironment containing Nf1+/-- and c-kit-dependent bone marrow.* Cell, 2008. **135**(3): p. 437-48.

88. Pollizzi, K., et al., *A hypomorphic allele of Tsc2 highlights the role of TSC1/TSC2 in signaling to AKT and models mild human TSC2 alleles.* Human molecular genetics, 2009. **18**(13): p. 2378-87.

89. Mo, W., et al., *CXCR4/CXCL12 mediate autocrine cell- cycle progression in NF1-associated malignant peripheral nerve sheath tumors.* Cell, 2013. **152**(5): p. 1077-90.

90. Lee da, Y., S.M. Gianino, and D.H. Gutmann, *Innate neural stem cell heterogeneity determines the patterning of glioma formation in children.* Cancer cell, 2012. **22**(1): p. 131-8.

91. Wu, J., et al., *Plexiform and dermal neurofibromas and pigmentation are caused by Nf1 loss in desert hedgehog-expressing cells.* Cancer Cell, 2008. **13**(2): p. 105-16.

92. Birnbaum, R.A., et al., *Nf1 and Gmcsf interact in myeloid leukemogenesis.* Mol Cell, 2000. **5**(1): p. 189-95.

93. Seizinger, B.R., et al., *Common pathogenetic mechanism for three tumor types in bilateral acoustic neurofibromatosis.* Science, 1987. **236**(4799): p. 317-9.

94. Plotkin, S.R., et al., *Hearing improvement after bevacizumab in patients with neurofibromatosis type 2.* The New England journal of medicine, 2009. **361**(4): p. 358-67.

95. Asthagiri, A.R., et al., *Mechanisms of hearing loss in neurofibromatosis type 2.* PLoS One, 2012. **7**(9): p. e46132.

96. Gouveris, H.T., A. Victor, and W.J. Mann, *Cochlear origin of early hearing loss in vestibular schwannoma.* The Laryngoscope, 2007. **117**(4): p. 680-3.

97. Prasher, D.K., et al., *Mechanisms of hearing loss in acoustic neuroma: an otoacoustic emission study.* Acta Otolaryngol, 1995. **115**(3): p. 375-81.

98. Sen, R. and D. Baltimore, *Multiple nuclear factors interact with the immunoglobulin enhancer sequences.* Cell, 1986. **46**(5): p. 705-16.

99. Sen, R. and D. Baltimore, *Inducibility of kappa immunoglobulin enhancer-binding protein Nf-kappa B by a posttranslational mechanism.* Cell, 1986. **47**(6): p. 921-8.

100. Baeuerle, P.A. and D. Baltimore, *Activation of DNA-binding activity in an apparently cytoplasmic precursor of the NF-kappa B transcription factor.* Cell, 1988. **53**(2): p. 211-7.

101. Bonizzi, G. and M. Karin, *The two NF-kappaB activation pathways and their role in innate and adaptive immunity.* Trends Immunol, 2004. **25**(6): p. 280-8.

102. Karin, M. and F.R. Greten, *NF-kappaB: linking inflammation and immunity to cancer development and progression.* Nat Rev Immunol, 2005. **5**(10): p. 749-59.

103. Hayden, M.S. and S. Ghosh, *Shared principles in NF-kappaB signaling.* Cell, 2008. **132**(3): p. 344-62.

104. Karin, M. and Y. Ben-Neriah, *Phosphorylation meets ubiquitination: the control of NF-[kappa]B activity.* Annu Rev Immunol, 2000. **18**: p. 621-63.

105. Dobrzanski, P., R.P. Ryseck, and R. Bravo, *Specific inhibition of RelB/p52 transcriptional activity by the C-terminal domain of p100.* Oncogene, 1995. **10**(5): p. 1003-7.

106. Senftleben, U., et al., *Activation by IKKalpha of a second, evolutionary conserved, NF-kappa B signaling pathway.* Science, 2001. **293**(5534): p. 1495-9.

107. Yilmaz, Z.B., et al., *RelB is required for Peyer's patch development: differential regulation of p52-RelB by lymphotoxin and TNF.* The EMBO journal, 2003. **22**(1): p. 121-30.

108. Basak, S., et al., *A fourth IkappaB protein within the NF-kappaB signaling module.* Cell, 2007. **128**(2): p. 369-81.

109. Liou, H.C., et al., *The NF-kappa B p50 precursor, p105, contains an internal I kappa B-like inhibitor that preferentially inhibits p50.* The EMBO journal, 1992. **11**(8): p. 3003-9.

110. Palombella, V.J., et al., *The ubiquitin-proteasome pathway is required for processing the NF-kappa B1 precursor protein and the activation of NF-kappa B.* Cell, 1994. **78**(5): p. 773-85.

111. Beinke, S. and S.C. Ley, *Functions of NF-kappaB1 and NF-kappaB2 in immune cell biology.* Biochem J, 2004. **382**(Pt 2): p. 393-409.

112. Arenzana-Seisdedos, F., et al., *Nuclear localization of I kappa B alpha promotes active transport of NF-kappa B from the nucleus to the cytoplasm.* Journal of cell science, 1997. **110 (Pt 3)**: p. 369-78.

113. Hoffmann, A., et al., *The IkappaB-NF-kappaB signaling module: temporal control and selective gene activation.* Science, 2002. **298**(5596): p. 1241-5.

114. Hu, Y., et al., *Abnormal morphogenesis but intact IKK activation in mice lacking the IKKalpha subunit of IkappaB kinase.* Science, 1999. **284**(5412): p. 316-20.

115. Xiao, G., E.W. Harhaj, and S.C. Sun, *NF-kappaB-inducing kinase regulates the processing of NF-kappaB2 p100.* Mol Cell, 2001. **7**(2): p. 401-9.

116. Lombardi, L., et al., *Structural and functional characterization of the promoter regions of the NFKB2 gene.* Nucleic Acids Res, 1995. **23**(12): p. 2328-36.

117. Stadanlick, J.E., et al., *Tonic B cell antigen receptor signals supply an NF-kappaB substrate for prosurvival BLyS signaling.* Nat Immunol, 2008. **9**(12): p. 1379-87.

118. Hannink, M. and H.M. Temin, *Structure and autoregulation of the c-rel promoter.* Oncogene, 1990. **5**(12): p. 1843-50.

119. Capobianco, A.J. and T.D. Gilmore, *Repression of the chicken c-rel promoter by vRel in chicken embryo fibroblasts is not mediated through a consensus NF-kappa B binding site.* Oncogene, 1991. **6**(12): p. 2203-10.

120. Ten, R.M., et al., *The characterization of the promoter of the gene encoding the p50 subunit of NF-kappa B indicates that it participates in its own regulation.* The EMBO journal, 1992. **11**(1): p. 195-203.

121. Bren, G.D., et al., *Transcription of the RelB gene is regulated by NF-kappaB.* Oncogene, 2001. **20**(53): p. 7722-33.

122. O'Dea, E. and A. Hoffmann, *The regulatory logic of the NF-kappaB signaling system.* Cold Spring Harb Perspect Biol, 2010. **2**(1): p. a000216.

123. Shinkura, R., et al., *Alymphoplasia is caused by a point mutation in the mouse gene encoding Nf-kappa b-inducing kinase.* Nature genetics, 1999. **22**(1): p. 74-7.

124. Yin, L., et al., *Defective lymphotoxin-beta receptor-induced NF-kappaB transcriptional activity in NIK-deficient mice.* Science, 2001. **291**(5511): p. 2162-5.

125. Liao, G., et al., *Regulation of the NF-kappaB-inducing kinase by tumor necrosis factor receptor-associated factor 3-induced degradation.* The Journal of biological chemistry, 2004. **279**(25): p. 26243-50.

126. Qing, G., Z. Qu, and G. Xiao, *Stabilization of basally translated NF-kappaB-inducing kinase (NIK) protein functions as a molecular switch of processing of NF-kappaB2 p100.* The Journal of biological chemistry, 2005. **280**(49): p. 40578-82.

127. Vallabhapurapu, S. and M. Karin, *Regulation and function of NF-kappaB transcription factors in the immune system.* Annu Rev Immunol, 2009. **27**: p. 693-733.

128. Vallabhapurapu, S., et al., *Nonredundant and complementary functions of TRAF2 and TRAF3 in a ubiquitination cascade that activates NIK-dependent alternative NF-kappaB signaling.* Nat Immunol, 2008. **9**(12): p. 1364-70.

129. Annunziata, C.M., et al., *Frequent engagement of the classical and alternative NF-kappaB pathways by diverse genetic abnormalities in multiple myeloma.* Cancer cell, 2007. **12**(2): p. 115-30.

130. Keats, J.J., et al., *Promiscuous mutations activate the noncanonical NF-kappaB pathway in multiple myeloma.* Cancer cell, 2007. **12**(2): p. 131-44.

131. Rosebeck, S., et al., *Cleavage of NIK by the API2-MALT1 fusion oncoprotein leads to noncanonical NF-kappaB activation.* Science, 2011. **331**(6016): p. 468-72.

132. Zarnegar, B., et al., *Control of canonical NF-kappaB activation through the NIK-IKK complex pathway.* Proceedings of the National Academy of Sciences of the United States of America, 2008. **105**(9): p. 3503-8.

133. Demchenko, Y.N., et al., *Classical and/or alternative NF-kappaB pathway activation in multiple myeloma.* Blood, 2010. **115**(17): p. 3541-52.

134. Liu, J., et al., *Structure of the nuclear factor kappaB-inducing kinase (NIK) kinase domain reveals a constitutively active conformation.* The Journal of biological chemistry, 2012. **287**(33): p. 27326-34.

135. Gilmore, T.D., *Multiple mutations contribute to the oncogenicity of the retroviral oncoprotein v-Rel.* Oncogene, 1999. **18**(49): p. 6925-37.

136. Braun, T., et al., *Targeting NF-kappaB in hematologic malignancies.* Cell death and differentiation, 2006. **13**(5): p. 748-58.

137. Li, Q. and I.M. Verma, *NF-kappaB regulation in the immune system.* Nat Rev Immunol, 2002. **2**(10): p. 725-34.

138. Karin, M., et al., *NF-kappaB in cancer: from innocent bystander to major culprit.* Nat Rev Cancer, 2002. **2**(4): p. 301-10.

139. Hinz, M., et al., *NF-kappaB function in growth control: regulation of cyclin D1 expression and G0/G1-to-S-phase transition.* Molecular and cellular biology, 1999. **19**(4): p. 2690-8.

140. Iwanaga, R., et al., *Activation of the cyclin D2 and cdk6 genes through NF-kappaB is critical for cell-cycle progression induced by HTLV-I Tax.* Oncogene, 2008. **27**(42): p. 5635-42.

141. Toth, C.R., et al., *Members of the nuclear factor kappa B family transactivate the murine c-myb gene.* The Journal of biological chemistry, 1995. **270**(13): p. 7661-71.

142. Duyao, M.P., et al., *Transactivation of the c-myc promoter by human T cell leukemia virus type 1 tax is mediated by NF kappa B.* The Journal of biological chemistry, 1992. **267**(23): p. 16288-91.

143. Kitamura, T., et al., *Involvement of poly(ADP-ribose) polymerase 1 in ERBB2 expression in rheumatoid synovial cells.* Am J Physiol Cell Physiol, 2005. **289**(1): p. C82-8.

144. Catz, S.D. and J.L. Johnson, *Transcriptional regulation of bcl-2 by nuclear factor kappa B and its significance in prostate cancer.* Oncogene, 2001. **20**(50): p. 7342-51.

145. Dai, J.Y., et al., *The Met protooncogene is a transcriptional target of NF kappaB: implications for cell survival.* Journal of cellular biochemistry, 2009. **107**(6): p. 1222-36.

146. Schmidt-Ullrich, R., et al., *NF-kappaB activity in transgenic mice: developmental regulation and tissue specificity.* Development, 1996. **122**(7): p. 2117-28.

147. Bhakar, A.L., et al., *Constitutive nuclear factor-kappa B activity is required for central neuron survival.* J Neurosci, 2002. **22**(19): p. 8466-75.

148. Kaltschmidt, B. and C. Kaltschmidt, *NF-kappaB in the nervous system.* Cold Spring Harb Perspect Biol, 2009. **1**(3): p. a001271.

149. Brambilla, R., et al., *Inhibition of astroglial nuclear factor kappaB reduces inflammation and improves functional recovery after spinal cord injury.* J Exp Med, 2005. **202**(1): p. 145-56.

150. Limpert, A.S., et al., *NF-kappaB forms a complex with the chromatin remodeler BRG1 to regulate Schwann cell differentiation.* J Neurosci, 2013. **33**(6): p. 2388-97.

151. Chen, Y., et al., *HDAC-mediated deacetylation of NF-kappaB is critical for Schwann cell myelination.* Nat Neurosci, 2011. **14**(4): p. 437-41.

152. Hung, G., et al., *Immunohistochemistry study of human vestibular nerve schwannoma differentiation.* Glia, 2002. **38**(4): p. 363-70.

153. Torres-Martin, M., et al., *Microarray analysis of gene expression in vestibular schwannomas reveals SPP1/MET signaling pathway and androgen receptor deregulation.* International journal of oncology, 2013. **42**(3): p. 848-62.

154. Gehlhausen, J.R., et al., *A murine model of neurofibromatosis type 2 that accurately phenocopies human schwannoma formation.* Human molecular genetics, 2015. **24**(1): p. 1-8.

155. Kim, J.Y., et al., *Inhibition of NF-kappaB activation by merlin.* Biochemical and biophysical research communications, 2002. **296**(5): p. 1295-302.

156. Ammoun, S., et al., *Axl/Gas6/NFkappaB signalling in schwannoma pathological proliferation, adhesion and survival.* Oncogene, 2014. **33**(3): p. 336-46.

157. Parker, M., et al., *C11orf95-RELA fusions drive oncogenic NF-kappaB signalling in ependymoma.* Nature, 2014. **506**(7489): p. 451-5.

158. Song, J., et al., *Cascleave: towards more accurate prediction of caspase substrate cleavage sites.* Bioinformatics, 2010. **26**(6): p. 752-60.

159. Wang, M., et al., *Cascleave 2.0, a new approach for predicting caspase and granzyme cleavage targets.* Bioinformatics, 2014. **30**(1): p. 71-80.

160. Verspurten, J., et al., *SitePredicting the cleavage of proteinase substrates.* Trends Biochem Sci, 2009. **34**(7): p. 319-23.

161. Edgar, R., M. Domrachev, and A.E. Lash, *Gene Expression Omnibus: NCBI gene expression and hybridization array data repository.* Nucleic Acids Res, 2002. **30**(1): p. 207-10.

162. Barrett, T., et al., *NCBI GEO: archive for functional genomics data sets--update.* Nucleic Acids Res, 2013. **41**(Database issue): p. D991-5.

163. Moriyama, T., et al., *Comparative analysis of expression of hepatocyte growth factor and its receptor, c-met, in gliomas, meningiomas and schwannomas in humans.* Cancer Lett, 1998. **124**(2): p. 149-55.

164. Hansen, M.R. and F.H. Linthicum, Jr., *Expression of neuregulin and activation of erbB receptors in vestibular schwannomas: possible autocrine loop stimulation.* Otol Neurotol, 2004. **25**(2): p. 155-9.

165. Ammoun, S., et al., *ErbB/HER receptor activation and preclinical efficacy of lapatinib in vestibular schwannoma.* Neuro Oncol, 2010. **12**(8): p. 834-43.

166. Xiao, G.H., et al., *The NF2 tumor suppressor gene product, merlin, inhibits cell proliferation and cell cycle progression by repressing cyclin D1 expression.* Molecular and cellular biology, 2005. **25**(6): p. 2384-94.

167. Dilwali, S., D. Roberts, and K.M. Stankovic, *Interplay between VEGF-A and cMET signaling in human vestibular schwannomas and schwann cells.* Cancer Biol Ther, 2015. **16**(1): p. 170-5.

168. Hovelmeyer, N., et al., *Regulation of B cell homeostasis and activation by the tumor suppressor gene CYLD.* J Exp Med, 2007. **204**(11): p. 2615-27.

169. Malinin, N.L., et al., *MAP3K-related kinase involved in NF-kappaB induction by TNF, CD95 and IL-1.* Nature, 1997. **385**(6616): p. 540-4.

170. Willmann, K.L., et al., *Biallelic loss-of-function mutation in NIK causes a primary immunodeficiency with multifaceted aberrant lymphoid immunity.* Nat Commun, 2014. **5**: p. 5360.

171. Yamada, T., et al., *Abnormal immune function of hemopoietic cells from alymphoplasia (aly) mice, a natural strain with mutant NF-kappa B-inducing kinase.* Journal of immunology, 2000. **165**(2): p. 804-12.

172. Ramakrishnan, P., W. Wang, and D. Wallach, *Receptor-specific signaling for both the alternative and the canonical NF-kappaB activation pathways by NF-kappaB-inducing kinase.* Immunity, 2004. **21**(4): p. 477-89.

173. Hu, W.H., *Activation of NF-kappa B by FADD, Casper, and Caspase-8.* Journal of Biological Chemistry, 2000. **275**(15): p. 10838-10844.

174. Sohn, D., K. Schulze-Osthoff, and R.U. Janicke, *Caspase-8 can be activated by interchain proteolysis without receptor-triggered dimerization*

during drug-induced apoptosis. The Journal of biological chemistry, 2005. **280**(7): p. 5267-73.

175. Fuentes-Prior, P. and G.S. Salvesen, *The protein structures that shape caspase activity, specificity, activation and inhibition.* Biochem J, 2004. **384**(Pt 2): p. 201-32.

176. Kurokawa, M. and S. Kornbluth, *Caspases and kinases in a death grip.* Cell, 2009. **138**(5): p. 838-54.

177. Graves, J.D., et al., *Caspase-mediated activation and induction of apoptosis by the mammalian Ste20-like kinase Mst1.* The EMBO journal, 1998. **17**(8): p. 2224-34.

178. Fischer, U., R.U. Janicke, and K. Schulze-Osthoff, *Many cuts to ruin: a comprehensive update of caspase substrates.* Cell death and differentiation, 2003. **10**(1): p. 76-100.

179. Kakeya, H., R. Onose, and H. Osada, *Caspase-mediated activation of a 36-kDa myelin basic protein kinase during anticancer drug-induced apoptosis.* Cancer research, 1998. **58**(21): p. 4888-94.

180. Lee, K.K., et al., *Proteolytic activation of MST/Krs, STE20-related protein kinase, by caspase during apoptosis.* Oncogene, 1998. **16**(23): p. 3029-37.

181. Huang, C.Y., et al., *Caspase activation of mammalian sterile 20-like kinase 3 (Mst3). Nuclear translocation and induction of apoptosis.* The Journal of biological chemistry, 2002. **277**(37): p. 34367-74.

182. Rudel, T., et al., *p21-activated kinase (PAK) is required for Fas-induced JNK activation in Jurkat cells.* Journal of immunology, 1998. **160**(1): p. 7-11.

183. Lee, N., et al., *Activation of hPAK65 by caspase cleavage induces some of the morphological and biochemical changes of apoptosis.* Proceedings of the National Academy of Sciences of the United States of America, 1997. **94**(25): p. 13642-7.

184. Chen, Y.R., et al., *Caspase-mediated cleavage and functional changes of hematopoietic progenitor kinase 1 (HPK1).* Oncogene, 1999. **18**(51): p. 7370-7.

185. Arnold, R., et al., *Caspase-mediated cleavage of hematopoietic progenitor kinase 1 (HPK1) converts an activator of NFkappaB into an inhibitor of NFkappaB.* The Journal of biological chemistry, 2001. **276**(18): p. 14675-84.

186. Cardone, M.H., et al., *The regulation of anoikis: MEKK-1 activation requires cleavage by caspases.* Cell, 1997. **90**(2): p. 315-23.

187. Deak, J.C., et al., *Fas-induced proteolytic activation and intracellular redistribution of the stress-signaling kinase MEKK1.* Proceedings of the National Academy of Sciences of the United States of America, 1998. **95**(10): p. 5595-600.

188. Widmann, C., et al., *MEK kinase 1, a substrate for DEVD-directed caspases, is involved in genotoxin-induced apoptosis.* Molecular and cellular biology, 1998. **18**(4): p. 2416-29.

189. Chaudhary, P.M., et al., *Activation of the NF-kappaB pathway by caspase 8 and its homologs.* Oncogene, 2000. **19**(39): p. 4451-60.

190. Shikama, Y., M. Yamada, and T. Miyashita, *Caspase-8 and caspase-10 activate NF-kappaB through RIP, NIK and IKKalpha kinases.* Eur J Immunol, 2003. **33**(7): p. 1998-2006.

191. Chun, H.J., et al., *Pleiotropic defects in lymphocyte activation caused by caspase-8 mutations lead to human immunodeficiency.* Nature, 2002. **419**(6905): p. 395-9.

192. Korenaga, M., et al., *Impaired protective immunity and T helper 2 responses in alymphoplasia (aly) mutant mice infected with Trichinella spiralis.* Immunology, 2001. **102**(2): p. 218-24.

193. Karrer, U., et al., *On the key role of secondary lymphoid organs in antiviral immune responses studied in alymphoplastic (aly/aly) and spleenless (Hox11(-)/-) mutant mice.* J Exp Med, 1997. **185**(12): p. 2157-70.

194. Su, H., et al., *Requirement for caspase-8 in NF-kappaB activation by antigen receptor.* Science, 2005. **307**(5714): p. 1465-8.

195. Pop, C. and G.S. Salvesen, *Human caspases: activation, specificity, and regulation.* The Journal of biological chemistry, 2009. **284**(33): p. 21777-81.

196. Wellington, C.L., et al., *Caspase cleavage of gene products associated with triplet expansion disorders generates truncated fragments containing the polyglutamine tract.* The Journal of biological chemistry, 1998. **273**(15): p. 9158-67.

197. Xiao, G. and S.C. Sun, *Negative regulation of the nuclear factor kappa B-inducing kinase by a cis-acting domain.* The Journal of biological chemistry, 2000. **275**(28): p. 21081-5.

198. Lee, S., et al., *Nuclear factor-kappaB-inducing kinase (NIK) contains an amino-terminal inhibitor of apoptosis (IAP)-binding motif (IBM) that potentiates NIK degradation by cellular IAP1 (c-IAP1).* The Journal of biological chemistry, 2014. **289**(44): p. 30680-9.

199. Razani, B., et al., *Negative feedback in noncanonical NF-kappaB signaling modulates NIK stability through IKKalpha-mediated phosphorylation.* Science signaling, 2010. **3**(123): p. ra41.

200. Yang, F., et al., *IKK beta plays an essential role in the phosphorylation of RelA/p65 on serine 536 induced by lipopolysaccharide.* Journal of immunology, 2003. **170**(11): p. 5630-5.

201. Lallemand, D., et al., *Merlin regulates transmembrane receptor accumulation and signaling at the plasma membrane in primary mouse Schwann cells and in human schwannomas.* Oncogene, 2009. **28**(6): p. 854-65.

202. Gutmann, D.H., et al., *Increased expression of the NF2 tumor suppressor gene product, merlin, impairs cell motility, adhesionand spreading.* Human molecular genetics, 1999. **8**(2): p. 267-75.

203. Sasaki, Y., et al., *NIK overexpression amplifies, whereas ablation of its TRAF3-binding domain replaces BAFF:BAFF-R-mediated survival signals*

in B cells. Proceedings of the National Academy of Sciences of the United States of America, 2008. **105**(31): p. 10883-8.

204. Bista, P., et al., *TRAF3 controls activation of the canonical and alternative NFkappaB by the lymphotoxin beta receptor.* The Journal of biological chemistry, 2010. **285**(17): p. 12971-8.

205. Thu, Y.M. and A. Richmond, *NF-kappaB inducing kinase: a key regulator in the immune system and in cancer.* Cytokine Growth Factor Rev, 2010. **21**(4): p. 213-26.

206. Gherardi, E., et al., *Targeting MET in cancer: rationale and progress.* Nat Rev Cancer, 2012. **12**(2): p. 89-103.

207. Yu, D. and M.C. Hung, *Overexpression of ErbB2 in cancer and ErbB2-targeting strategies.* Oncogene, 2000. **19**(53): p. 6115-21.

208. Neklason, D.W., et al., *Activating mutation in MET oncogene in familial colorectal cancer.* BMC Cancer, 2011. **11**: p. 424.

209. Herter-Sprie, G.S., H. Greulich, and K.K. Wong, *Activating Mutations in ERBB2 and Their Impact on Diagnostics and Treatment.* Front Oncol, 2013. **3**: p. 86.

210. Garratt, A.N., et al., *A dual role of erbB2 in myelination and in expansion of the schwann cell precursor pool.* The Journal of cell biology, 2000. **148**(5): p. 1035-46.

211. Houshmandi, S.S., et al., *The neurofibromatosis 2 protein, merlin, regulates glial cell growth in an ErbB2- and Src-dependent manner.* Molecular and cellular biology, 2009. **29**(6): p. 1472-86.

212. Karajannis, M.A., et al., *Phase II trial of lapatinib in adult and pediatric patients with neurofibromatosis type 2 and progressive vestibular schwannomas.* Neuro Oncol, 2012. **14**(9): p. 1163-70.

213. Clemence, A., R. Mirsky, and K.R. Jessen, *Non-myelin-forming Schwann cells proliferate rapidly during Wallerian degeneration in the rat sciatic nerve.* J Neurocytol, 1989. **18**(2): p. 185-92.

214. Stoll, G., S. Jander, and R.R. Myers, *Degeneration and regeneration of the peripheral nervous system: from Augustus Waller's observations to neuroinflammation.* J Peripher Nerv Syst, 2002. **7**(1): p. 13-27.

215. Tofaris, G.K., et al., *Denervated Schwann cells attract macrophages by secretion of leukemia inhibitory factor (LIF) and monocyte chemoattractant protein-1 in a process regulated by interleukin-6 and LIF.* J Neurosci, 2002. **22**(15): p. 6696-703.

216. Goethals, S., et al., *Toll-like receptor expression in the peripheral nerve.* Glia, 2010. **58**(14): p. 1701-9.

217. Kim, D., et al., *Toll-like receptor 2 contributes to chemokine gene expression and macrophage infiltration in the dorsal root ganglia after peripheral nerve injury.* Mol Pain, 2011. **7**: p. 74.

218. Boivin, A., et al., *Toll-like receptor signaling is critical for Wallerian degeneration and functional recovery after peripheral nerve injury.* J Neurosci, 2007. **27**(46): p. 12565-76.

219. Lee, H., et al., *Necrotic neuronal cells induce inflammatory Schwann cell activation via TLR2 and TLR3: implication in Wallerian degeneration.*

Biochemical and biophysical research communications, 2006. **350**(3): p. 742-7.

220. Barrette, B., et al., *Transcriptional profiling of the injured sciatic nerve of mice carrying the Wld(S) mutant gene: identification of genes involved in neuroprotection, neuroinflammation, and nerve regeneration.* Brain Behav Immun, 2010. **24**(8): p. 1254-67.

221. Limpert, A.S. and B.D. Carter, *Axonal neuregulin 1 type III activates NF-kappaB in Schwann cells during myelin formation.* The Journal of biological chemistry, 2010. **285**(22): p. 16614-22.

222. Morton, P.D., et al., *Nuclear factor-kappaB activation in Schwann cells regulates regeneration and remyelination.* Glia, 2012. **60**(4): p. 639-50.

223. Mitchell, L.S., et al., *Expression of myelin protein gene transcripts by Schwann cells of regenerating nerve.* J Neurosci Res, 1990. **27**(2): p. 125-35.

224. Kandathil, C.K., et al., *Aspirin intake correlates with halted growth of sporadic vestibular schwannoma in vivo.* Otol Neurotol, 2014. **35**(2): p. 353-7.

225. Dilwali, S., et al., *Nonsteroidal anti-inflammatory medications are cytostatic against human vestibular schwannomas.* Transl Res, 2015.

226. Hong, B., et al., *Cyclooxygenase-2 supports tumor proliferation in vestibular schwannomas.* Neurosurgery, 2011. **68**(4): p. 1112-7.

227. Yamamoto, Y. and R.B. Gaynor, *Therapeutic potential of inhibition of the NF-kappaB pathway in the treatment of inflammation and cancer.* The Journal of clinical investigation, 2001. **107**(2): p. 135-42.

228. Yamamoto, K., et al., *Transcriptional roles of nuclear factor kappa B and nuclear factor-interleukin-6 in the tumor necrosis factor alpha-dependent induction of cyclooxygenase-2 in MC3T3-E1 cells.* The Journal of biological chemistry, 1995. **270**(52): p. 31315-20.

229. Ackerman, W.E.t., et al., *Nuclear factor-kappa B regulates inducible prostaglandin E synthase expression in human amnion mesenchymal cells.* Biol Reprod, 2008. **78**(1): p. 68-76.

230. Kaltschmidt, B., et al., *Cyclooxygenase-2 is a neuronal target gene of NF-kappaB.* BMC Mol Biol, 2002. **3**: p. 16.

231. Wang, C.Y., et al., *NF-kappaB antiapoptosis: induction of TRAF1 and TRAF2 and c-IAP1 and c-IAP2 to suppress caspase-8 activation.* Science, 1998. **281**(5383): p. 1680-3.

232. Lin, X., et al., *Molecular determinants of NF-kappaB-inducing kinase action.* Molecular and cellular biology, 1998. **18**(10): p. 5899-907.

233. Basak, C., et al., *NF-kappaB- and C/EBPbeta-driven interleukin-1beta gene expression and PAK1-mediated caspase-1 activation play essential roles in interleukin-1beta release from Helicobacter pylori lipopolysaccharide-stimulated macrophages.* The Journal of biological chemistry, 2005. **280**(6): p. 4279-88.

234. Gnesutta, N., J. Qu, and A. Minden, *The serine/threonine kinase PAK4 prevents caspase activation and protects cells from apoptosis.* The Journal of biological chemistry, 2001. **276**(17): p. 14414-9.

235. Rudel, T. and G.M. Bokoch, *Membrane and morphological changes in apoptotic cells regulated by caspase-mediated activation of PAK2.* Science, 1997. **276**(5318): p. 1571-4.

236. Gnesutta, N. and A. Minden, *Death receptor-induced activation of initiator caspase 8 is antagonized by serine/threonine kinase PAK4.* Molecular and cellular biology, 2003. **23**(21): p. 7838-48.

237. Barbero, S., et al., *Caspase-8 association with the focal adhesion complex promotes tumor cell migration and metastasis.* Cancer research, 2009. **69**(9): p. 3755-63.

238. Foryst-Ludwig, A. and M. Naumann, *p21-activated kinase 1 activates the nuclear factor kappa B (NF-kappa B)-inducing kinase-Ikappa B kinases NF-kappa B pathway and proinflammatory cytokines in Helicobacter pylori infection.* The Journal of biological chemistry, 2000. **275**(50): p. 39779-85.

239. Frost, J.A., et al., *Stimulation of NFkappa B activity by multiple signaling pathways requires PAK1.* The Journal of biological chemistry, 2000. **275**(26): p. 19693-9.

240. Yang, F.C., et al., *Neurofibromin-deficient Schwann cells secrete a potent migratory stimulus for Nf1+/- mast cells.* J Clin Invest, 2003. **112**(12): p. 1851-61.

CURRICULUM VITAE

Jeff R. Gehlhausen

EDUCATION

2009-present: Indiana University School of Medicine; Indianapolis, IN

MSTP (MD/PhD) student

2009-2011 (First two years of medical school): Earned "Honors" grade in the following courses in the first two years of medical school: Biochemistry, Cellular and Molecular Biology, Histology, Physiology, Immunology, Microbiology, General Pathology, Systemic Pathology, Neuroscience, Pharmacology, Introduction to Clinical Medicine, and Medical Genetics.

2011-2015: PhD student in lab of Dr. Wade Clapp. PhD conferred in May 2015 from Indiana University.

Present-2017: 3rd and 4th years of medical school.

2003-2007: Indiana University, Bloomington

B.S. in Informatics; Minors in Information Technology, Computer Science

Graduated Summa Cum Laude; 1st in class with overall 3.97 GPA, 4.0 Science GPA

ACADEMIC AND PROFESSIONAL HONORS

2014 1 of 5 students campus-wide to receive Indiana University School of Medicine Educational Affairs' Award for Outstanding Student Contribution to curricular reform

2014 Marilyn Hester Scholarship for students conducting pediatric oncology research ($8,000 award); Indiana University School of Medicine, Indianapolis, IN

2005, 2006 Informatics Dean's Advisory Council Scholarship ($1,000 award); Indiana University, Bloomington, IN

2004 Telamon Scholarship ($2,500 award); Indiana University, Bloomington, IN

2003 Indiana University Fee Remission Scholarship (75% reduction in tuition costs annually, worth roughly $12,000/yr); Indiana University, Bloomington, IN

RESEARCH EXPERIENCE

2011-present Graduate Student, Lab of Dr. Wade Clapp; Indiana University School of Medicine, Indianapolis, IN

2008-2009 Research Technician, Lab of Dr. Wade Clapp; Indiana University School of Medicine, Indianapolis, IN

2007 Research Assistant, Lab of Dr. Justen Andrews; Indiana University, Bloomington, IN

CLINICAL EXPERIENCE

2010-present Volunteer, Indiana School of Medicine Student Outreach Center; Indianapolis, IN

2009-present Medical Student; Indiana University School of Medicine, Indianapolis, IN

2007 Emergency Room Volunteer, Bloomington Hospital; Bloomington, IN

POSITIONS AND EMPLOYMENT

2013-present Student member of Indiana University School of Medicine Curricular Reform team for Host Defense course (combined Immunology/Microbiology course); Indianapolis, IN

2012-present Indiana University School of Medicine Curriculum Council Steering Committee; Indianapolis, IN

2013 Medical Student tutor; Indianapolis, IN

2012-13 Indiana University School of Medicine Student Research Committee; Indianapolis, IN

2009, 2012-15 Molecular Medicine in Action (MMIA), Faculty Selected Instructor; Indianapolis, IN

2006-2008 Microsoft Student Partner Technical Representative; Bloomington, IN

2006-2007 Software Developer, Fossil Visualization Application; Bloomington, IN

2006-2007 Intern, Microsoft Academic Division; Bloomington, IN

2006-2007 Associate Instructor for Introductory Computing laboratory; Bloomington, IN

2005-2006 Software Developer, Midwest Proton Radiotherapy Institute; Bloomington, IN

PROFESSIONAL SOCIETIES

2012-present Medical Student Member, American Medical Association

2011-present Associate Member, American Association of Cancer Research

2006 Iota Nu Phi Informatics Honor Society Inductee; Indiana University, Bloomington, IN

TRAINING GRANTS AND FELLOWSHIPS

2014-present NRSA F30 training grant from National Institute for Deafness and Communication Disorders (NIDCD); Fellowship covers all tuition and related fees for graduate/medical school, along with a yearly stipend of $22,500 and $4,000 in supplemental allowance.

2014 American Physician Scientist Association annual meeting travel award recipient (750$ in supplemental allowance)

2013 IUSM Graduate Student travel award ($500 in supplemental allowance)

2013 Simon Cancer Center AACR annual meeting travel grant awardee ($500 in supplemental allowance)

2012-2014 Children's Tumor Foundation Young Investigator Award; $64,000 Predoctoral stipend over two years with $5,000 in travel/supplemental allowances

2012 Indiana Clinical and Translational Sciences Institute (CTSI) Predoctoral Award – NIH Training Grant #TR000162 (Declined due to receipt of CTF Young Investigator Award); $24,500 Predoctoral stipend per year (competitive renewal)

2009-present Medical Scientist Training Program (MSTP) Fellow; Indiana University School of Medicine, Indianapolis, IN

2007 Informatics Graduate School Barwise Scholarship (full graduate school tuition and stipend, value exceeding $30,000/yr); Indiana University, Bloomington, IN

2007 Hutton Honors College Summer Research Grant ($1,000 award); Indiana University, Bloomington, IN

ABSTRACTS AND POSTERS

1. A novel murine model of NF2 with manifestations of human NF2 disease. Gehlhausen JR, Shew MA, Park SJ, Staser KW, Rhodes SD, Clapp DW, Yates CW. Children's Tumor Foundation Annual NF meeting. Monterey, California (June, 2013).

2. A conditional model of schwannoma genesis that recapitulates human NF2 disease. Gehlhausen JR, Shew MA, Park SJ, Staser KW, Rhodes SD, Clapp DW, Yates CW. American Association for Cancer Research (AACR) annual meeting. Washington, DC (April 2013).

3. Normal Hematopoesis and Nf1-deficient myeloproliferative disease require Erk.. Staser K, Park SJ, He YZ, Shew MA, Rhodes SD, Gehlhausen JR, Cerabonna D, Li Y, Nalepa G, Yang FC, Clapp DW. International Society for Experimental Hematology (ISEH) Annual Meeting, Amsterdam, The Netherlands (August 2012).

4. A novel murine model of Neurofibromatosis Type 2. Gehlhausen JR, Shew MA, Park SJ, Clapp DW, Yates CW. Children's Tumor Foundation Annual Neurofibromatosis Meeting. New Orleans, LA (June 2012).

5. Development of a novel murine model of Neurofibromatosis Type 2. Gehlhausen JR, Shew MA, Park SJ, Clapp DW, Yates CW. International NF2 Conference, Manchester, UK (May 2012).

6. Myelopoiesis Requires Erk. Staser KW, Park SJ, He YZ, Shew MA, Gehlhausen JR, Rhodes SD, Li Y, Nalepa G, Yang FC, Clapp DW. Cancer Biology Training Consortium Annual Meeting, Tucson, AZ (November 2010)

7. Marrow repopulation and stem cell expansion requires ERK. Staser KW, Park SJ, He YZ, Shew MA, Gehlhausen JR, Rhodes SD, Li Y, Nalepa G, Yang FC, Clapp DW. International Society for Experimental Hematology (ISEH) Annual Meeting, Melbourne, Australia (September 2010).

8. Genetic evidence that myeloid proliferation requires ERK. Staser K, Park SJ, He YZ, Shew MA, Gehlhausen JR, Robinson MB, Li Y, Rhodes SD, Nalepa G, Yang FC, Clapp DW. American Society of Clinical Investigators (ASCI) Annual Meeting, Chicago, IL (April 2010).

9. Erk1 negatively regulates SCF-dependent mast cell function via Erk2 and β-catenin interactions. Staser K, Park SJ, Gehlhausen JR, Clapp DW. Howard Hughes Medical Institute Annual Scholars/Fellows Meeting, Bethesda, MD (May 2009).

ORAL PRESENTATIONS

1. A conditional NF2 mouse model of schwannoma genesis that recapitulates human disease. Gehlhausen JR, Park SJ, Yates CW, Clapp DW. Abstract selected for oral presentation in plenary session. 2014 American Society for Clinical Investigation/American Physician Scientist Association Joint Meeting. Chicago, IL (April 2014).

2. A new murine model of Neurofibromatosis Type 2. Gehlhausen JR, Shew MA, Park SJ, Clapp DW, Yates CW. Selected platform presentation. Children's Tumor Foundation Annual Neurofibromatosis Meeting. New Orleans, LA (June 2012).

3. Current Research in Neurofibromatosis Type 2. Gehlhausen JR, Shew MA, Park SJ, Yates CW, Clapp DW. Neonatology Working Group Seminar Series, Indianapolis, IN (July 2011).

4. Visualization of Fossil Records Using Microsoft Virtual Earth. Gehlhausen JR, Dalkilic MM, Microsoft eScience Workshop, Chapel Hill, NC (May 2007).

PEER-REVIEWED PUBLICATIONS

1. Gehlhausen JR, Park SJ, Hickox AE, Shew M, Staser K, Rhodes SD, Menon KM,Lajiness JD, Mwanthi M, Yang X, Yuan J, Territo P, Hutchins G, Nalepa G, Yang FC,Conway SJ, Heinz MG, Stemmer-Rachamimov A, Yates CW, Clapp DW. A murine model of neurofibromatosis type 2 that accurately phenocopies human schwannoma formation. Hum mol genet. 2015 Jan 1;24(1):1-8. doi: 10.1093/hmg/ddu414. Epub 2014 Aug 11. PMID: 25113746; PMCID: PMC4262489.

2. Grzegorz Nalepa, Jill Barnholtz-Sloan, Rikki Enzor, Dilip Dey, Ying He, Jeff R. Gehlhausen, Amalia S. Lehmann, Yanzhu Yang1, Xianlin Yang, Shi Chen, Xiaowei Guan, Yanwen Chen, Jamie Renbarger, Feng-Chun Yang, Luis F. Parada, Wade Clapp. Tumor Suppressor CDKN3 Controls Mitosis. J Cell Biol. 2013 Jun 24;201(7):997-1012. doi: 10.1083/jcb.201205125. Epub 2013 Jun 17. PMID: 23775190; PMCID: PMC3691455.

3. Staser K,Park SJ, Rhodes SD,Zeng Y,He Y,Shew MA, Gehlhausen JR,Cerabonna D,Menon KM,Chen S,Sun Z,Yuan J, Ingram DA,Nalepa G,Yang FC, Clapp DW. Normal hematopoiesis and neurofibromin-deficient myeloproliferative disease require Erk. J Clin Invest. 2013;123(1):329–334. doi:10.1172/JCI66167. PMCID: PMC3533306; PMID: 23221339.

4. Costello JC, Dalkilic MM, Beason SM, Gehlhausen JR, Patwardhan R, Middha S, Eads BD, Andrews JR. Gene networks in Drosophila melanogaster: integrating experimental data to predict gene function. Genome biol. 10 (2009), pp. R97. PMCID: PMC2768986; PMID: 19758432.

5. Costello JC, Schrider D, Gehlhausen JR, Dalkilic M. Data-driven ontologies. Pac Symp Biocomput. 2009:15-26. Prepublished on 2009/02/13 as DOI. PMID: 19213131.